Development of advanced methods for the analysis of star and highly branched polymers

by
Douglas Murima

This thesis is presented in partial fulfilment of the requirements for the degree of
Doctor of Philosophy (Polymer Science)
at the
University of Stellenbosch

Supervisor: Professor Harald Pasch
Faculty of Science
Department of Chemistry and Polymer Science

March 2020

Declaration

By submitting this thesis electronically, I, **Douglas Murima**, hereby declare that the entirety of the work contained therein is my own, original work, that I am the sole author thereof (save to the extent explicitly otherwise stated), that reproduction and publication thereof by Stellenbosch University will not infringe any third party rights and that I have not previously in its entirety or in part submitted it for obtaining any qualification.

Date March 2020

Abstract

Branched polymers are a unique class of materials with broad applications in fields such as automobile parts, textiles, lubricants, packaging, medicine, construction, soil binders in agriculture, and so on. Much of their attractive properties when compared to their linear counterparts are a result of variations in chemical composition, molar mass and architectural distributions. Branching in polymers may exist naturally (e.g. polysaccharides, natural rubber) or deliberately induced (e.g. in synthetic rubber and packaging materials from polyolefins, rheology modifiers). Advances in the synthesis of branched polymers with complex architectures for various targeted applications have continued to add to the growing need of more advanced characterization methods for structure-property correlations. In this current work, the development of various advanced methods for separation and characterization of lowly and highly branched polymers with distributions that include molar mass, degree of branching and chemical composition were investigated. Monodisperse star-branched polystyrenes with varying numbers of arms (3, 4, and 6 arms) provided a clean model systems for the analysis of crude star-branched polybutadienes with 3 and 4-arms, miktoarm-polystyrene-polyisoprene, and then a more complex hyperbranched Bd-PS. The first experimental part described the preparation of 3-arm, 4-arm and 6-arm star polystyrenes from multi-armed RAFT agents. Here, for the first time, the comprehensive characterization of star functionality (number of arms) via triple detector SEC and correlating with average functionalities determined by offline ^{1}H-NMR and comparing the resolution of different chromatographic techniques was presented. The second part extended the comparison between the separation capabilities of HPLC in both 1D and 2D modes to resolve highly branched block copolymers. The novelty of the work was highlighted regarding the comprehensive analysis of hyperbranched block copolymers using liquid chromatographic techniques in combination with spectroscopic techniques and remarkable correlations were established. The third experimental part of this work discussed, for the first time, the application of multidetector Thermal field-flow fractionation as a channel-based separation technique for determining polymer conformations from Mark-Houwink plots and the degree of branching using functionality plots for a set of 3-, 4-, and 6-arm star polystyrenes, and a more complex hyperbranched polybutadiene-polystyrene (PBd-PS) copolymer in a single experiment.

Opsomming

Vertakte polimere is 'n unieke klas materiale met breë toepassings in velde soos motoronderdele, tekstiele, smeermiddels, verpakking, medisyne, konstruksie, grondbinders in die landbou, ensovoorts. Baie van hul aantreklike eienskappe in vergelyking met hul lineêre eweknieë is die resultaat van variasies in chemiese samestelling, molmassa en argitektoniese verdeling. Vertakkings in polimere kan natuurlik bestaan (b.v. polisakkariede, natuurlike rubber) of doelbewus veroorsaak word (b.v. in sintetiese rubber en verpakkingsmateriaal van poli-olefiene, reologie-modifiseerders). Die vooruitgang in die sintese van vertakte polimere met komplekse argitekture vir verskillende doelgerigte toepassings het steeds bygedra tot die groeiende behoefte aan meer gevorderde karakteriseringsmetodes vir struktuureienskap korrelasies. In hierdie huidige werk is die ontwikkeling van verskillende gevorderde metodes vir die skeiding en karakterisering van lae en sterk vertakte polimere met verspreidings wat molêre massa, die mate van vertakking en chemiese samestelling insluit, ondersoek. Monodisperse stervertakte polistireen met wisselende aantal arms (3, 4 en 6 arms) het 'n skoon modelstelsels voorsien vir die ontleding van ru-vertakte polibutadiëne met 3 en 4-arms, miktoarm-polistireen-poli-isopreen, en dan nog 'n meer komplekse hipervertakte Bd-PS. Die eerste eksperimentele deel het die bereiding van 3-arm-, 4-arm- en 6-arm-ster-polistireen van mult-arm RAFT-middels beskryf. Hier is die eerste keer die uitgebreide karakterisering van sterfunksionaliteit (hoeveelheid arms) via die drievoudige detector SEC en korreleer met die gemiddelde funksionaliteite wat deur offline 1H-NMR bepaal is, en die resolusie van verskillende chromatografiese tegnieke vergelyk. Die tweede deel het die vergelyking tussen die skeidingsvermoëns van HPLC in beide 1D- en 2D-modusse uitgebrei om hoogs vertakte blokkopolimere op te los. Die nuwigheid van die werk is uitgelig met betrekking tot die uitgebreide analise van hipervertakte blokkopolimere met behulp van vloeistofchromatografiese tegnieke in kombinasie met spektroskopiese tegnieke en merkwaardige korrelasies is vasgestel. Die derde eksperimentele deel van hierdie werk het vir die eerste keer die toepassing van multidetektor termiese veldvloei-fraksionering bespreek as 'n kanaalgebaseerde skeidingstegniek vir die bepaling van polimeerkonformasies vanaf Mark-Houwink grafieke en die mate van vertakking deur gebruik te maak van funksionele plotte vir 'n stel van 3-, 4- en 6-arm ster-polistireen, en 'n meer komplekse hipervertakte polibutadiëen-polistireen (PBd-PS) -kopolymeer in 'n enkele eksperiment.

Acknowledgements

First and foremost, I would like to thank **God** for the countless blessings in all aspects of my everyday life and making this study possible.

Secondly, I would like to express my heartfelt gratitude and immeasurable appreciation to my promoter, **Professor Harald Pasch**, for the guidance, patience, encouragement, and enthusiastic support throughout my studies.

I would like to thank **Dr. Helen Pfukwa,** for her immense knowledge and motivation. Furthermore, I would like to thank **Professor Lian Hutchings** for assistance and contribution on the basics of Temperature gradient interaction chromatography.

My sincere thanks also go to members of **Professor Pasch's research group** (past and present): **Khumo, Kerissa, Mohau, Mawande, Anthony, Paul, Guillaume, Zanelle, Chelsea, Noni, Carlo, Josh, Clement, Ndumiso** and **Upenyu.**

I would like to extend my appreciation to all members of the Polymer Science Division especially **Mrs. Erinda Cooper, Mrs. Aneli Fourie, Mr. Deon Koen, Mr. Calvin Maart** and **Mr. Jim Motshweni** and **all staff members** at the Department of Chemistry and Polymer Science.

I would also like to thank **Elsa Malherbe** and **Dr Brand** for NMR analysis.

I would like to thank **Professor Harald Pasch** and the Polymer Science Division for the financial support of this research.

Finally, a special thanks goes to **my beloved family** for the moral support, and **all my friends** and anyone not mentioned. All your contributions are greatly appreciated.

Table of Contents

List of Figures

List of Tables

List of Abbreviations

α	Mark-Houwink exponent
2D-LC	comprehensive two-dimensional liquid chromatography
% v/v	percentage by volume
AIBN	Azobisisobutyronitrile
C-Hex	cyclohexane
DLS	dynamic light scattering
dRI	differential refractive index detector
dVisc	differential viscometer detector
ELSD	evaporative light scattering detector
^{1}H-NMR	proton nuclear magnetic resonance spectroscopy
IV	intrinsic viscosity
MALS	multiangle light scattering detector
PBd-PS	hyperbranched polybutadiene-polystyrene block copolymer
PS	polystyrene
PS-PI_2	miktoarm star-branched polystyrene-polyisoprene
RAFT	reversible addition-fragmentation chain transfer polymerization
R_g	radius of gyration
R_h	hydrodynamic radius
SEC	size exclusion chromatography
SGIC	solvent gradient interaction chromatography
TGIC	temperature gradient interaction chromatography
THF	tetrahydrofuran
ThFFF	Thermal field-flow fractionation
t_R	retention time
V_E	elution volume

1.

Introduction and aims

1.1 Introduction

The continued development of robust, synthetic as well as post-synthesis modification methods used to prepare polymers with desirable functionalities and properties consistently adds to the demand of state-of-the-art analytical methods.[1-3] This is predominantly because polymers often exist as complex macromolecular mixtures which may contain multiple distributions regarding chemical composition, functionality, molecular weight (M_W), chain architecture, and so on[4,5] Figure 1.1 shows the distinctive molecular distributions usually present in polymers.

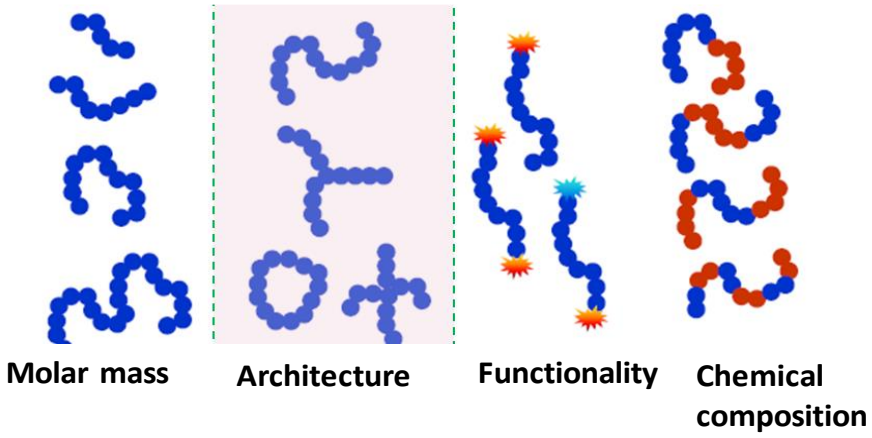

Figure 1.1 Various molecular heterogeneities present in synthetic polymers

As such, these distributions affect the final materials' properties and the comprehensive characterization of the distributions is important in the development and quality control of polymeric materials for various targeted end-use applications. [4-8] Most frequently, reversible deactivation radical polymerization (RDRP) techniques such as atomic transfer radical polymerization (ATRP) as well as reversible addition-fragmentation chain transfer (RAFT); or living polymerization methods that include anionic polymerization are used to tailor a variety of the desired properties in polymers for structural-property correlations.[9-12] Although the designing of such polymers can be achieved relatively easily, there are still grey areas in

their characterization, particularly if branching co-exists with two or more of the other molecular distributions.[13,14]

The development of multidimensional separation and characterization techniques is an area of ongoing research in order to address and break down the complexity of polymeric mixtures regarding their multiple distributions.[1,15-18] High performance liquid chromatography (HPLC) separation techniques that include size exclusion chromatography (SEC), interaction chromatography (IC) as well as liquid chromatography at critical conditions (LCCC) in one-dimensional or two-dimensional modes are frequently employed due to their availability in most research centres.[19-25] Alternatively, channel-based separation techniques such as asymmetric flow field-flow fractionation (AF4) and Thermal field-flow fractionation are used if available.[26-30]

The work discussed in this thesis involves novel contributions towards the comprehensive analysis of low and highly branched block copolymers for structure-property correlations by means of a combination of chromatographic techniques coupled to multiple detection methods. The application of multidetector ThFFF to address the influence of the degree of branching on separation and elution behaviour of hyperbranched PBd-PS block copolymers is also highlighted.

1.2 Aims and Objectives

The main aim of this study was to develop advanced liquid chromatography based analytical methods in one- and two-dimensional modes for the characterization of miktoarm star-branched polystyrene-polyisoprene (PS-PI_2) and hyperbranched polybutadiene-polystyrene (PBd-PS) block copolymers. A set of star-shaped polystyrenes with (3, 4, and 6 arms) and star-shaped polybutadienes with 3 and 4 arms provided a clean model for the method development and analysis. Thermal field-flow fractionation was to be employed to provide complementary branching information on star polystyrenes with 3, 4, and 6 arms and the more complex hyperbranched PBd-PS.

The objectives of this study were to analyse the effect of branching and size distribution on the solution behaviour of star-branched polymers by

a) Preparing multi-arm RAFT agents.
- Prepare 3-arm, 4-arm and 6-arm star polymers from the multi-arm RAFT agents

- Determine the absolute molecular weights of the star-branched polymers by multiangle light scattering
- Determine the intrinsic viscosity properties of the star-branched polymers by viscometry and compare the average functionalities with those determined by offline ^{1}H-NMR
- Fractionate the star-branched species from the linear species via TGIC, SGIC and 2D-LC

b) Preparing model miktoarm star-branched PS-PI_2 and hyperbranched PBd-PS via coupling chemistry using building blocks made by anionic polymerization

- Characterize the miktoarm star PS-PI_2 and the hyperbranched PBd-PS by triple-detector SEC
- 2D-LC analysis of the miktoarm star PS-PI_2 and the hyperbranched PBd-PS comparing the two liquid adsorption chromatography (LAC) methods (TGIC and SGIC) on normal and reversed phase LC
- Analyse the individual fractions (collected from one-dimensional normal phase and reversed phase TGIC) using offline ^{1}H-NMR for tentative structural assignments

c) Characterizing the star-branched PS and the hyperbranched PBd-PS block copolymer using multi-detector ThFFF

- Determine the size distributions and conformations from Mark-Houwink plots and the dimensionless shape factors (R_g/R_h) as well as hydrodynamic average sizes, using star-shaped polystyrenes with 3, 4, and 6 arms as the models, from offline dynamic light scattering (DLS)

1.3 Thesis Layout

A short introduction together with the aims and objectives of this study are given in Chapter 1.

The broad theoretical base of this work is presented in Chapter 2. It includes a brief overview of branched and hyperbranched polymers, outlining the separation techniques. The last part focuses on the methods of detection used for branching analysis.

Chapter 3 describes the preparation of 3-arm, 4-arm and 6-arm star polystyrenes from the multi-armed RAFT agents. Here, for the first time, the comprehensive characterization of star

functionality (number of arms) via triple detector SEC and correlating with average functionalities determined by offline ^{1}H-NMR and comparing the resolution of TGIC, SGIC, 2D-LC is presented.

Chapter 4 extends the comparison between the separation capabilities of SGIC and TGIC in both 1D and 2D modes to separate highly branched block copolymers. To the best of our knowledge, there is very little work done on the comprehensive analysis of hyperbranched block copolymers using liquid chromatographic techniques in combination with spectroscopic techniques.

Chapter 5 highlights the characterization of complex hyperbranched PBd-PS copolymers using multi-detector Thermal field-Flow Fractionation (ThFFF). This chapter particularly highlights the application of Thermal field-flow fractionation as a means of characterizing low and highly branched block copolymers based on their compositional and size/architectural polydispersities.

1.4 References

1. H. Pasch; M. Adler; F. Rittig; S. Becker. *Macromolecules Rapid. Commun* 2005, **26**: 438-444.
2. B. W. J. Pirok; D. R. Stoll; P. J. Schoenmakers. *Anal. Chem.* 2018, **91**:240-263.
3. Y. Pakzad; M. Fathi; M. Mozafari In *Advanced Functional Polymers for Biomedical Applications*; Elsevier: 2019, p 359-381.
4. D. Murima; H. Pfukwa; I. Tiggelman; P. C. Hartmann; H. Pasch. *Macromolecules Mater.Eng.* 2016, **301**: 836-845.
5. R. Nagarajan, In *Amphiphiles: Molecular Assembly and Applications*, American Chemical Society 2011, **1070**: p1-22.
6. M. Nichifor; X. X. Zhu. *Colloid. Polym. Sci.* 2003, **281**: 1034-1039.
7. Y. Liu; W. Radke; H. Pasch. *Macromolecules.* 2005, **38**: 7476-7484.
8. N. Li; T. Yan; Z. Li; T. Thurn-Albrecht; W. H. Binder. *Energ. Environ. Sci.* 2012, **5**: 7888-7892.
9. K. Matyjaszewski. *Macromolecules.* 2012, **45**: 4015-4039.
10. G. Moad; E. Rizzardo; S. H. Thang. *Polym. Int.* 2011, **60**: 9-25.
11. M. Tanishima; A. Goto; L. Lei; A. Ohtsuki; H. Kaji; A. Nomura; Y. Tsujii; Y. Yamaguchi; H. Komatsu; M. Miyamoto. *Polymers* 2014, **6**: 311-326.
12. N. Hadjichristidis; A. Hirao *Anionic Polymerization*; Springer, Japan 2015, p 1082
13. S. Lee; H. Lee; T. Chang; A. Hirao. *Macromolecules.* 2017, **50**: 2768-2776.
14. S. Lee; H. Choi; T. Chang; B. Staal. *Anal. Chem.* 2018, **90**: 6259-6266.
15. P. Kilz; R. Kruger; H. Much; G. Schulz. *Adv. Chem. Ser.* 1995, **247**: 223-241.
16. H. Pasch *Adv. Polym. Sci*., 2000, **150**: 1-66.
17. A. Ndiripo; P. S. Eselem Bungu; H. Pasch. *Polym. Int.* 2019, **68**: 206-217.
18. W. Radke. *J. Chromatogr. A.* 2019, **1593**: 17-23.
19. J. Gerber; W. Radke. *Polymers.* 2005, **46**: 9224-9229.
20. P. Dugo; F. Cacciola; T. Kumm; G. Dugo; L. Mondello. *J. Chromatogr. A.* 2008, **1184**: 353-368.

21. K. Im; H.-W. Park; S. Lee; T. Chang. *J. Chromatogr. A.* 2009, **1216**: 4606-4610.
22. A. de Villiers; P. Venter; H. Pasch. *J. Chromatogr. A.* 2016, **1430**: 16-78.
23. T. Chang In *Recent Progress in Separation of Macromolecules and Particulates*; ACS Publications: 2018, p 1-17.
24. L. R. Hutchings. *Macromolecules* 2012, **45**: 5621-5639.
25. L. R. Hutchings; S. Agostini; M. E. Oti; J. Keth. *Eur. Polym. J.* 2015, **73**: 105-115.
26. J. C. Giddings; M. N. Myers; J. Janča. *J. Chromatogr. A.* 1979, **186**: 37-44.
27. M. E. Schimpf. *J. Chromatogr. A.* 1990, **517**: 405-421.
28. J. R. Runyon; S. K. R. Williams. *J. Chromatogr. A* 2011, **1218**: 7016-7022.
29. G. Greyling; A. Lederer; H. Pasch. *Macromolecules Chem. Phys.* 2018, **219**: 1800417.
30. U. L. Muza; H. Pasch. *Anal. Chem.* 2019, **91**, 6926-6933

2.

Overview of branched polymers

2.1 Properties and applications

In generic terms, a branched polymer constitutes of molecules with more than one backbone chain, therefore, it is a nonlinear polymer.[1,2] The existence of branching in polymers is a unique structural variable that can be used advantageously to modify the processing characteristics and properties of polymers. Branching affects the chemical and physical properties of polymers that include crystallinity, viscoelastic properties, and solubility.[3-5] To the same degree, this has opened doors for further research in a wide range of industrial applications that include flocculants for waste-water/crude oil recovery, drug delivery, synthetic rubber materials, flexible films for packaging, toys and a bucket list of household items as presented in Figure 2.1.[6-11]

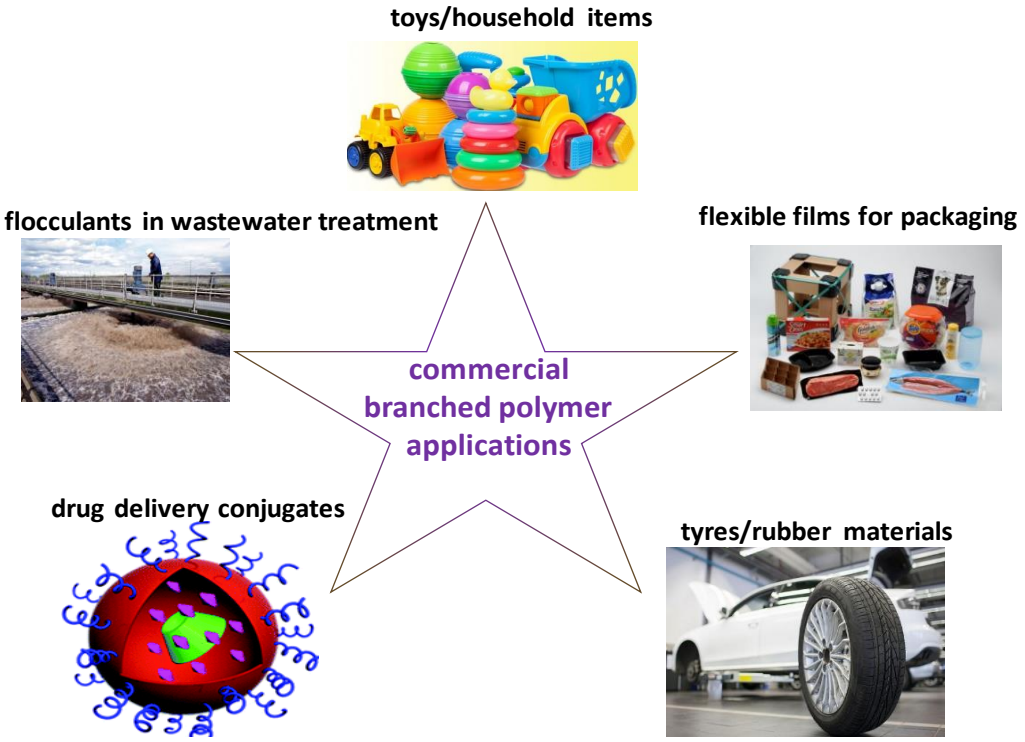

Figure 2.1 Selected commercial applications of branched polymers

However, it is difficult to predict the relationship between branching and properties based on the behavior of most branched polymers because the branching reaction most frequently occurs in a random fashion. Therefore, the numbers and types of branches per macromolecule

are difficult to define except on an average basis. Fundamental understanding of the effects of chain branching on polymer properties requires the availability of a variety of model branched polymers with well-defined structures and low degrees of compositional heterogeneity.[12-15] Reversible deactivation radical polymerization (RDRP) techniques such as reversible addition-fragmentation chain transfer (RAFT) and anionic polymerization are particularly suited for the preparation of these "model" polymers since they allow to adjust important parameters that include molar mass and molar mass distribution, copolymer composition, architecture as well as chain end functionality.[16-22] The aim of this study is to develop a combination of advanced liquid chromatographic methods based on model regular star-branched, miktoarm star-branched and hyperbranched block copolymers prepared via RAFT (for star polystyrenes) together with anionic polymerization combined with classical Williamson coupling reactions (for miktoarm star-branched and hyperbranched polymers).[14,23] The application of Thermal field-flow fractionation (ThFFF) as a non-column based fractionation technique is also assessed with an overall objective of achieving a comprehensive separation and characterization of complex polymer mixtures driven by a particular interest on the composition, molar mass and degree of branching. The detailed separation principles of the column- and channel-based techniques employed in this work are discussed in the following sections.

2.2 Star-branched and hyperbranched polymers

2.2.1 Star-branched polymers

These consist of several 'arms' radiating from a central core. This can be achieved by growing the polymer arms from a central core–the 'core first or divergent' approach.[24] According to this procedure multifunctional compounds capable of simultaneously initiating the polymerization of several arms are used. There are several requirements that a multifunctional initiator has to fulfil in order to produce star polymers with invariable arms of low molecular weight distribution, and uniform molecular weights. To achieve this, all present initiation sites must be equally reactive, and the initiation rate must be higher than the propagation rate. The characterization of the star polymers produced by this method is difficult, since the molecular weight of the arms cannot be measured directly. The number of the arms can be defined indirectly by several methods, such as endgroup analysis, determination of the branching parameters (which are the ratios of the mean square radius of gyration, intrinsic viscosity, or hydrodynamic radius of the star to the corresponding linear one with the same molecular weight).[25-28]

Alternatively, star polymers can be prepared by synthesizing the individual arms first then attaching them to a central molecule–the 'arms first or convergent' approach.[29,30]. This is probably the most efficient way to synthesize well-defined star polymers because of the absolute control that can be achieved in all synthetic steps, since the living arms can be isolated before linking and characterized independently along with the final star.[31] In addition, the functionality of the linking agent determines the number of branches of the star polymer, provided that the linking reaction is quantitative. Consequently, the functionality of the star can be measured directly and with accuracy. Disadvantages of the method include the long time required for the linking reaction in most cases and the need to perform fractionation in order to obtain the pure star polymer, since a small excess of the living arms is needed to ensure that the linking reaction goes to completion.[32] Regular star-branched polymers have arms that exhibit low degrees of compositional heterogeneity with respect to composition, molecular weight, and molecular weight distribution. Mixed arm star-branched polymers (often described as mikto-arm star polymers, see Figure 2.2), also have a single branch point, but the arms differ in either molecular weight or composition.[33] When the arms differ in composition, mixed star-branched polymers can be considered as a special type of graft copolymer. [34]

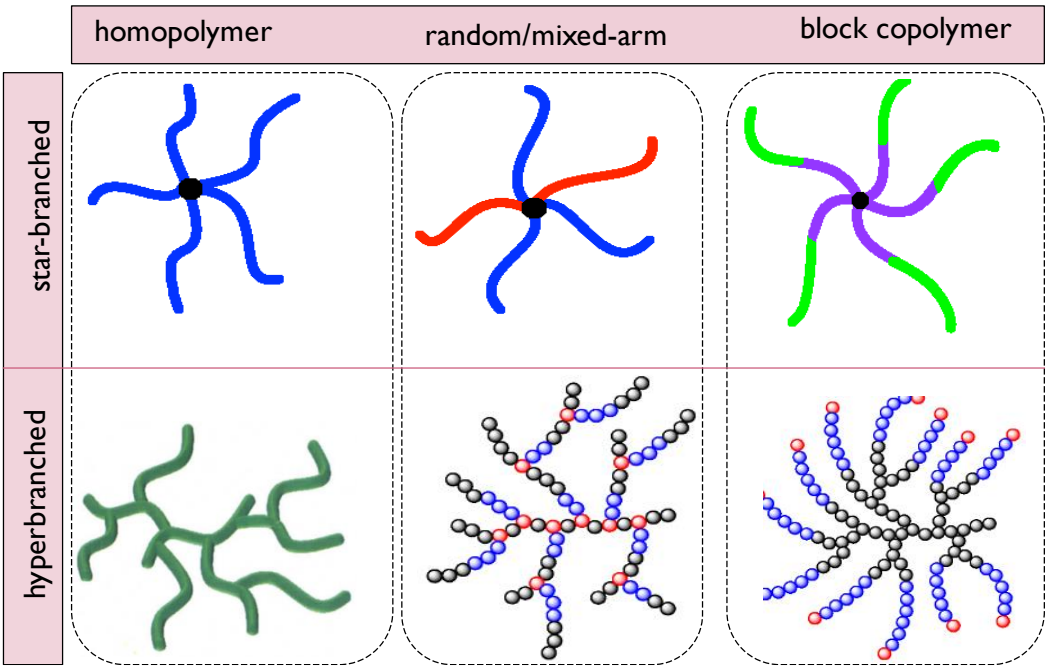

Figure 2.2 Schematic illustration of the different star-branched and hyperbranched structures

2.2.2 Hyperbranched polymers

Hyperbranched polymers are a special type of highly branched dendrimer-like macromolecules, whose 3-dimensional globular structures are not regular nor highly symmetrical, yet they display comparable physical and chemical properties such as higher solubility and lower viscosity.[35,36] The combined bulk and solution properties of hyperbranched polymers have lately found much of their designs in macromolecular structures that include tubules, micelles and fibers (through the self-assembly of hyperbranched polymers).[37-39] Of significant importance is their potential application in areas such as tissue engineering, drug delivery systems, adhesives and fabrication of organic-inorganic hybrids.[40-43] Unlike dendrimers which require many synthetic steps, hyperbranched polymers are prepared by direct, one-step polycondensation of AB_x monomers/macromonomers with two different types of functional groups (A and B) that can react with each other to form a covalent bond. For the macromonomer approach, Reversible deactivation radical polymerization (RDRP) methods such as reversible addition-fragmentation chain-transfer polymerization (RAFT) and living polymerization techniques that include anionic polymerization are often used to synthesize the polymeric arms – "macromonomers".[44-51] The resultant living arms are usually end-functionalized with reactive groups such as azides, alcohols or halides to prepare the building blocks, which are then efficiently coupled via azide coupling, click coupling or Williamson coupling reactions.[44-46, 52-54]

Compared with other polymer coupling methods, the Williamson coupling reactions are widely employed in both lab-scale and industrial synthesis. This is made viable due to the simplicity of the reaction steps of the method which makes it a versatile route to prepare model branched and highly branched polymers.[55] However, like any other synthetic procedure in organic chemistry the Williamson coupling reaction has its own demerits and a careful optimization of the experimental conditions is required. Although Williamson coupling reactions are favoured particularly by aprotic solvents with high dielectric constants such as dimethylformamide (DMF) or dimethylacetamide (DMAc), macromonomers like polybutadiene are insoluble in these solvents. After a systematic study on optimizing the ideal solvent system, improved conditions consisting of a mixed solvent system of THF (good solvent for butadiene but with a modest dielectric constant) and DMF or DMAc (poor solvent for polybutadiene but with a high dielectric constant) in a 50/50 % v/v ratio were established by Hutchings et al. as the optimum conditions.[56] Based on these insights, the above solvent system conditions were also employed in this work. Owing to that, the building blocks chosen

for the Williamson coupling reactions in this work were synthesized by high-vacuum living anionic polymerization techniques in order to produce well-defined block structures with narrow molar mass distributions.

2.3 Selected approaches for characterization of branched polymers

The complexity of polymers poses unique challenges with respect to their characterization. Numerous methods of polymer characterization have been developed due to the potential for multiple molecular distributions in a sample such as variations in chemical composition (composition distribution), differences in architectural traits (architectural distribution) and molar mass. The separation techniques commonly used can be broken down into categories of column-based (i.e. size exclusion – SEC and high performance liquid chromatography – HPLC) as well as channel-based that include asymmetric flow field-flow fractionation (AF4) and Thermal field-flow fractionation (ThFFF) combined with multiple detection techniques for characterization.[3,57-63 64]

2.3.1 Size exclusion chromatography with triple detection

Although SEC is broadly applied to characterize synthetic polymers, its limitations become exposed because branching has a notable effect on the size of macromolecules in solution.[3] The main characterization challenge for conventional size-sensitive methods such as size exclusion chromatography (SEC) arises from the fact that high molar mass branched macromolecules may co-elute with low molar mass linear macromolecules due to the phenomenon shown in Figure 2.3.[65]

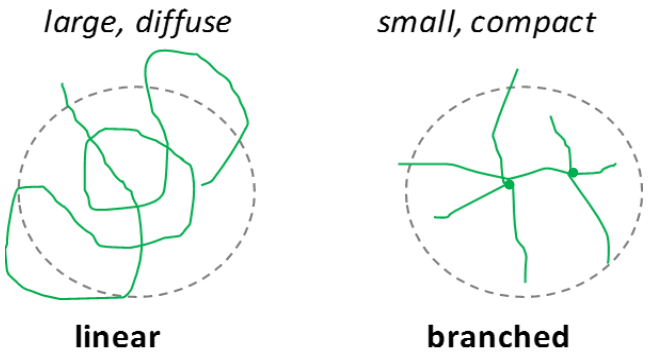

Figure 2.3 Effect of branching on hydrodynamic size in solution

This challenge can be primarily tackled by using SEC coupled with a concentration detector (typically a refractive index detector–RI) combined with a viscometer and applied to investigate the branched structures. When the RI and viscometer are then coupled to a light

scattering detector, MALS, the absolute molecular weights and radii of gyration of the branched polymers can be determined.[59,66,67] Figure 2.4 shows a scheme of the SEC-triple detection system setup.

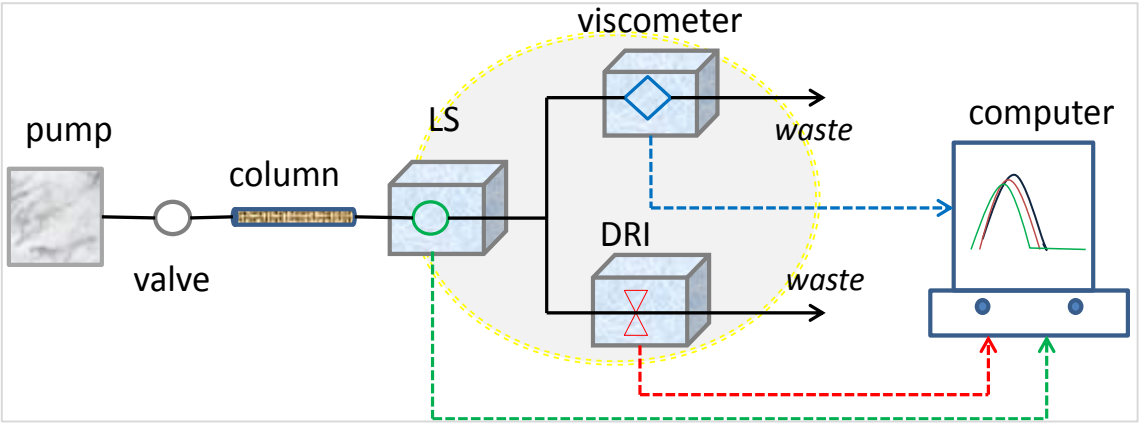

Figure 2.4 Scheme of the SEC-triple detection system setup

2.3.2 Solvent gradient interaction chromatography (SGIC) and temperature gradient interaction chromatography (TGIC)

In solvent gradient interaction chromatography (SGIC) the extent of analyte-stationary phase interactions is controlled by changing the chemical composition of the carrier liquid (mobile phase).[65,68] The analyte is dissolved and injected in a carrier solvent system that promotes adsorption onto the stationary phase. As the strength of the good solvent component in the mobile phase is increased, the interactions of the analyte with the stationary phase also change. Although separations based on other molecular distributions such as molar mass or architecture are possible theoretically, the SGIC technique is commonly used for the characterization of composition distributions in copolymers.[69-73] The challenge associated with a successful SGIC method development lies in the monotonous optimization of an effective mobile phase system, choice of proper stationary phase, separation at isothermal conditions and the option of detectors that are suitable for the constantly changing mobile phase composition.[74]

An alternative method to adjust retention is to regulate the temperature in temperature gradient interaction chromatography (TGIC).[58,75] This is a mode of interaction chromatography where the column temperature is precisely controlled via a programmable temperature compartment in order to adjust the strength of interactions between the analyte and the stationary phase. The main drawback with TGIC is that there is no one-size-fits-all-approach and like SGIC, a successful method development relies on trial and error steps. In

addition, TGIC is characterized with potentially lengthy waiting period(s) between analyses since the column temperature(s) must return to the suitable initial starting point. In most cases, the temperature starts at a low value and is then increased at a controlled rate to decrease polymer-stationary phase interactions. The polymer chains that weakly interact with the stationary phase are eluted first while speeding up elution of strongly interacting components as the temperature increases. One of the variations of TGIC is the normal phase (NP) TGIC which is characterized by a polar stationary phase such as bare silica, amino or diol bonded silica and a less polar mobile phase. Unlike (RP) TGIC, (NP) TGIC has a potential to be useful in the characterisation of polymers in terms of functionality. Since the chain-end functionalization of high molar mass polymers has attracted attention in the rubber and tyre industry. This is largely because the functionalized chain ends can not only significantly improve the dispersion of filler particles such as silica and carbon black, but can also lead to improved rolling resistance which aids in fuel efficiency.[76] Lee et al. used NP-TGIC for the analysis of hydroxyl chain-end functionalised polystyrene polymers.[77] Hutchings et al. also showed that NP-TGIC is selective to polar end-groups on the characterisation of two classes of chain end-functionalised polymer (polystyrene and polybutadiene) by (NP)-TGIC for high molar masses over 200 000 g/mol.[78]

On the contrary, the widely employed reversed phase (RP) TGIC is a variation of TGIC which achieves separation by means of regulating the analyte interactions between a non-polar, hydrophobic stationary phase, such as C_8 or C_{18} bonded silica, and a mobile phase that is more polar than the stationary phase. The (RP) TGIC technique enables the separation of polymers on the basis that it is sensitive to total molecular weight and has a much higher resolution compared to SEC and SGIC in that regard.[79] Through careful optimization of the separation conditions (RP) TGIC has in recent times demonstrated to be selective with regard to structural dispersity, although the separation ultimately occurs on the basis of molar mass, therefore, making branching in polymers to be effectively characterized.[56,80-83]

Liquid chromatography at critical conditions

Liquid chromatography at critical conditions (LCCC) is a mode of separation which is distinctively useful in characterizing block copolymers and functionalized branched polymers.[84-87] Separations in LCCC of block copolymers are optimized such that one block of the copolymer is considered to be chromatographically invisible whereas the other block elutes either under size exclusion chromatography (SEC) or liquid adsorption chromatography (LAC) conditions. For example, The application of LCCC can be considered for a series of

polystyrene (PS)–poly(butadiene) (PBd) block copolymers.[85,88] The chemistry of the mobile phase, stationary phase, and the column temperature would be selected to eliminate the effects of the PS block on retention, thereby, yielding a separation based solely on the size of the PBd block. This offers insight into the size distribution and composition of the PBd block without the influence of the PS block. Similarly, for a functionalized branched polymer with known endgroups of a unique chemistry, the separation could be adjusted to be selective towards the targeted endgroups, eventually adjusting a separation based solely on the degree of branching.[89,90] However, akin to the other chromatography techniques discussed in the previous sections, this approach is often trial-based and iterative. Therefore, it is a challenge to establish the optimized conditions for a given polymer chemistry, where adjustments to the stationary phase, mobile phase, and column temperature are required. .

2.3.3 2D liquid chromatography

Stand-alone one-dimensional liquid chromatographic techniques (1D-LC) are often not sufficient to have the peak capacity required to efficiently resolve components in a complex mixture which prompts the use of more advanced separation techniques.[91] Peak capacity is a standard of measurement that defines the highest number of equal-height peaks, that can be fit side-by-side at equal resolution within a given separation space.[92] The peak capacity of a stationary phase is restricted by the peak width which depends on the efficiency of the column and the width of the distribution of a particular property.[93] The relationship between peak capacity and column efficiency in 1D-LC is described by Equation 1:

$$n = 1 + \frac{\sqrt{N}}{4} \times \ln \frac{V_P}{V_o} \qquad \textbf{[1]}$$

where, n is peak capacity, N is the plate number, V_p is the pore volume and V_0 is the interstitial volume.[94] Ideally, the peak capacity of a LC × LC method will be the product of the peak capacities of the two 1D separations that contribute to the 2D separation.[95,96] In order to obtain a more comprehensive understanding of the complexity of polymers regarding the multiple distributions, it can be useful to analyse them using two-dimensional liquid chromatography (2D-LC).[97,98] The relationship between column efficiency and peak capacity of a 2D-LC separation is given by Equation 2:

$$n_{LC\times LC} = \left(1 + \frac{\sqrt{N_1}}{4} \times \ln \frac{V_{p,1}}{V_{0,1}}\right) \times \left(1 + \frac{\sqrt{N_2}}{4} \times \ln \frac{V_{p,2}}{V_{0,2}}\right) \times \sin(\theta) \qquad \textbf{[2]}$$

Where, $n_{LC\ x\ LC}$ is the peak capacity of a two-dimensional system and θ is the separation angle between the two 1D-LC methods. When the two separation methods are completely independent of one another, a separation angle of 90° is obtained. The two primary coupling systems that are commonly used for 2D-LC are (a) the coupling of LCCC in the first dimension with SEC in the second dimension, and (b) coupling of gradient HPLC in the first dimension with SEC in the second dimension.[99-101] Practically, there are several other ways to set up a 2D-LC system, however, some systems are easier and more practical to use than others. A diagram of the hardware that was used for online comprehensive 2D-LC separations in this work is shown in Figure 2.5. The first dimension (SGIC or TGIC) was connected to the second dimension (SEC) by an electronically controlled transfer valve which transferred fractions from the first dimension into the second dimension. The flow rates of both dimensions were adjusted such that the time it took to fill one storage loop was equal to the time taken to analyse the other loop contents in the second dimension. The column type, dimension, particle size, eluent and flow rates in the different dimensions were chosen in such a way that they were compatible in order to optimise peak capacity.

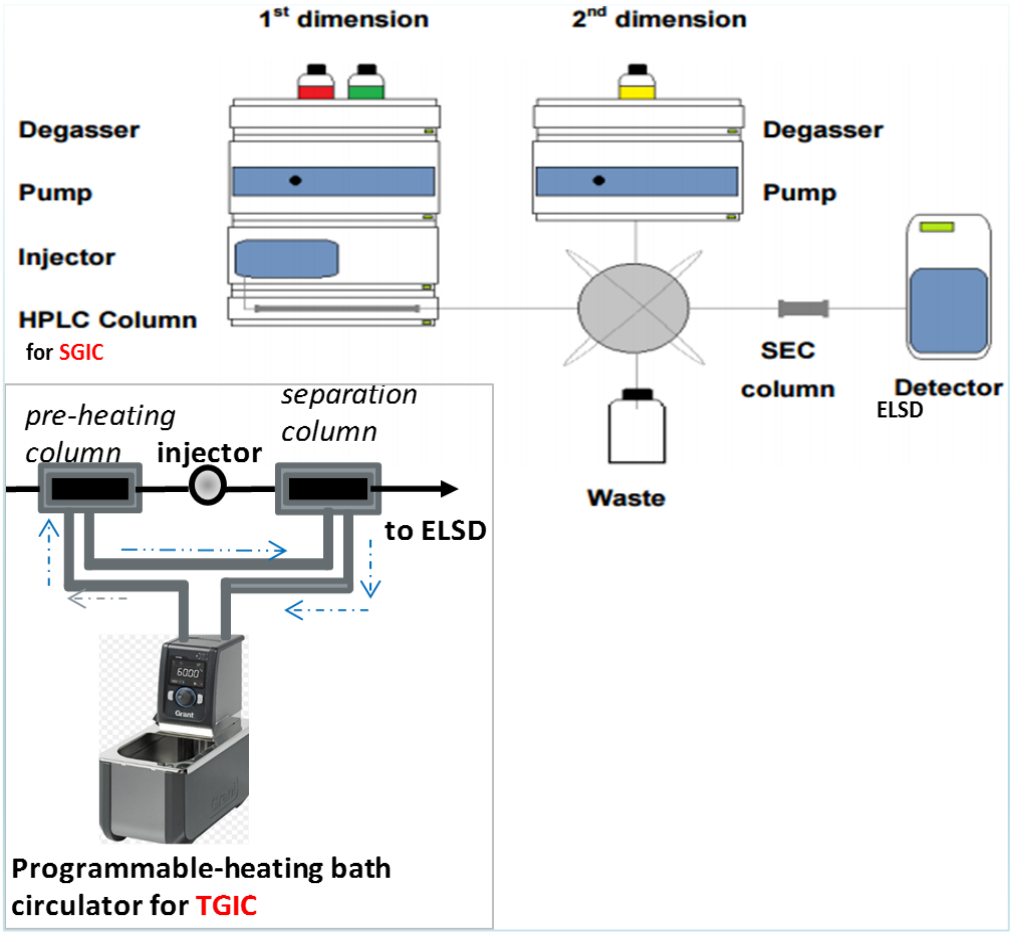

Figure 2.5 Scheme showing the two 2D-LC (TGIC × SEC and SGIC × SEC) set-up**.**

Having a common solvent in both dimensions is known to minimize breakthrough effects in addition to the interferences of the solvent that is coming from the first dimension with the separation in the second dimension.[101] From the work covered in this thesis the primary objective of employing LC × LC was to gain comprehensive information on branched samples regarding their molar mass, chemical composition and degree of branching from single 2D chromatograms.

2.3.4 Thermal field-flow fractionation (ThFFF)

The separation in ThFFF takes place in a thin and open "ribbon-like" channel where a carrier fluid transports components down the separation axis of the channel.[102] The frictional drag at the channel walls facilitated by a low-enough flow rate creates a parabolic flow profile spanning the channel thickness, with the fastest flows in the centre of the channel and the slowest flows near the walls (see Figure 2.6).

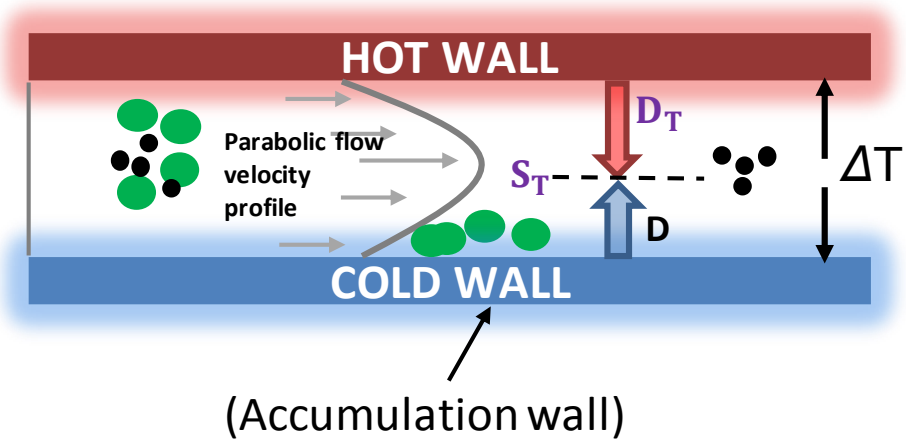

Figure 2.6 Scheme of the ThFFF channel separation mechanism.

An external thermal field is applied transversal to the separation axis of the channel to drive components from the hot wall towards the cold wall (accumulation wall) via thermophoresis, and is quantified by the thermal diffusion coefficient (D_T).[103] This field-induced transport is neutralized by the diffusion of components away from the high concentration region near the accumulation wall known as the ordinary diffusion (D). An equilibrium state is reached when the two transport processes are balanced, expressed as the Soret coefficient ($S_T = D_T/D$) and there is no net flux of sample in either direction. This equilibrium position is unique to each sample component depending on various factors such as the magnitude of their interaction with the applied field and their diffusion coefficient.[102,104] As such, components of smaller sizes diffuse further into the channel than larger components based on the inverse relationship between diffusion coefficient (D) and hydrodynamic diameter (D_h) given by the Stokes-Einstein equation for spherical analytes shown in Equation 3.

$$D = \frac{kT}{3\pi\eta D_h} \qquad [3]$$

where k is Boltzmann's constant, η is the intrinsic viscosity of the carrier liquid, and T is the temperature in Kelvins.[105] ThFFF is particularly useful in the characterization of complex polymers in a fashion that resembles a 2D-LC separation because the movement of a polymer in a temperature field is dependent on the ratio of D_T (a function of chemical composition of the polymer and solvent) to that of D (depends on the size of the analyte and magnitude of the applied thermal field).[106,107]. In addition, ThFFF can also be modelled to determine molar mass averages, molecular weight distributions and degrees of branching of polymers because the molar mass versus elution volume as well as the conformation plot are not affected by co-

elution issues such as those encountered in SEC.[108] Mathematically, the retention time in ThFFF is described by Equation 4 as:

$$t_r = \frac{D_T \Delta T t^o}{6D} = \frac{D_T \Delta \pi \eta t^o}{2kT} D_h \qquad [4]$$

where t^0 is the void time or time it takes to elute a complete channel volume and t_r is the retention time of the analyte.[109,110]

2.4 On-line detectors for separation methods

Detection methods are required to obtain information about polymer components as they elute from the separation device. Additionally to concentration monitoring, on-line detectors can provide information about specific polymer properties. Most frequently, these detectors include UV-visible light absorbance (UV-Vis), differential refractive index (dRI), evaporative light scattering (ELS), viscometry and light scattering detectors.

2.4.1 Evaporative light scattering detector (ELSD)

An evaporative light scattering detector (ELSD) is a universal detection method that delivers a signal for all compounds that do not evaporate (less volatile than the eluent) or decompose.[111] Principally, an ELSD measures the amount of light scattered by particles of the analyte that have been dried through evaporation. Although design characteristics differ from one manufacturer to another, a general detection mechanism is common to all evaporative light scattering detectors and it comprises three stages: nebulization, mobile phase evaporation and detection (see Figure 2.7).

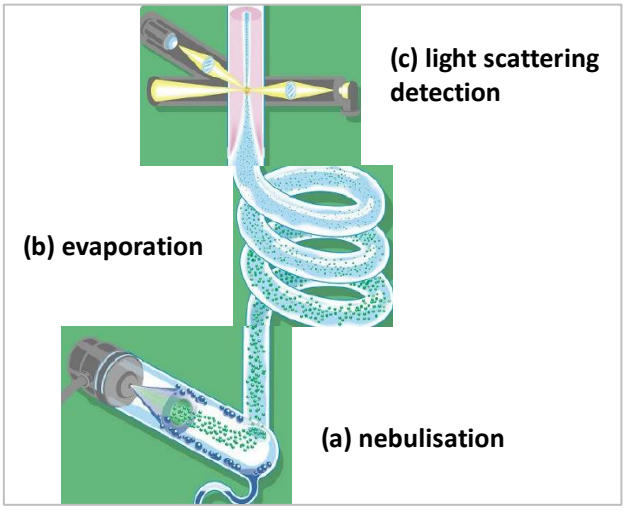

Figure 2.7 Scheme showing the three main stages of evaporative light scattering detection mechanism

The nebulizer combines a gas flow of air (N_2 gas) with the column effluent to produce an aerosol of micro- and nanodroplets which are channelled into the heated evaporating tube (where the solvent is removed). The analyte particles are transferred into the detection cell where they are irradiated by a light emitting diode (LED) and a photomultiplier positioned at a fixed angle from the incident light.[112] Although ELSD offers advantages over other detection methods in that it is compatible with a much wider range of solvents and modifiers and produces stable baselines during gradient elution chromatography, it cannot be reliably used as a quantitative detection method without calibration.[113]

2.4.2 Differential refractive index detector (dRI)

The refractive index detector, also called the Differential Refractive Index Detector, detects solutes by monitoring the refractive index of the column eluent relative to a reference cell containing air, mobile phase, or a transparent material with a specified refractive index.[114] The change in refractive index with respect to an analyte's concentration is described by Equation 5 as:

$$\mathrm{dRI} = \left(\frac{\mathrm{dn}}{\mathrm{dc}}\right)\mathrm{C} \qquad \textbf{[5]}$$

where *(dn/dc)* is the analyte's refractive index increment and *C* is its concentration. A refractive index detector is considered a universal detector since it monitors a bulk property of the solution. Unfortunately, RI detectors have a very low sensitivity (mg/L range) and are subject to factors such as density of the medium, flow rate variations, wavelength of light, temperature and pressure.[115]

2.4.3 Static Light Scattering

The application of light-scattering detectors to measure molecular weight in gel permeation chromatography (GPC) experiments is now commonplace. The attraction for most users is that the molecular weight is measured from the light-scattering (LS) detector signal directly, avoiding the need to use polymer or protein standards to calibrate the GPC elution volume. Additionally, the molecular weight measured by the LS detector is independent of polymer type and structure. In a typical light scattering experiment, a well collimated, single frequency, polarized light beam (i.e., from a laser) is used to illuminate a solution containing a suspension of the macromolecules or nanoparticles of interest. The electric field of the polarized light beam is preferably produced perpendicular to the plane in which the intensity and angular dependence of the subsequently scattered light is to be measured (by convention,

the polarization direction is denoted 'vertical' and the measurement plane 'horizontal') . The overall intensity carries information about the molar mass, while the angular dependence within the horizontal plane carries information about the size of the macromolecule. In accordance to theories developed from the expression in Equation 6, commercially there are three types of static light scattering detectors. Each has its merits as well as shortfalls and the three can be described as follows:

1. Multi-angle light scattering (MALS) - Measures the scattered light at two or more angles and extrapolate the data back to the zero angle. Multi angle light scattering (MALS) detectors are often chosen, in some instances because they provide the most accurate data for the measurement of the radius of gyration (Rg), and in others because they have become an accepted industry standard.

2. Right-angle light scattering (RALS) - Measures the scattered light at 90º and when coupled to online viscometry detection uses the viscosity data to correct to the zero angle. For flexible linear polymers, the application of RALS provides a low-cost, reliable measurement of the radius of gyration and also gives improved capability for small molecular sizes when compared to MALS.

3. Low-angle light scattering (LALS) - Measures at a low angle — close to zero — where the angular effects are negligible. No correction needed. However at low angles close to 0º it becomes a challenge to measure the scattered light because of the presence of the incident laser beam.

In this work, the MALS was employed largely due to availability within our facilities and as a result of the confidence afforded by multiple measurements as well as the technique's unique ability to accurately measure radius of gyration (Rg) - a useful parameter for describing polymer size that also contains information on the polymer structure.

Multiangle light scattering detector (MALS)

Multiangle light scattering detection (MALS) is typically used to measure larger sample species, such as protein aggregates, high molar mass macromolecules and particles. MALS is carried out by shining a laser light on analytes and detecting the light scattered by the analytes in all directions.[59] The intensity of light scattering increases with analyte size and concentration (measured by an online concentration detector such as UV-Vis or dRI). The

fundamental equation for the scattering of light from dilute polymer solutions is the Zimm expression (see Equation 6):[116]

$$\frac{KC}{R_\vartheta} = \left(\frac{1}{M_w} + 2A_2C\right) \times \frac{1}{P_\theta} \quad \textbf{[6]}$$

where K is an optical constant describing the behaviour of the light in the system, C is the analyte concentration, P_θ is the particle scattering factor, which is a measure of the angular dissymmetry of the scattered light and is related to the size and the angle at which the scattering is determined, M_W is the molar mass of the polymer and A_2 is the second virial coefficient, which describes the change in scatter intensity with respect to polymer-solvent interactions. R_θ is the excess Rayleigh scattering ratio of the solution above that of the pure solvent, measured at angle θ with respect to the incident laser beam and can be expressed with Equation 7 as follows:

$$R_\theta = k\frac{MALS_{l_\theta}}{l_o} \quad \textbf{[7]}$$

Where l_0 is the irradiance of the incident laser and I_θ is the excess intensity of the scattered light above that of the pure solvent at angle θ. Based on this, it is possible to determine the radius of gyration (R_g) and the absolute molecular mass of the polymer. When used in an on-line capacity with a separation technique such as HPLC or ThFFF, MALS presents an orthogonal method for determining the size, molar mass distributions and branching characteristics present in a polymer sample.[117,118]

2.4.4 Differential Viscometer

The differential viscometry evaluates changes in the viscosity of a solution by use of a four-capillary bridge design via a balanced bridge configuration, similar to the Wheatstone bridge common in electrical circuits as shown in Figure 2.8.[119] Four capillary tubes (R1–R4) are arranged with differential pressure (DP) transducers measuring the pressure difference across the midpoint of the bridge and the pressure difference from the inlet to the outlet (IP). A delay volume is deliberately inserted in the circuit before capillary R4 to provide a reference flow of solvent through capillary R4 during sample elution. However, the delay volume should (a) have an internal volume larger than the total permeation volume of the SEC column and (b) have a flow resistance which is negligible relative to the capillary resistances. Accurate molar mass determination can be obtained through universal calibration, which relates intrinsic viscosity to polymer molar mass.

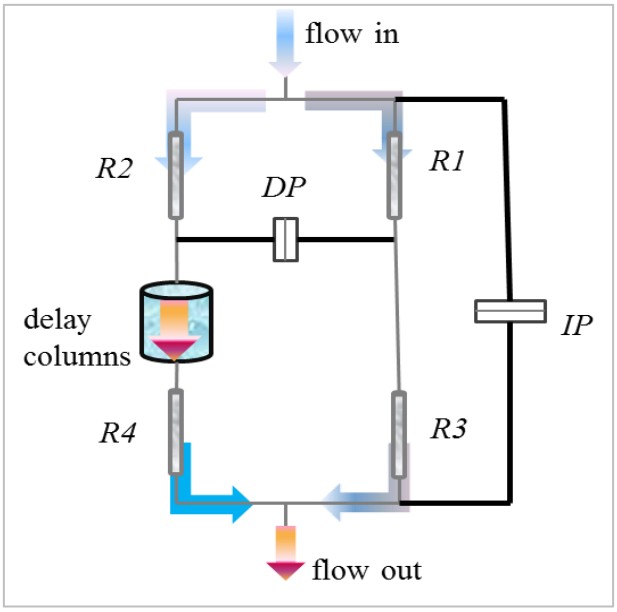

Figure 2.8 Scheme of the differential viscometer 4-capillary bridge design

The Mark–Houwink plot is a very useful approach for branching analysis, which is the logarithm of the intrinsic viscosity (obtained e.g. using online viscometry) plotted against the logarithm of the molar mass (obtained using universal calibration or light scattering detection). The general relationship of the Mark-Houwink plot can be expressed as follows (see Equation. 8):

$$[\eta] = KM^{\alpha} \quad \textbf{[8]}$$

Where the parameters α (describes the coil density of the polymer) and K (related to the polymer backbone structure) are constants which depend on the polymer-solvent system. The Mark–Houwink parameters are determined from the universal calibration. They are estimated from the intercept and slope of a straight line fitting the bi-logarithmic plot of intrinsic viscosity [η] versus molar mass [M] as shown in Equation 9.[120]

$$\log[\eta] = \log[K] + \alpha\log[M] \quad \textbf{[9]}$$

The slope of the Mark–Houwink plot (Mark–Houwink exponent, α) is dependent on the shape (branching) of the molecules in solution. If the intrinsic viscosity has no molar mass dependence, which is the case for ideal solid spheres, a slope of 0 is expected. The Mark–Houwink exponent of rigid rods is 2. Typical random coil polymers exhibit Mark-Houwink exponents in the range of 0.5 to 0.8, depending on the solvent quality.

2.4.5 Dynamic Light Scattering

Dynamic light scattering (DLS) is a non-invasive, well-established technique for measuring the hydrodynamic size and hydrodynamic size distribution of molecules and particles typically in the submicron region (lower than 1μm).[121,122] In principle, DLS works similar to MALS with respect to the concept of examining the intensity of laser light scattered by a particle but differs in that it evaluates small changes in the intensity of the scattered light in relation to the movement of the analyte.[123,124] The Brownian motion of particles or polymer molecules in suspension causes the laser light to be scattered at different intensities. Analysis of these intensity fluctuations yields the velocity of the Brownian motion and hence the particle size using the Stokes-Einstein relationship (see Equation 3). Larger particles have smaller diffusion coefficients and move slower, while smaller particles have larger diffusion coefficients and move faster.[125]

2.5 References

1. S. G. Gaynor; S. Edelman; K. Matyjaszewski. *Macromolecules.* 1996, **29**: 1079-1081.
2. D. Boschmann; R. Edam; P. J. Schoenmakers; P. Vana. *Macromol. Symp.* 2009, **275-276**: 184-196.
3. W. H. Stockmayer; M. Fixman. *Ann.NY. Acad. Sci* 1953, **57**: 334-352.
4. G. C. Berry; T. G. Fox In *Fortschritte der Hochpolymeren-Forschung*; Springer: 1968, p 261-357.
5. W. Radke; G. Litvinenko; A. H. Mueller. *Macromolecules.* 1998, **31**: 239-248.
6. T. Tripathy; N. Karmakar; R. Singh. *J.Appl. Polym. Sci.* 2001, **82**: 375-382.
7. D. A. Wever; L. M. Polgar; M. C. Stuart; F. Picchioni; A. A. Broekhuis. *Ind. Eng. Chem. Res.* 2013, **52**: 16993-17005.
8. W. B. Liechty; D. R. Kryscio; B. V. Slaughter; N. A. Peppas. *Ann. Rev.* 2010, **1**: 149-173.
9. T. Otte; H. Pasch; T. Macko; R. Brüll; F. Stadler; J. Kaschta; F. Becker; M. Buback. *J. Chromatogr. A.* 2011, **1218**: 4257-4267.
10. J. Lange; E. Stenroos; M. Johansson; E. Malmström. *Polymer.* 2001, **42**: 7403-7410.
11. P. M. Hergenrother. *Angew. Chem. Int. Ed.* 1990, **29**: 1262-1268.
12. S. Bywater In *Physical Chemistry*; Springer, Berlin: 1979, p 89-116.
13. W. Burchard In *Branched polymers II*; Springer, Berlin: 1999, p 113-194.
14. L. R. Hutchings. *Soft Matter.* 2008, **4**: 2150-2159.
15. T. Masuda; Y. Ohta; S. Onogi. *Macromolecules.* 1971, **4**: 763-768.
16. M. L. Koh; D. Konkolewicz; S. Perrier. *Macromolecules.* 2011, **44**: 2715-2724.
17. H. Iatrou; N. Hadjichristidis. *Macromolecules.* 1992, **25**: 4649-4651.
18. T. Higashihara; M. Hayashi; A. Hirao. *Prog. Polym. Sci.* 2011, **36**: 323-375.
19. N. Hadjichristidis; A. Hirao *Anionic Polymerization*; Springer, Japan, 2015, P1082
20. R. P. Quirk; B. Lee. *Macromol. Symp.* 1992, **53**: 201-210.
21. Y. H. Kim. *J. Polym. Sci. A: Polym. Chem.* 1998, **36**: 1685-1698.
22. A. H. Müller; D. Yan; M. Wulkow. *Macromolecules.* 1997, **30**: 7015-7023.
23. L. R. Hutchings; J. M. Dodds; S. J. Roberts-Bleming. *Macromol. Symp.* 2006, **240**: 56-67.
24. A. Hirao; M. Hayashi; S. Loykulnant; K. Sugiyama; S. W. Ryu; N. Haraguchi; A. Matsuo; T. Higashihara. *Prog. Polym. Sci.* 2005, **30**: 111-182.

25. J. Xia; X. Zhang; K. Matyjaszewski. *Macromolecules.* 1999, **32**: 4482-4484.
26. K. Matyjaszewski. *Polym. Int.* 2003, **52**: 1559-1565.
27. H. Gao; S. Ohno; K. Matyjaszewski. *J. Am. Chem. Soc.* 2006, **128**: 15111-15113.
28. S. Abraham; J. H. Choi; C. S. Ha; I. Kim. *J. Polym. Sci. A: Polym. Chem.* 2007, **45**: 5559-5572.
29. H. Gao; K. Matyjaszewski. *J. Am. Chem. Soc* 2007, **129**: 11828-11834.
30. G. Moad; R. T. Mayadunne; E. Rizzardo; M. Skidmore; S. H. Thang. *Macromol. Symp.* 2003, **192**: 1-12.
31. J. Ferreira; J. Syrett; M. Whittaker; D. Haddleton; T. P. Davis; C. Boyer. *Polym. Chem.* 2011, **2**: 1671-1677.
32. M. Pitsikalis; S. Sioula; S. Pispas; N. Hadjichristidis; D. C. Cook; J. Li; J. W. Mays. *J. Polym. Sci. A: Polym. Chem.* 1999, **37**: 4337-4350.
33. T. Tsoukatos; N. Hadjichristidis. *J. Polym. Sci. A: Polym. Chem.*2002, **40**: 2575-2582
34. T. Witten; P. Pincus. *Macromolecules.* 1986, **19**: 2509-2513.
35. Y. Segawa; T. Higashihara; M. Ueda. *Polym. Chem.* 2013, **4**: 1746-1759.
36. F. Sun; X. Luo; L. Kang; X. Peng; C. Lu. *Polym. Chem.* 2015, **6**: 1214-1225.
37. B. Guo; Y. Sun; A. Finne-Wistrand; K. Mustafa; A.-C. Albertsson. *Acta. Biomater.* 2012, **8**: 144-153.
38. S.-E. Stiriba; H. Kautz; H. Frey. *J. Am. Chem. Soc.* 2002, **124**: 9698-9699.
39. S. Burkinshaw; P. Froehling; M. Mignanelli. *Dyes. Pigments.* 2002, **53**: 229-235.
40. J. L. Hedrick; C. J. Hawker; R. D. Miller; R. Twieg; S. Srinivasan; M. Trollsås. *Macromolecules.* 1997, **30**: 7607-7610.
41. S. Chen; X.-Z. Zhang; S.-X. Cheng; R.-X. Zhuo; Z.-W. Gu. *Biomacromolecules.* 2008, **9**: 2578-2585.
42. Y. Zhou; W. Huang; J. Liu; X. Zhu; D. Yan. *Adv. Mat.* 2010, **22**: 4567-4590.
43. G. G. Buonocore; L. Schiavo; I. Attianese; A. Borriello. *Compos. Part B-Eng.* 2013, **53**: 187-192.
44. R. P. Quirk; J. Yin; S.-H. Guo; X.-W. Hu; G. J. Summers; J. Kim; L.-F. Zhu; J.-J. Ma; T. Takizawa; T. Lynch. *Rubber. Chem. Technol.* 1991, **64**: 648-660.
45. S. G. Gaynor; J.-S. Wang; K. Matyjaszewski. *Macromolecules.* 1995, **28**: 8051-8056.
46. K. Matyjaszewski; S. Gaynor; J.-S. Wang. *Macromolecules.* 1995, **28**: 2093-2095.
47. H. Hsieh; R. P. Quirk *Anionic polymerization: principles and practical applications*; CRC Press, 1996, p 744
48. K. Matyjaszewski; J. Spanswick In *Handbook of Polymer Synthesis*; CRC Press: 2004, p 907-954.
49. N. Hadjichristidis; H. Iatrou; S. Pispas; M. Pitsikalis. *J.Polym. Sci. A: Polym. Chem.* 2000, **38**: 3211-3234.
50. J. Tonnar; P. Lacroix-Desmazes; B. Boutevin. *Macromolecules.* 2007, **40**: 186-190.
51. M. Morton *Anionic polymerization: principles and practice*; Elsevier, 2012
52. N. V. Tsarevsky; B. S. Sumerlin; K. Matyjaszewski. *Macromolecules.* 2005, **38**: 3558-3561.
53. D. Fournier; R. Hoogenboom; U. S. Schubert. *Chem. Soc. Rev.* 2007, **36**: 1369-1380.
54. L. R. Hutchings; S. J. Roberts-Bleming. *Macromolecules.* 2006, **39**: 2144-2152.
55. A. Pagliarulo; L. R. Hutchings. *Macromol. Chem. Phys.* 2018, **219**: 1700386-400.
56. L. R. Hutchings. *Macromolecules.* 2012, **45**: 5621-5639.
57. J. C. Giddings; F. J. Yang; M. N. Myers. *Anal. Chem.* 1976, **48**: 1126-1132.
58. H. C. Lee; T. Chang; S. Harville; J. W. Mays. *Macromolecules.* 1998, **31**: 690-694.
59. S. Podzimek; T. Vlcek; C. Johann. *J. Appl. Polym. Sci.* 2001, **81**: 1588-1594.
60. T. Chang. *J.Polym. Sci. B: Polym. Phys.* 2005, **43**: 1591-1607.
61. K. Im; S. Park; D. Cho; T. Chang; K. Lee; N. Choi. *Anal. Chem.* 2004, **76**: 2638-2642.
62. S. K. Ratanathanawongs Williams; D. Lee. *J. Sep. Sci.* 2006, **29**: 1720-1732.
63. H. Pasch; B. Trathnigg *Multidimensional HPLC of polymers*; Berlin, Springer, 2013, p 37-90

64. J. R. Runyon; S. K. R. Williams. *J. Chromatogr. A.* 2011, **1218**: 7016-7022.
65. T. Otte; T. Klein; R. Brüll; T. Macko; H. Pasch. *J. Chromatogr. A.* 2011, **1218**: 4240-4248.
66. C. Gao; D. Yan. *Prog. Polym. Sci.* 2004, **29**: 183-275.
67. M. Gaborieau; P. Castignolles. *Anal. Bioanal. Chem.* 2011, **399**: 1413-1423.
68. W. Radke. *J. Chromatogr. A.* 2014, **1335**: 62-79.
69. T. C. Schunk. *J. Chromatogr. A.* 1993, **656**: 591-615.
70. T. C. Schunk. *J. Chromatogr. A.* 1994, **661:**: 215-226.
71. H. Pasch In *New Developments in Polymer Analytics I*; Springer: 2000, p 1-66.
72. F. Fitzpatrick; R. Edam; P. Schoenmakers. *J. Chromatogr. A.* 2003, **988**: 53-67.
73. T. Macko; A. Ginzburg; K. Remerie; R. Bruell. *Macromol. Chem. Phys.* 2012, **213**: 937-944.
74. N. Miller; B. Karger. *J. Chromatogr. A.* 1985, **326**: 45-61.
75. T. Chang; H. C. Lee; W. Lee; S. Park; C. Ko. *Macromol. Chem. Phys.* 1999, **200**: 2188-2204.
76. B. Seo; K. Kim; H. Lee; J.-Y. Lee; G.-h. Kwag; W. Kim. *Macromol. Res* 2015, **23**: 466-473.
77. W. Lee; D. Cho; B. O. Chun; T. Chang; M. Ree. *J. Chromatogr. A.* 2001, **910**: 51-60.
78. L. R. Hutchings; S. Agostini; M. E. Oti; J. Keth. *Eur. Polym. J.* 2015, **73**: 105-115.
79. T. Chang In *Liquid Chromatography/FTIR Microspectroscopy/Microwave Assisted Synthesis*; Springer: 2003, p 1-60.
80. S. W. Li; H. E. Park; J. M. Dealy; M. Maric; H. Lee; K. Im; H. Choi; T. Chang; M. S. Rahman; J. Mays. *Macromolecules* 2010, **44**: 208-214.
81. A. Alghyamah; J. B. P. Soares. *Ind. Eng. Chem. Res.* 2013, **53**: 9228-9235.
82. T. Chang In *Recent Progress in Separation of Macromolecules and Particulates*; ACS Publications: 2018, p 1-17.
83. D. Murima; H. Pasch. *Anal. Bioanal. Chem.* 2019: **411**, 5063-5078.
84. L. Gao; J. Oh; Y. Tu; T. Chang. *Polymer* 2018, **135**: 279-284.
85. . Wang, W. Gao, S. Orski, X. M. Liu. In *Recent progress in Separation of Macromolecules and ParticulatesACS. Ser.* 2018. p 9-15.
86. W. Radke. *J. Chromatogr. A.* 2019, **1593**: 17-23.
87. Y. Pakzad; M. Fathi; M. Mozafari In *Advanced Functional Polymers for Biomedical Applications*; Elsevier: 2019, p 359-381.
88. S. Lee; H. Choi; T. Chang; B. Staal. *Anal. Chem.* 2018, **90**: 6259-6266.
89. R. Epping; U. Panne; J. Falkenhagen. *Anal. Chem.* 2018, **90**: 3467-3474.
90. J. Wang; S. Yang; K. Zhang. *J Pharm Biomed Anal.* 2019, **164**: 452-459.
91. P. Dugo; F. Cacciola; T. Kumm; G. Dugo; L. Mondello. *J. Chromatogr. A.* 2008, **1184**: 353-368.
92. U. D. Neue. *J. Chromatogr. A.* 2005, **1079**: 153-161.
93. J. Dolan; L. Snyder; N. Djordjevic; D. Hill; T. Waeghe. *J. Chromatogr. A.* 1999, **857**: 1-20.
94. N. Marchetti; A. Cavazzini; F. Gritti; G. Guiochon. *J. Chromatogr. A.* 2007, **1163**: 203-211.
95. X. Li; D. R. Stoll; P. W. Carr. *Anal. Chem.* 2008, **81**: 845-850.
96. J. M. Davis; J. C. Giddings. *Analytical chemistry* 1983, **55**: 418-424.
97. H. Pasch; K. Mequanint; A. Jörg. *e-Polymers* 2002, **2**.1-19.
98. P. Kilz. *Chromatographia* 2004, **59**: 3-14.
99. B. Trathnigg; M. Kollroser. *Int. J. Polymer Analysis and Characterization* 1995, **1**: 301-313.
100. K. Im; H.-w. Park; S. Lee; T. Chang. *J. Chromatogr. A.* 2009, **1216**: 4606-4610.
101. W. Hiller; M. Hehn; P. Sinha; J.-A. Raust; H. Pasch. *Macromolecules* 2012, **45**: 7740-7748.
102. J. C. Giddings; F. Yang; M. N. Myers. *Science* 1976, **193**: 1244-1245.
103. S. Wiegand. *J. Phys Condens. Matter.* 2004, **16**: R357.
104. M. E. Hovingh; G. H. Thompson; J. C. Giddings. *Anal. Chem.* 1970, **42**: 195-203.
105. C. C. Miller. *Proceedings of the Royal Society of London. Series A, Containing Papers of a Mathematical and Physical Character* 1924, **106**: 724-749.
106. G. Liu; J. Giddings. *Chromatographia* 1992, **34**: 483-492.

107. P. M. Shiundu; S. M. Munguti; B. M. Wamalwa. *Bulletin of the Chemical Society of Ethiopia* 2002, **16**: 91-101.
108. M. E. Schimpf; J. C. Giddings. *Macromolecules* 1987, **20**: 1561-1563.
109. J. C. Giddings; M. N. Myers; J. Janča. *J. Chromatogr. A.* 1979, **186**: 37-44.
110. P. M. Shiundu; J. C. Giddings. *J. Chromatogr. A.* 1995, **715**: 117-126.
111. G. Bear. *J. Chromatogr. A.* 1988, **459**: 91-107.
112. T. H. Mourey; L. E. Oppenheimer. *Anal. Chem.* 1984, **56**: 2427-2434.
113. A. Hopia; V.-M. Ollilainen. *J Liq Chrom Relat Tech.* 1993, **16**: 2469-2482.
114. H. Binder. *J. Chromatogr.* 1980, **189**: 414-420.
115. R. D. Rocklin. *J. Chromatogr. A.* 1991, **546**: 175-187.
116. B. H. Zimm. *J. Chem. Phys.* 1948, **16**: 1093-1099.
117. S. Grcev; P. Schoenmakers; P. Iedema. *Polymer* 2004, **45**: 39-48.
118. C. Augsten; K. Mäder. *Int. J. Pharm. Pharm. Sci.* 2008, **351**: 23-30.
119. W. W. Yau; S. W. Rementer. *J. Liq. Chromatogr.* 1990, **13**: 627-675.
120. T. G. Scholte; N. Meijerink; H. Schoffeleers; A. Brands. *J. Appl. Polym. Sci.* 1984, **29**: 3763-3782.
121. W. Brown *Dynamic light scattering: the method and some applications*; Clarendon press Oxford, 1993; Vol. 313
122. R. Shaw. *Dynamic Light Scattering Training.Malvern Instruments Ltd* 2014
123. M. Kaszuba; D. McKnight; M. T. Connah; F. K. McNeil-Watson; U. Nobbmann. *J. Nanopart. Res.*2008, **10**: 823-829.
124. R. Xu. *Particuology* 2015, **18**: 11-21.
125. W. Schärtl *Light scattering from polymer solutions and nanoparticle dispersions*; Springer Science & Business Media, 2007

3.

Comprehensive branching analysis of star-shaped polystyrenes using a liquid chromatography-based approach[1]

Douglas Murima, Harald Pasch *

Correspondence to: Harald Pasch, email:hpasch@sun.ac.za

Abstract: The comprehensive branching analysis of complex polymers is still a challenge in advanced polymer analysis. Average branching information (average number and length of branches) can be obtained by spectroscopic methods, mainly NMR spectroscopy. The determination of the branching distribution, i.e. the concentration of macromolecules with a given number of branches, however, requires fractionation. Typically, size exclusion chromatography is used that separates the complex mixture regarding molecular size in solution and not strictly regarding the number of branches. In the present approach, model star-shaped polystyrenes were synthesized with a pre-determined architecture to give theoretical three-arm, four-arm and six-arm structures. The branched samples were compared to a linear analogue of comparable molar mass known not to contain branching. Triple detector size exclusion chromatography with refractive index, multiangle light scattering and online viscometer detection was used to determine absolute molar masses, radii of gyration and branching distributions of the star-shaped polymers. ^{1}H-NMR was used to calculate the average functionality and a reasonable agreement between the results of the two methods was obtained. Temperature gradient interaction chromatography and solvent gradient interaction chromatography were employed to separate the complex reaction products according to chemical composition (number of branches) and to resolve by-products. The separation capabilities of the two chromatographic techniques were compared and evaluated. Comprehensive two-dimensional liquid chromatography was used to separate the polydisperse star-shaped polystyrenes regarding both branching and molar mass.

Keywords: Star-shaped polymers, polystyrene, size exclusion chromatography, multiple detectors, solvent gradient interaction chromatography, temperature gradient interaction chromatography

[1] D. Murima; H. Pasch. *Anal. Bioanal. Chem.* 2019: **411**, 5063-5078.

3.1 Introduction

Star-shaped polymers consist of a number of linear polymer chains (arms) joined together at a central point (core) with a given number of chain end groups (functionalities).[1-6] The preparation of star-shaped polymers can be achieved by growing the polymer arms from a central core–the 'core first' approach, or by synthesizing the individual arms and then attaching them to a central molecule–the 'arms first' approach (Figure 3.1).[6,7] Most frequently, methods of controlled free radical polymerization are used for the core first approach. One of these methods is the reversible addition-fragmentation chain transfer polymerization (RAFT) that is used in the present work.[8-13]

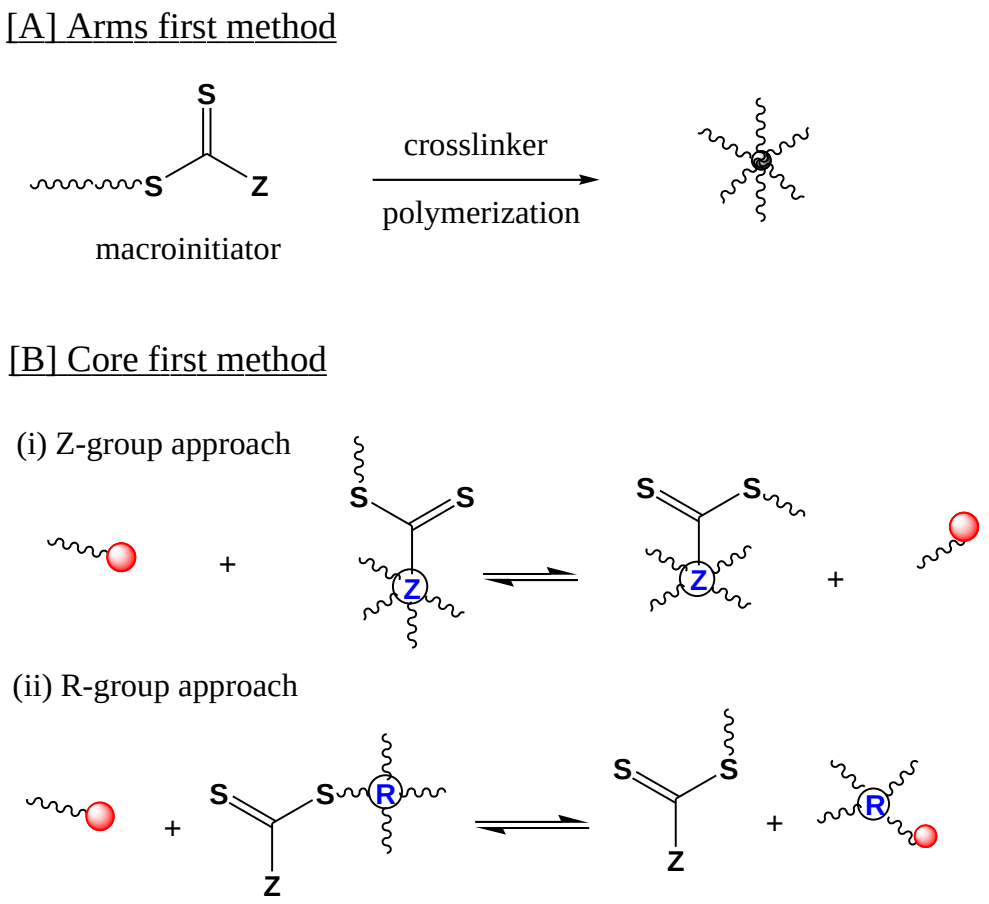

Figure 3.1 Schematic representation of the arms first (A) and core first (B) methods for star polymer synthesis using the RAFT technique; together with the Z-group and R-group approaches B (i) and B (ii), respectively. Red oval/dot represents the propagating free radical.

The mechanism of the RAFT method allows for two alternative approaches towards star polymer synthesis, namely the R-group approach and the Z-group approach.[14-16] This allows for increased flexibility when designing star polymers within the concept of the core first method where the mediating RAFT moiety is attached to the core either via the leaving R-group or via the stabilizing Z-group as shown in Figure 3.1.

3.1.1 The RAFT mechanism

The initiation, chain propagation and chain termination in RAFT polymerization resemble those in conventional radical polymerization.[17] From the RAFT mechanism depicted in Figure 3.2, following the activation step (a and b) between radical from the initiator ($I^{\cdot}$) and the monomer (M), the propagating radical ($P_n^{\cdot}$) adds to the C=S group originating from the RAFT agent or chain transfer agent, CTA and an intermediate radical (step c) will be generated.

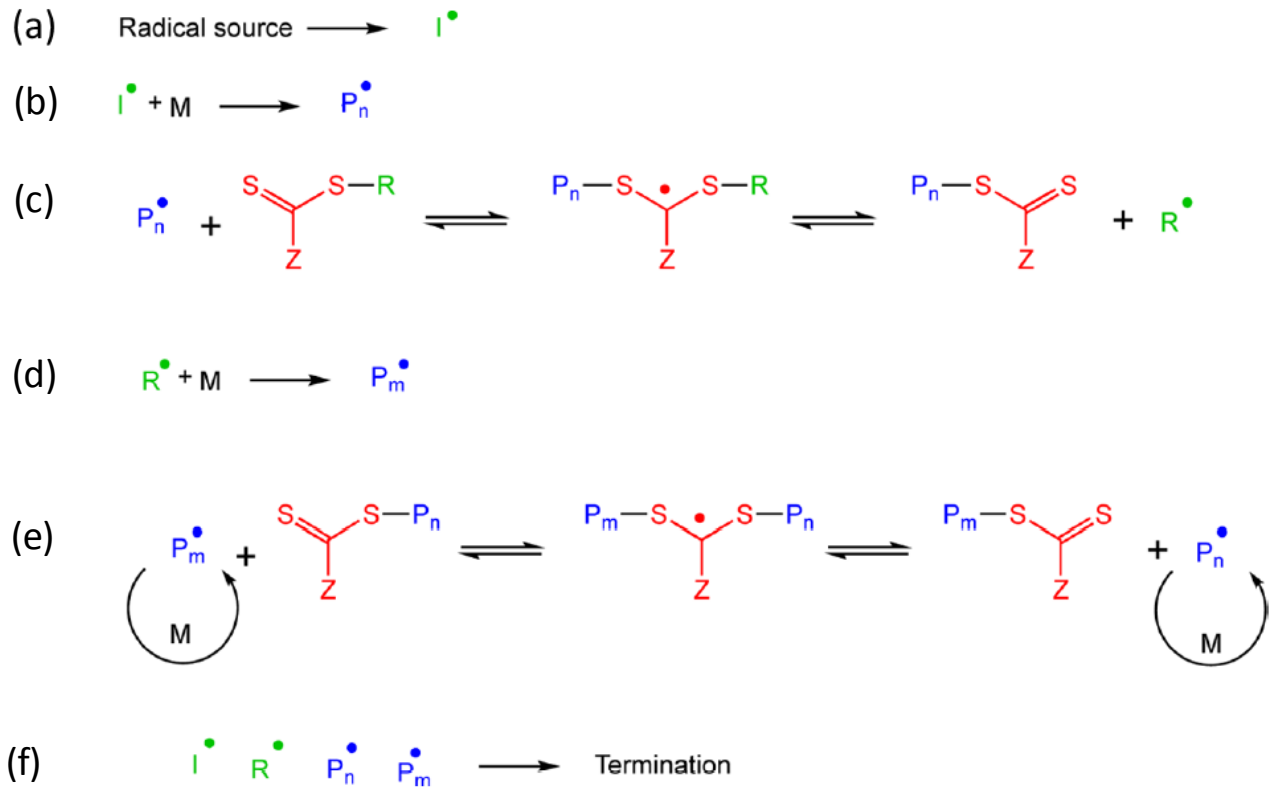

Figure 3.2 Example of the reversible addition-fragmentation chain transfer polymerization mechanism

The chain transfers steps that form the basis of the RAFT mechanism are degenerate as they involve a reversible transfer of the functional chain end-group (typically a thiocarbonylthio group, Z−C(═S)S−R) between the dormant chains (macroRAFT agent or macroCTA) and the propagating radicals.[18] In an effective process, the rate of addition/fragmentation equilibrium is higher than that of the propagation, so there should be less than one monomer unit added per activation cycle to ensure that all growing chains have a similar degree of polymerization (DP) at a given time. The overall process (step d and e) is comprised of the insertion of monomers between the R- and Z−C(=S)S-groups of a RAFT agent, which form the end-groups of the majority of the resulting polymeric chains. The termination reaction (step f) is often inevitable in a radical polymerization system, usually yielding dead polymer chains.[19] For RAFT polymerization, the termination reaction could be minimized, due to the existence

of the thiocarbonylthio end-group in resulting polymeric chains, which also enables participating in the RAFT polymerization as done by the RAFT agent. By making use of a macroinitiator, other monomers can be polymerized to prepare multiblock polymers. In addition, the activity of C=S group in RAFT agent plays a critical role in controlling molar mass and molar mass dispersity, as well as regulating the polymerization process. The realization of function depends greatly on the Z group, which often regulates the activity of C=S bond and stabilizes the intermediate radical. At the same time, the latter R-group should be an excellent leaving group when the C=S bond of RAFT agent undergoes the addition of propagating radical, and it also can reinitiate polymerization rapidly and effectively.

Part of the motivation of this study was based on published work carried out in our research group which highlighted on the capabilities of a novel tetrafunctional RAFT agent to prepare star polymers.[13,20] As such, we extended the knowledge to prepare regular stars with varying number of arms in order to model a comprehensive analytical approach.

In this work, the star polymers were synthesized using the Z-group approach because unlike the R-group approach, the RAFT trithiocarbonyl functionality is not departing from the star molecule which prevents the formation of living linear polymer and excludes star-star coupling via the conventional radical-radical termination process.[17,18] Owing to their exclusive structure, star polymers exhibit some remarkable characteristics and properties unattainable by simple linear polymers.[19] Quantitative information about branching topology is very important in order to gain a better understanding of the polymerization process, structure-property correlations and to develop innovative polymer-based materials with novel or improved bulk and solution properties.[20,21] Furthermore, the precise understanding of the dynamic properties of model star-shaped polymers can provide fundamental insight into the development and characterization of even more complex branched polymers that include hyperbranched, comb-shaped, dendritic and H-shaped molecules.[22-25] The methodical analysis of synthetic polymers with multivariate distributions is a difficult task and a single separation (or analysis) method is often not able to provide comprehensive information.[26]

A logical strategy to characterize such complex samples is to find liquid chromatographic methods that each separates exclusively or at least predominantly according to a single molecular characteristic (molar mass, chemical composition).[27,28] In a next step these selective methods could be combined to carry out a multidimensional mapping of the multivariate distribution. Multidetector size exclusion chromatography (SEC) comprising a concentration detector (typically a refractive index detector–RI) combined with an online viscometer and a

multiangle laser light scattering detector (MALLS) has been used to investigate the branching distribution of star-shaped polymer structures.[29,30] Although this is a powerful approach, it typically does not provide comprehensive information on the concentration of molecules with different numbers of arms in a complex sample. SEC separates polymer molecules according to their hydrodynamic size in solution.[31] Most importantly, SEC does not differentiate between linear and branched molecules as long as they have the same size in solution causing linear and branched molecules of different molar masses to co-elute.[32,33] This suggests that SEC alone cannot resolve all products of a complex reaction mixture, which might not differ much in hydrodynamic size.

In contrast to SEC, interaction chromatography (IC) has proven to be a powerful technique for the structural analysis of branched polymers.[12,27,34] In most cases the crude product mixture is first purified by fractionation (to remove low molar mass impurities) and the structural uniformity of the isolated components is investigated by conventional analytical methods such as SEC and nuclear magnetic resonance (NMR).[35] To overcome the problems of long retention times in interaction chromatography, the mobile phase strength is often increased over the duration of the experimental run which can be achieved by applying gradients of the eluent (solvent gradient interaction chromatography, SGIC)[36-39] or temperature (temperature gradient interaction chromatography, TGIC).[40-42] Chang et al. and Lee et al. conducted some extensive work on the fractionation of various branched polymers using TGIC.[43-46] In one of their latest reviews, Lee at al. and co-workers analyzed polybutadiene stars in which they contrasted triple detector SEC with triple detector TGIC and concluded that TGIC showed remarkable resolution while branching analysis of individual polybutadiene star species from TGIC fractionation was made possible with triple detection. In their review, they also demonstrated that in principle, with careful control of the TGIC operating parameters, it is possible to carry out branching analysis for model branched polymers without the bias of local dispersity.[47]

Drawing motivation from this and other work, we propose a combination of different liquid chromatographic methods to comprehensively analyse model branched polymers by correlating conventional triple detector SEC data to SGIC/TGIC fractionation data and ^{1}H-NMR analysis. In this present study, we aim at comparing the separation capabilities of SGIC and TGIC in fractionating and isolating star-shaped polystyrenes. Offline ^{1}H-NMR is employed to determine the average star functionalities of the star-shaped polystyrene. The experimental data from ^{1}H-NMR are contrasted to the branching distribution and average star functionality information obtained from triple detector SEC. As no single mode of liquid

chromatography can achieve complete separation of the star polystyrenes by molar mass and by topology, the use of two-dimensional liquid chromatography with TGIC in the 1st dimension and SEC in the 2nd dimension is highlighted. Kilz et al. reported on the automated multidimensional analysis of polymers and since then the concept of 2D-LC has gained popularity in separation science.[48] As prototypical star-shaped samples, polystyrenes were synthesized using the 'core first' approach to produce three-arm (PS3), four-arm (PS4) and six-arm (PS6) structures that are representative samples for branching analysis.

3.2 Experimental

3.2.1 Materials

Styrene (Sigma-Aldrich) was washed successively with a 0.03M aqueous potassium hydroxide (KOH) solution and distilled water to remove the inhibitor. The washed styrene was then distilled at 40 °C under reduced pressure to remove impurities and possible oligomers, which could result from auto-polymerization. Azobisisobutyronitrile (AIBN) was supplied by Sigma-Aldrich and purified by recrystallization from methanol. Dipentaerithritol, 2,2-bis{[(3-sulfanylpropanoyl) oxy] methyl} butyl3-sulfanylpropanoate and 3-[(3-sulfanylpropanoyl) oxy]-2,2-bis[(3-sulfanylpropanoyl) oxy] methyl) propyl3-sulfanylpropanoate were supplied by Sigma-Aldrich and used as received. Column-chromatographic purification of the RAFT agents was performed using silica gel (Merck, Kieselgel60). Technical grade *n*-pentane and ethyl acetate were supplied by Sigma-Aldrich and used without further purification.

3.3 Synthesis of multi-arm RAFT agents

Dipentaerythritolhexakis(3-(*S*-benzyltrithiocarbonyl) propionate), 1.

All multi-arm RAFT agents were synthesized according to a method first proposed by Mayadune et al. as a guideline.[9] Dipentaerythritol (1.25 g, 4.9 mmol), 2-mercaptopropanoic acid (4.77 g, 44 mmol) in the presence of a catalytic amount of p-toluene sulfonic acid (100 mg) was heated to reflux in toluene for 24 hr until the theoretical amount of water was collected using a Dean-Stark apparatus. The reaction mixture was poured into 100 mL of saturated $NaHCO_3$ in water, extracted with 3×100 mL $CHCl_3$. The solution of combined extracts was washed with 10% HCl, saturated aqueous NaCl solution and dried with $MgSO_4$. The solids were filtered from the heterogeneous mixture and the solvent evaporated. The product was used in the next step without purification. Triethylamine (6.06 g in 20 mL) in

$CHCl_3$ was added to a stirred solution of the hexamercapto derivative (3.89 g, 4.8 mmol), and carbon disulfide (CS_2, 4.54 g, 58 mmol) in $CHCl_3$ (20 mL) at room temperature. The solution was stirred for 1 hr before benzyl bromide (5.64 g, 33 mmol) was added. The mixture was stirred for 2 hr, poured into a cold solution of aqueous 10% HCl, and extracted three times with ethyl acetate (3×50 mL) to afford a thick yellow oil. The crude product was purified by column chromatography using 30% ethyl acetate in pentane to afford the six-arm chain-transfer agent (5.10 g, 68% yield) with 83% purity. ^{1}H NMR (300 MHz, DMSO-d_6) δ (ppm) 2.75 (*f*,12H), 3.4 (*e*,4H), 3.6 (*d*,12H), 4.02 (*c*,12H), 4.6 (*b*,12H), 7.3 (*a*,30$H_{aromatics}$), see Figure 3.3. The protons around 1.2 and 2ppm were attributed to residual ethyl acetate used during the solvent extraction steps.

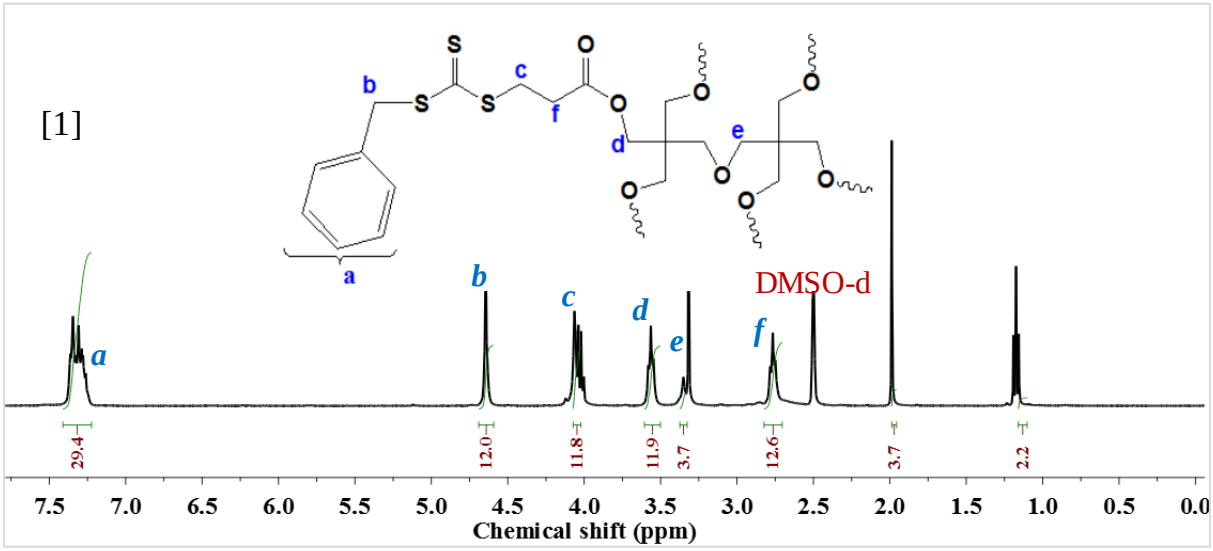

Figure 3.3 ^{1}H NMR spectrum of the reaction product of six arm RAFT dipentaerythritol-hexakis-3-(S-benzyl-trithiocarbonyl) propanoate, solvent: deuterated dimethylsulfoxide.

3-[(3-sulfanylpropanoyl) oxy]-2,2-bis[(3-sulfanylpropanoyl) oxy] methyl) propyl 3-sulfanylpropanoate, 2.

A solution of 3-[(3-sulfanylpropanoyl)oxy]-2,2-bis[(3-sulfanylpropanoyl)oxy]methyl)propyl 3-sulfanylpropanoate (0.71 mL, 1.44 g, 5.00 mmol) in chloroform was carefully mixed with an aliquot of 100 mL chloroform in triethylamine (5.56 mL, 4.08 g, 42.0 mmol, 8 equiv). After stirring the reaction mixture for 1 hr at room temperature 10 mL of CS_2 and (1-bromoethyl) benzene (3.02 mL, 4.07 g, 22.0 mmol, 4.1 equiv) were added slowly. The mixture was stirred for 15 hr and afterwards the reaction was quenched by adding 100 mL of 10% HCl. The organic phase was separated and washed twice with 100 mL of water and dried over Na_2SO_4. Solvent was removed in vacuum and the crude product was purified on silica

with CH_2Cl_2 (Rf =0.38) as eluent. A yield of 2.61 g (43.7% yield) of the four-arm chain transfer agent was received as yellow oil with 94% purity.

^{1}H NMR (300 MHz, $CDCl_3$) δ (ppm): 1.75 (d, J= 7.1 Hz, 12H, $C\underline{H}_3$–CH), 2.76 (t, J =7.0 Hz, 8H, CH_2), 3.56 (t, J =7.0 Hz, 8H, CH_2), 4.02 (s, 8H, CH_2), 5.32 (q, J= 7.1 Hz, 4H, CH), 7.32 (m, 20H, $H_{aromatics}$), (See Figure 3.4).

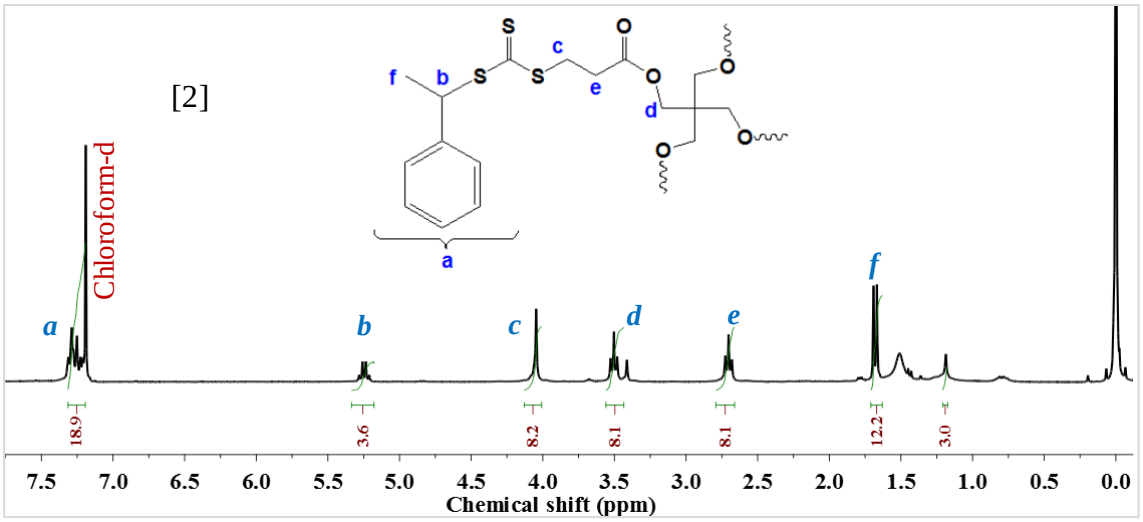

Figure 3.4 ^{1}H-NMR for the synthesis of four arm RAFT; 3-[(3-sulfanylpropanoyl) oxy]-2,2-bis({[(3-sulfanylpropanoyl) oxy] methyl}) propyl 3-sulfanylpropanoate in deuterated chloroform, 400 MHz

2,2-bis[(3-sulfanylpropanoyl) oxy] methyl) butyl 3-sulfanylpropanoate, 3.

To a solution of 2,2-bis[(3-sulfanylpropanoyl) oxy] methyl) butyl 3-sulfanylpropanoate (1.00 mL, 1.22 g, 3.06 mmol) in 50 mL chloroform, triethylamine (1.51 mL, 1.10 g, 10.6 mmol, 3.6 equiv) was added. After stirring the reaction mixture for 1 hr at room temperature, 5mL of CS_2 and (1-bromoethyl) benzene (1.50 mL, 2.04 g, 11.1 mmol, 3.6 equiv) were added slowly. The mixture was stirred for 15 hr and the reaction was then quenched by adding 50 mL of 10% HCl. The organic phase was separated and washed two times with 50 mL of water and dried over Na_2SO_4. Traces of solvent and non-reacted starting materials were removed in vacuum. 2.68 g (97.2%yield) of the three-arm chain transfer agent were received as a yellow liquid with 96% purity. ^{1}H NMR (300 MHz, $CDCl_3$) δ (ppm): 0.86 (t, J = 7.6 Hz, 3H, CH_3), 1.45 (q, J= 7.6 Hz, 2H, CH_2), 2.78 (t, = 7.0 Hz, 6H, CH_2), 3.62 (t, J =7.0 Hz, 6H, CH_2), 4.03 (s, 6H, CH_2), 4.62 (s, 6H, CH), 7.32 (m, 15H, $H_{aromatics}$), See Figure 3.5.

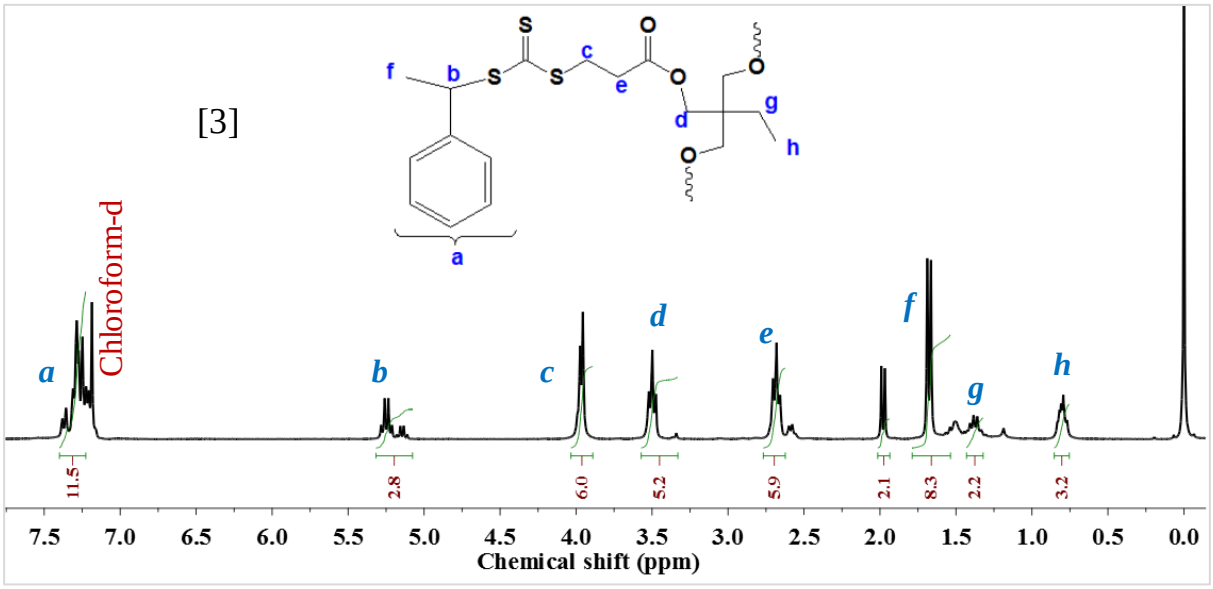

Figure 3.5 ^{1}H-NMR for the synthesis of three arm RAFT; 2,2-bis{[(3-sulfanylpropanoyl)oxy]methyl}butyl 3-sulfanylpropanoate in deuterated chloroform, 400 MHz [9]

3.4 Z-star RAFT polymerizations

Styrene (1.92 g; 0.0184 mol) was degassed via three freeze–pump–thaw cycles, transferred along with the RAFT agent and the AIBN initiator into argon-filled Schlenk flasks. The reaction mixture was subsequently inserted into a preheated oil bath thermostated at 70 ± 0.1 °C. The polymerizations were carried out using Toluene (2.32 mL) as the solvent. The reaction scheme is presented in Figure 3.6. The reaction was stopped by cooling the solution in an ice bath. The reaction times were up to 24 hr. The star-branched samples were isolated by precipitation in cold methanol and analysed as obtained relative to a linear analogue of comparable molar mass known not to contain branching. The linear polystyrene was prepared via conventional radical polymerization using toluene as the solvent and AIBN as the initiator. Samples for the linear PS polymerization were withdrawn after every hour and analyzed via SEC.

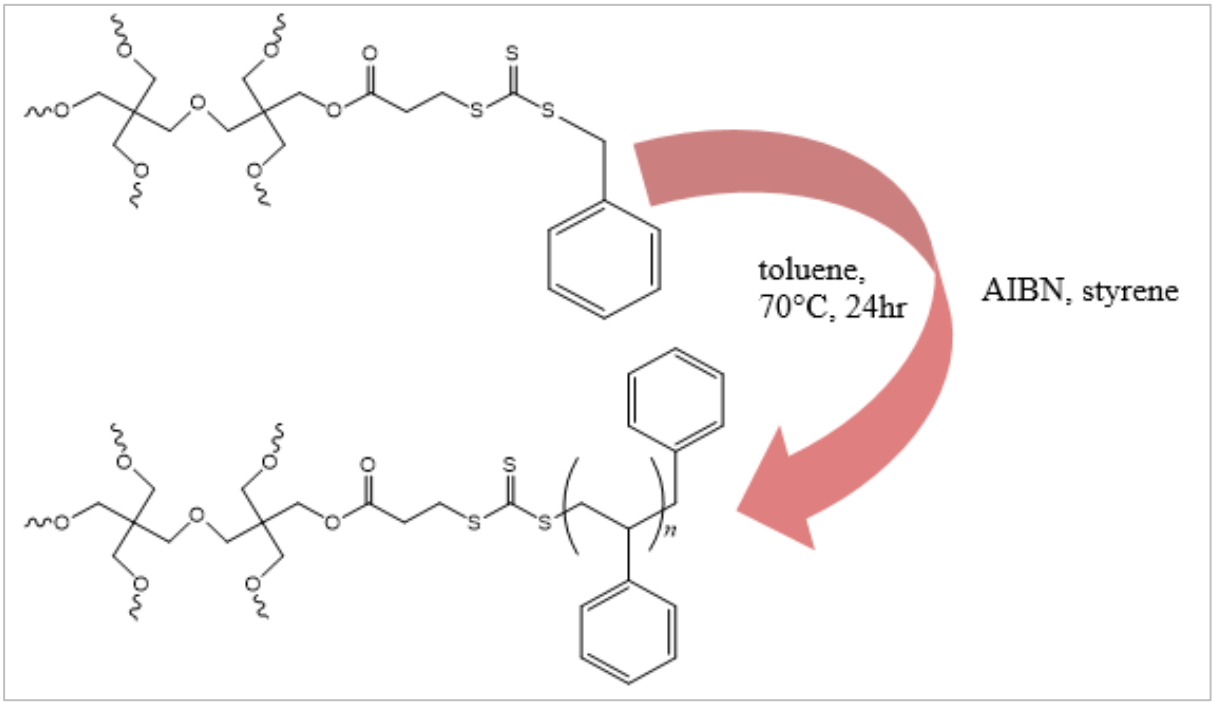

Figure 3.6: Reaction scheme for the Z-star RAFT solution polymerization of six-arm star polystyrene carried out in toluene.

The amounts of chain transfer agents (RAFT) and initiator (AIBN) used are given in Table 3.1.

Table 3.1 Amounts of chain transfer agents (RAFT) and initiator (AIBN) used for the polymerization reactions.

Sample	Initiator	RAFT agent (g; moL)
	AIBN (g; moL)	
Star PS 3-arm	3.15×10^{-3}; 1.92×10^{-5}	1.58×10^{-2} 1.67×10^{-5}
Star PS 4-arm	4.07×10^{-3}; 2.48×10^{-5}	2.04×10^{-2}; 1.68×10^{-5}
Star PS 6-arm	1.22×10^{-2}; 7.45×10^{-5}	6.12×10^{-2}; 3.44×10^{-5}

3.5 Characterization techniques

3.5.1 Chemical structure identification and molar mass analysis

3.5.1.1 ^{1}H-NMR

The dried samples of the star-branched polystyrenes were dissolved in either deuterated chloroform ($CDCl_3$) or deuterated dimethyl sulfoxide (DMSO-d_6). The signals were recorded on a Varian Inova 400 MHz NMR spectrometer by averaging 16 scans with a 0.3µsec pulse delay.

3.5.1.2 Triple detector (SEC)

The dried polymer samples were completely dissolved in THF at a concentration of 3mg/mL to obtain a good signal-to-noise ratio. The flow rate was 1mL/min. The signals were recorded on the Postnova SC2000 modular triple SEC/GPC instrument (Postnova Analytics, Landsberg, Germany) comprised of a PN 1130 isocratic HPLC pump and autosampler, PN 3150 refractive index (RI) detector, PN 3310 capillary bridge-viscometer and a PN3621 MALS detector. Data processing was performed using NovaSec V1.5.0.7 software. Separation was achieved using two PLgel (Polymer Laboratories) 5 µm Mixed-C (300 × 7.5 mm) columns connected in series along with a PLgel 5µm guard column (50 × 7.5 mm). The columns were kept at a constant temperature of 30 °C. THF Chromasolv HPLC grade solvent (0.125% BHT stabilised, Sigma-Aldrich) was employed as the mobile phase at a flow rate of 1mL/min and 100 µL injection volumes were used. Each solution contained 3 mg/mL of the crude sample in order to obtain a good signal-to-noise ratio. The hydrodynamic radii were determined using intrinsic viscosity data obtained from the online viscometry and molar mass information from MALS. The dn/dc values were measured online (in-house) with the samples using the peak areas detected by the PN 3150 refractive index detector. Branching distribution and star functionality information was obtained using the Postnova SC2000 modular triple SEC/GPC instrument (Postnova Analytics, Landsberg, Germany) comprising a PN 1130 isocratic HPLC pump and autosampler, PN 3150 refractive index (RI) detector, PN 3310 capillary bridge-viscometer and a PN3621 MALS detector. The system was calibrated using the viscosity-based universal calibration method.

3.5.2 Branching analysis

3.5.2.1 Temperature gradient (TGIC) and solvent gradient interaction chromatography (SGIC)

TGIC and SGIC experiments were carried out on an Agilent 1200 HPLC instrument (Agilent Technologies, Waldbronn, Germany) comprising the following: autosampler, on-line degasser, quaternary pump unit and a thermostated column compartment. The HPLC system was equipped with a C18 bonded silica column(Macherey-Nagel, Nucleosil C18, 100 Å pore size, 250 × 4.6 mm I.D., 5 µm particle size)for reversed phase (RP) IC; and a bare silica column (Macherey-Nagel, Nucleosil, 100 Å pore size, 250 × 4.6 mm I.D., 5 µm particle size) for normal phase (NP) IC. The polymer sample was dissolved at a concentration of 3 and 0.5mg/mL for TGIC and SGIC and the injection volume was 100 and 30µL for TGIC and SGIC, respectively. The mobile phase compositions and flow rates are stated in section 3.6.4 and 3.6.5. The column temperature was controlled via a programmable heated bath circulator through home-made fluid column jackets for the TGIC set-up. To estimate the molar mass for the sample corresponding to each TGIC fraction, linear standards of known molar masses were also run under the same SGIC and TGIC conditions. The chromatograms were recorded and processed on the PSS WinGPC Unichrom software (8.2). An evaporative light scattering detector (ELSD, Agilent 1260 Infinity) was used at a set temperature of 100 °C and a gain of 6.

3.5.2.2 Two-dimensional liquid chromatography

The sample concentration for the 2D-LC experiments was approximately 3 mg/mL with an injection volume of 100 µL. The first-dimension separation with respect to topology was carried out on the Nucleosil C18 column with the specifications mentioned above (see section 3.5.2.1) at a flow rate of 0.08 mL/min using a linear temperature ramp rate of 0.15 °C/min from 5-40 °C. The runtime was 240 minutes for the first dimension. The second dimension separated according to molar mass using THF as the eluent on a styrene-divinylbenzene (SDVB) stationary phase with the following dimensions: 5 µm particle size, 50 mm length and 20 mm internal diameter. The flow rate used for the second dimension was 4 mL/min. An evaporative light scattering detector (ELSD, Agilent 1260 Infinity) was used as the detector at a temperature of 100 °C and a gain of 8. The coupling of TGIC and SEC was achieved by an electronically controlled eight-port valve EC8 W (VICI VALCO instruments, Texas, USA) equipped with two 200 µL loops. After the initial injection (100 µL), fractions from the first

dimension were transferred into the second dimension every 2.5 min in order to inject 200 µL of eluent from the first dimension into the second dimension.

3.6 Results and discussion

The general synthetic approaches used to prepare star polymers in this study are not in their entirety novel. As continuation of an ongoing research, part of the motivation for this work was based on published findings carried out in our research group which highlighted on the capabilities of a novel tetrafunctional RAFT agent to prepare star polymers via the core first approach.[13,20] The tetrafunctional RAFT agent, tetrabenzyl(1,3-dithietane-2,2,4,4-tetrayl)-tetracarbanotrithioate, was successfully used to prepare four-arm star polystyrene.

Owing to these insights, the primary idea of this work was to prepare a series of simple branched polymers in the form of three, four and six-arm stars using the same core first approach. After preparation of the series of star-shaped polymers with varying number of arms, the main objective was then to develop a combination of spectroscopic and liquid chromatography-based analytical methods to comprehensively characterize the resultant star polymers with regard to the size as well as branching distributions.

3.6.1 Chemical structure elucidation

NMR spectroscopy is commonly used to determine the average degree of branching (DB) of branched polymers. It is quite frequently difficult to calculate DB of highly branched polymers by ^{1}H NMR spectroscopy owing to the overlapping of typical signals. [49] However, in this study, the model star-branched polystyrenes constitute of simple branches. The CH_2 RAFT core protons around 3.8-4.1ppm and the CH polystyrene protons around 4.6ppm were used for the calculation of the average star functionality as they were not overlapping with any other typical signal in the spectra as shown in the example in Figure 3.7. The average number of arms per star were calculated according to the following expression:

$$\int \frac{\mathbf{CH}_{\mathbf{styrene}}/_{1}}{\mathbf{CH}_{\mathbf{2}\,\mathbf{core}}/_{2}} \times \text{theoretical number of arms.}$$

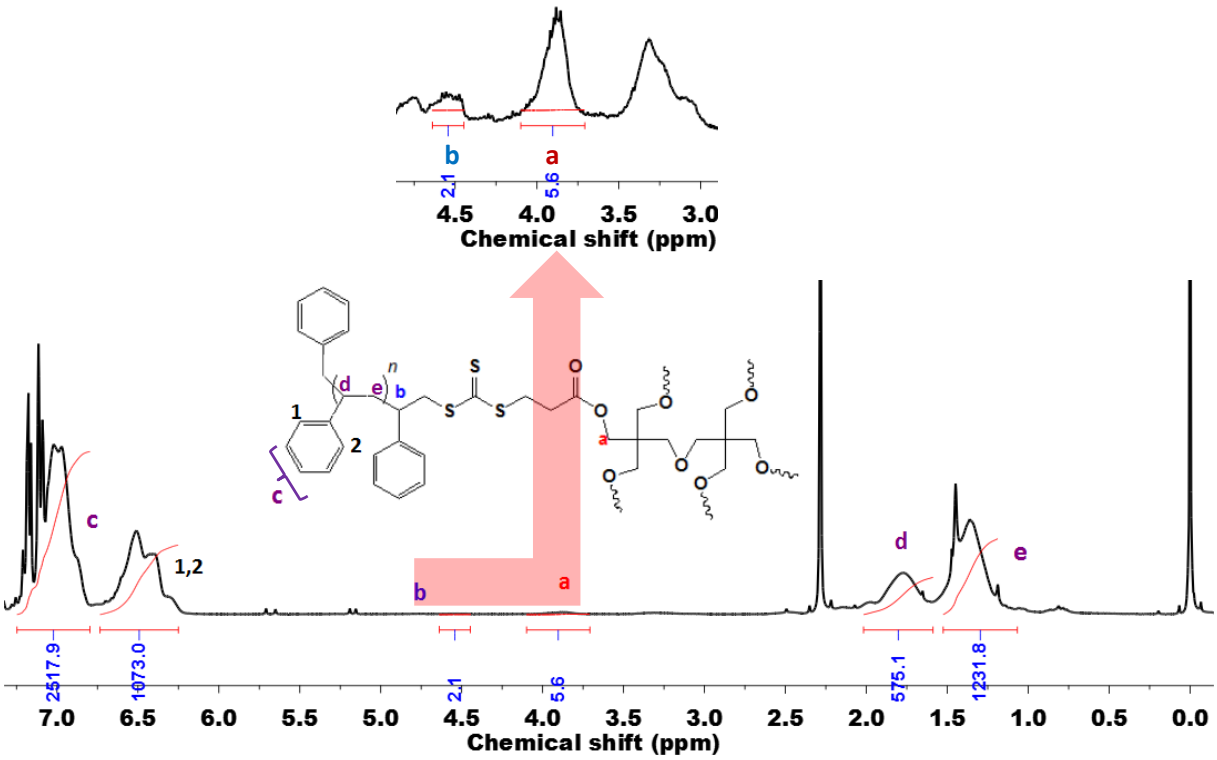

Figure 3.7: [1]HNMR spectrum of star PS 6-arm, solvent: deuterated chloroform.

The average star functionality for the six-arm star polystyrene was calculated using the RAFT core CH_2 and the polystyrene CH proton integrals providing an average number of arms of **4.50**. The same calculation method was adopted to determine the average star functionality in four-arm and three-arm star PS (using the protons at similar positions to the ones used for the star PS 6-arm in Figure 3.7) to give **3.26** and **2.53** arms, respectively. The lower than expected average branching numbers indicate complex mixtures of star-shaped polymers with a different number of arms and linear polymer chains from the RAFT, core first strategy employed to prepare the stars. These complex mixtures will contain molecules with the target functionality, i.e. 6, 4 and 3, respectively, but in addition, will have by-products of lower functionality. Additionally, the NMR approach to calculate the average star functionalities had its challenges due to the poor signal to noise ratio for the polystyrene C**H** proton (labelled ***b*** in Figure 3.7). However, of the available polystyrene protons to facilitate the calculation, it was the only distinct as well as non-overlapping choice. NMR provides just an average number of arms and, therefore, fractionation is required to obtain information on the different sample components and their compositions.

3.6.2 Molar mass analysis

Figure 3.8 (A) shows the MALS detector response versus elution volume plots of the star-shaped polystyrenes compared to the linear analogue. The molar mass distributions of the

star-shaped samples agree with Gaussian peak distributions characteristic of polymers prepared via a living radical process. Some peak tailing at higher elution volumes was apparent for all the star-branched samples, indicative of the inevitable formation of dead polymer chains (chains with no reactive end groups) formed during the RAFT polymerization process. [50] It is clear that the formation of dead polymer chains is a limitation for obtaining pure and narrowly dispersed star polymers. [51]

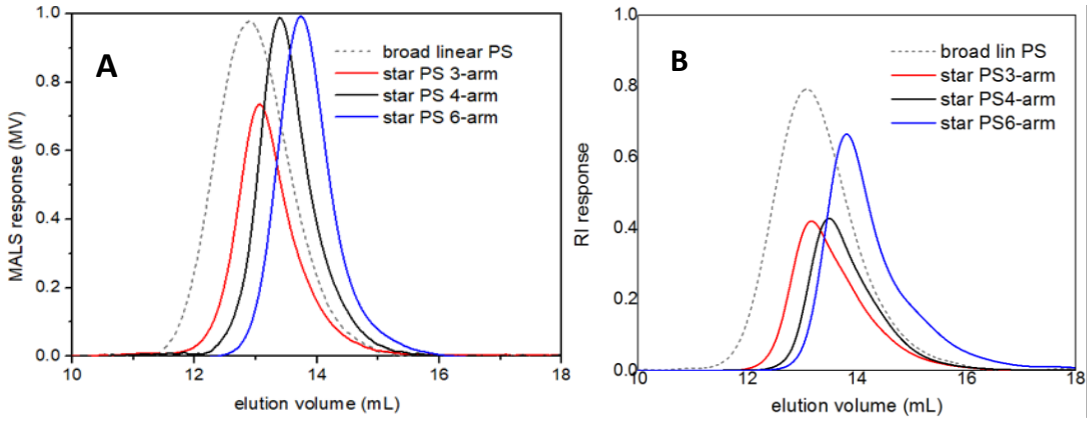

Figure 3.8: Overlaid MALS chromatograms (A) and corresponding RI signals (B) as a function of elution volume of the crude star-shaped polystyrenes and the linear polystyrene reference

However, considering the co-elution of the different species as evidenced in the RI signals of the SEC elution profiles (Figure 3.8 B), the crude star-shaped polymers prepared in this work exhibited reasonably narrow molar mass dispersities as shown in Table 3.2 which is indicative of polymers prepared via the controlled radical process - RAFT. [8] In RAFT, the exchange between the dormant species (carrying RAFT moiety) and the active propagating polymeric chains is rapid and offers an equal probability for the end-capped polymeric chains to activate via the fragmentation of the intermediate radical and add more monomer units, while deactivation of the polymeric radicals proceeds via the addition to the dormant agent. Thus, polymers with controlled molecular weights and dispersity index (PDI) can be produced for a wide range of monomers, while their end groups can be maintained active at the end of the reaction. Additionally, the molar ratio of monomer to RAFT agent to initiator determines the targeted chain length and dispersity of the polymer product at complete conversion. As a rule of thumb, the polymer molecular weight (typically derived from size exclusion chromatography (SEC)) should increase linearly with monomer conversion, such that at 100% conversion the molecular weight corresponds to the initial ratio of monomer to initiator (or chain transfer agent (CTA) in the case of RAFT) in the system. In this study, the targeted molar masses per star was 120 000 g/mol. However low conversions (56% for 3-arm, 38% for

4-arm and 45% for the 6-arm star) as determined by gravimetric analyses resulted in the low average molar masses obtained.

As expected, there was no pronounced separation of the star-shaped polymers from the linear analogue because the molecular size resolution of SEC is poor when comparing branched polymers and linear analogues of similar molar masses. In addition, the relationship between molar mass and size in solution is a function of the branching topology and this implies that a fraction of a given size may contain linear and branched molecules with different molar masses. This proves the necessity of using further fractionation techniques and detection methods that are more specific regarding branching topology.

Table 3.2: Molar mass and dispersity (DI) values of the star-shaped polystyrenes.

Sample	**M_w MALS (g/mol)**	**DI**
Broad linear PS	69000	1.8
Star PS 3-arm	67000	1.5
Star PS 4-arm	46000	1.4
Star PS 6-arm	54000	1.5

3.6.3 Star functionality – conformation plots

The presence of branches at a polymer backbone leads to a contraction of the polymer coil in solution and, accordingly, to a decrease in hydrodynamic size relative to a linear polymer analogue of the same molar mass. [47] Zimm and Stockmayer mathematically treated the hydrodynamic size contraction in branched polymers of various chain architectures assuming random walk statistics of the polymer chains. They defined chain contraction factor (***g***) as the ratio of the mean square radius of gyration (R_g^2) of a branched polymer to that of a linear polymer analogue having the same molar mass using Equation 10. [52]

$$g \equiv \frac{(R_g^2)\text{branched}}{(R_g^2)\text{linear}} \qquad \textbf{[10]}$$

For a regular star-shaped polymer with ***f*** number of arms (branches), the geometric contraction factor was described using Equation 11 as follows:

$$g_{rw} = \frac{3f-2}{f^2} \qquad \textbf{[11]}$$

where ***rw*** stands for the random walk statistics. Considering the difficulty in precisely determining the radius of gyration by light scattering, particularly for low molar mass polymers, and the inherent precision of intrinsic viscosity measurements, intrinsic viscosity has a technical advantage over the radius of gyration and g′ (based on viscosity measurements) is more frequently measured in the branching analysis. On the other hand, while g is a function of chain architecture only and the theoretical relationship between chain structure and the corresponding contraction factor has been developed for g, the hydrodynamic contraction factor, g′ (described using the relationship in Equation 12), includes the hydrodynamic interaction of polymer chain segments in solution, which is not trivial to treat theoretically. Therefore, the establishment of a reliable relationship between g and g′ is a prerequisite for the branching analysis using g′. In their quest to improve the branching analysis theories, Zimm and Kilb suggested the use of intrinsic viscosity **(**η**)** from viscometric experiments instead of the radius of gyration from light scattering in order to determine the extent of chain contraction relative to the degree of branching using Equation 12:

$$g' = \left(\frac{[\eta]_{\mathbf{branched}}}{[\eta]_{\mathbf{linear}}}\right) \qquad \textbf{[12]}$$

where [η] is the intrinsic viscosity of the branched and linear polymer chains having the same molar mass, respectively. [53] The relationship between (radius of gyration dependent) *g* and (intrinsic viscosity dependent) g' is described via the so-called 'draining parameter' ε expressed by Equation 13:

$$g' = g^{\varepsilon} \qquad \textbf{[13]}$$

The draining parameter varies between 0.5 (long branches with a very short, or without a backbone) to 1.5 for comb-shaped polymers (short branches attached on a long backbone). Podzimek et al. investigated the effects of varying the draining parameter on the branching ratio and established that the value changes with molar mass. [54]

Branching analysis is more straight forward if one compares the data obtained from a branched polymer sample to that of a linear polymer chain of identical chemical structure and molar mass. The Mark–Houwink plot is a very useful approach for branching analysis, which is the logarithm of the intrinsic viscosity (obtained e.g. using online viscometry) plotted against the logarithm of the molar mass (obtained using universal calibration or light

scattering detection). The general relationship of the Mark-Houwink plot is described in Chapter 2 (see Equation. 8 and 9).[55]

In the present study, Mark–Houwink plots were prepared for the star-shaped polystyrenes and then compared to polystyrene reference that was known not to contain branching. Figure 3.9 shows an overlay of the Mark–Houwink plots of the star-shaped polymers and the linear reference. The intrinsic viscosity data were obtained from the online viscometer while the molar mass information was derived from the MALS also attached to the SEC instrument. Relative to the linear PS material, which adopts a random coil conformation in solution, the star-shaped polymers adopt more compact spherical conformations. [54] The Mark–Houwink exponent of the linear polystyrene was determined to be 0.73, which is in line with literature data. [54] From Figure 3.9, it can be observed that the linear polystyrene exhibits the highest intrinsic viscosity at a given molar mass, the lowest density and the most extended random coil structure, while the intrinsic viscosity values of the star-shaped polystyrenes fall below that of the linear (at a fixed molar mass as branching increases the polymer coil density decreases in solution). The Mark–Houwink plots for the star-shaped polystyrenes PS 3-arm (0.46) and star PS 4-arm (0.42) were overlapping at some point across the log M scale which indicates the presence of molecules that have similar molar masses and degree of branching. For the star PS 4-arm, another variation around log (M) = 4.8 was also seen. For the sample PS6-arm, however, the Mark–Houwink exponent significantly varied across the molar mass scale as a result of the more complex nature and coelution of species in the star-shaped sample containing macromolecules with different numbers of arms. There is also evidence of the presence of high molar mass species characterized by a Mark–Houwink exponent of 0.78 attributable to that of linear molecules. During synthesis of the Hexafunctional RAFT agent , Dipentaerythritolhexakis(3-(*S*-benzyltrithiocarbonyl) propionate), the final product was obtained with 83% purity according to NMR analysis. The presence of impurities in the final product (linear and/or bifunctional) may have led to formation of high molar mass linear polymer chains during the RAFT polymerization process, while it is also possible that the star individual arms may not grow at the same rate. The Mark–Houwink exponents of 0.48 for the lower molar masses and 0.36 for medium molar masses signify that molecules of different molar masses have different numbers of arms.

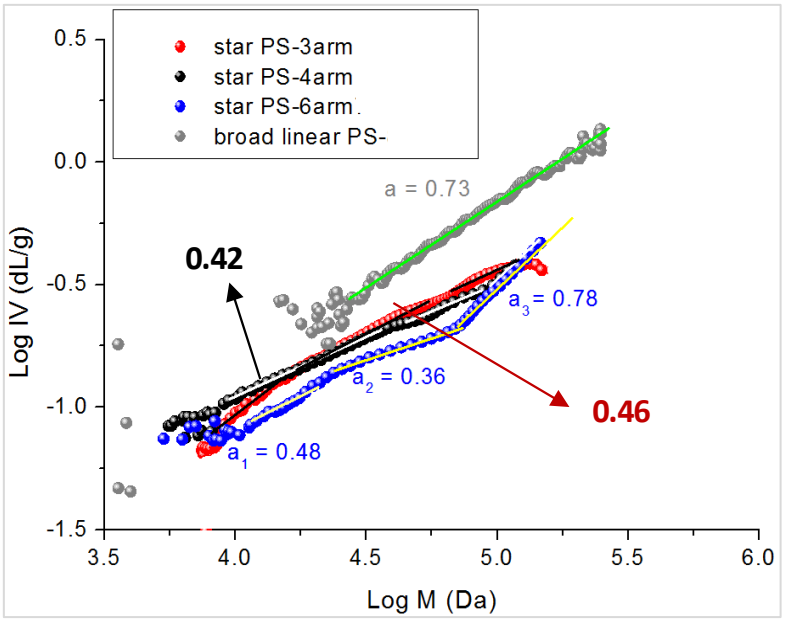

Figure 3.9: Overlaid Mark-Houwink plots for different star-shaped polystyrene and a linear polystyrene reference.

It is without a doubt that if the constants in the Mark–Houwink equation are known, the application of SEC with viscometric detection yields a viscosity average molecular weight while the application of SEC with light scattering detection results in a weight-average molar mass. However, even though the combination of both detection systems allows for the determination of the local dispersity due to coeluting polymers varying in molar mass, the coelution of polymers varying in other molecular species is still inevitable as shown by the Mark–Houwink exponent of 0.78 for the crude PS 6-arm star in Figure 3.9. Therefore, a combination of non-SEC separation techniques needs to be developed in order to comprehensively characterize branched polymers and that is where the basis of the argument of our work emanates from. The average branching ratio (branching parameter, contraction factor) g' was calculated from the intrinsic viscosities of the branched polystyrenes and the linear polystyrene of similar molar mass fractions using Equation 13. The molar masses were determined by MALS while the intrinsic viscosities were measured by online viscometry. The overlaid plots of the branching ratios as a function of molar mass are shown in Figure 3.10A. The contraction factor for the linear reference is 1 and decreases for the branched PS with increasing chain density and, hence, the increasing number of arms. From the branching ratio plots there was compelling evidence on the overal influence of branching on the size of the polymer molecules in solution and the fact that different samples had different numbers of arms. As was expected, the number of arms increased from star PS 3-arm to star PS 4-arm and star PS 6-arm which agrees with the NMR results. The plots also indicate that samples

star PS 3-arm and star PS 4-arm have a rather homogeneous distribution of the number of arms as a function of molar mass.

There still is an experimental consensus on the precise value of the draining parameter and it would be helpful if one considers evaluating the effects of varying the draining parameter on the values of the contraction factor obtained. However, with supporting information from Ahn et al. and Lee et al., experimentally a draining parameter value between 0.70–0.8 is reliably used for regular star-branched polymers. [56,57] Based on this logic, in this work the star functionality (the number of arms) f was determined from the contraction factor (g′) and a draining parameter of 0.75. The star functionality plots are displayed in Figure 3.10B.

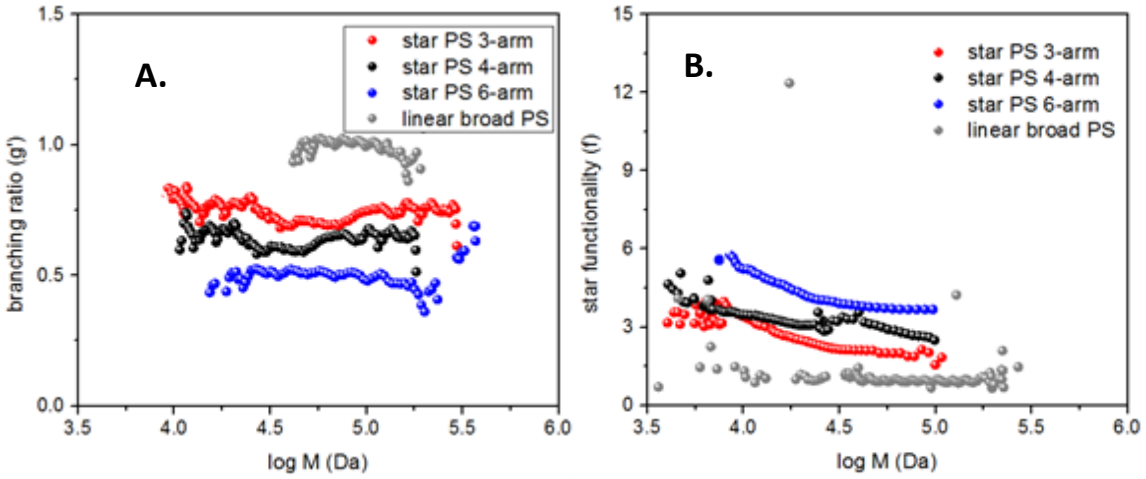

Figure 3.10: Branching ratio, g', as a function of molar mass plots (A) and star functionality plots showing the number of arms, f, as a function of molar mass (B) for the star-shaped and linear polystyrene samples.

The functionalities of the linear polystyrene approached unity as is expected for a linear chain polymer and in line with findings from the calculated branching ratios. It can be argued that Mark–Houwink plot gives information on the extent of branching in a complex polymer mixture relative to a linear analogue in one picture. While neither the g´(M) nor the f(M) plots did not individually give a complete picture of the complex mixtures when compared to the logIV(logM) plots, they provided additional and very useful data to supplement our argument based on the Mark-Houwink exponents. Looking at the more complex six arm PS, the expectation from the shape of the contraction factor - g´(M) plot, and the functionality plots – f(M) plot would be to resemble the log(IV) vs log(M) plot regarding structural variations between the branched and linear species. The synthesis mechanism offered no direct and convenient explanation to the deviation observed. However, in addition to the data scattering at the lower and higher molar mass regime for the g´(M) plot, the experimental consensus surrounding the precise value of the draining parameter may have contributed to the

inconsistent data obtained for the f(M) plot. To verify and eliminate this phenomena, it would be helpful if one considers evaluating the effects of varying the draining parameter on the values of the contraction factor obtained, and therefore, the shape of the g´(M) as well as the f(M) plots. Additionally, the log(M) scales in Figures 3.10A and 3.10B do not represent homogeneous polymer mixtures but weight-average based molecular weights of the linear and star-shaped molecules that have the same chain size. The functionalities of the star-shaped polystyrenes, however, were all distinctively above that of the linear reference. For similar molecular weights, the branching ratio decreases with an increase in chain density approaching unity for linear polymers. [58]

When the dn/dc value is known, the RI signal can be used to determine the concentration and a sample of unknown concentration can be analyzed. Following that, the calculated concentration value is then applied to other detector equations such as the MALS and viscometer which allows for the determination of molecular weight and intrinsic viscosity as shown by Equations 14 and 15.

$$\text{LS output (mV)} = K_{LS} \times Mw \times \left(\frac{dn}{dc}\right)^2 \times \text{Concentration} \quad \textbf{[14]}$$

$$\text{Viscometer output (mV)} = K_{visc} \times IV \times \text{Concentration} \quad \textbf{[15]}$$

Where (***K)*** is the detector constant. The knowledge of the dn/dc value is, therefore, critical because it is the link that translates the raw RI signal to sample concentration. The intrinsic viscosity and refractive index increment (dn/dc) values for the star-shaped polystyrene samples are summarized in Table 3.4.

Table 3.3: Intrinsic viscosity and dn/dc data for the star-shaped and linear polystyrene samples.

Sample	**IV (dL/g)**	**dn/dc**
Broad linear PS	0.561	0.184
Star PS 3-arm	0.226	0.180
Star PS 4-arm	0.191	0.181
Star PS 6-arm	0.165	0.176

The dn/dc values of the star-branched polystyrenes were generally not significantly different from that of the linear polystyrene reference. However, the slight variation of the dn/dc value of the star PS 6-arm compared to the star PS 4-arm, PS 3-arm and the linear analogue can be

attributed to the larger core which might have contributed to a slight chemical composition difference influenced by the RAFT agent structures (which formed the cores), although this deduction is still inconclusive at this stage.

Figure 3.11 shows the plots of the hydrodynamic radius versus elution volume for the star-shaped and linear polystyrene samples. The hydrodynamic radii were determined using intrinsic viscosity data obtained from the online viscometry and molar mass information from MALS. As expected, at similar elution volumes similar hydrodynamic radii for the linear and branched samples are obtained. This confirms that SEC separates according to hydrodynamic size irrespective of molecular topology. [54] From the intrinsic viscosity values in Table 3.5 and the branching information obtained from the conformation plots it is clear, however, that the star-shaped polymers form more compact polymer coils in solution relative to the linear analogue. At very high molar masses (low elution volumes) the data are more scattered and different behaviours are seen for the different stars and the linear reference. This different behaviour will be the subject of future studies.

For the separation of polymers according to properties other than size, e.g. chemical composition or molecular topology, has led to the development of other chromatographic separation methods that include liquid adsorption chromatography (LAC), gradient liquid adsorption chromatography, precipitation–redissolution chromatography and liquid chromatography at critical conditions (LCCC).[59,60] Gradient elution is the method of choice for the separation of samples with wide ranges of molar mass and/or chemical composition. Gradients may be formed either by changing the composition of the mobile phase at isothermal conditions or by running a temperature gradient in isocratic solvent conditions.

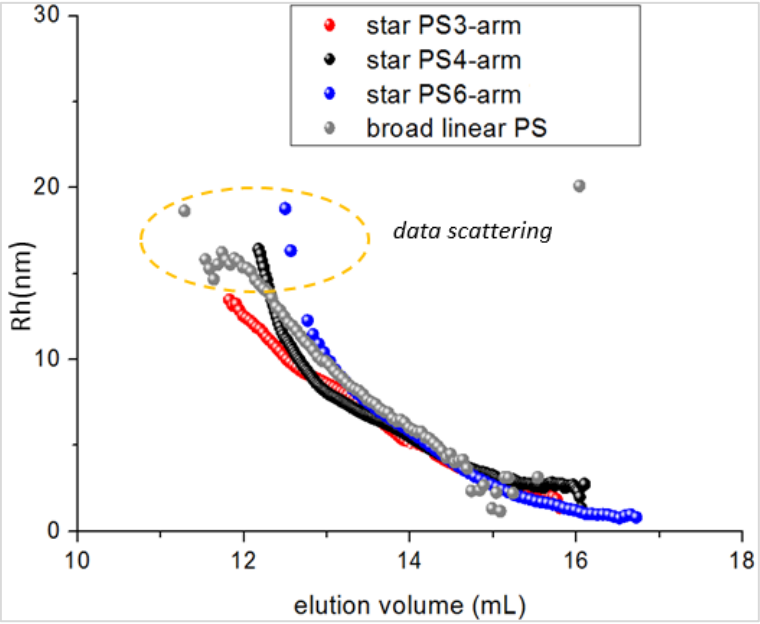

Figure 3.11: Plots of hydrodynamic radius as a function of elution volume.

In this current study, we address the capabilities of solvent gradient interaction chromatography (SGIC) versus temperature gradient interaction chromatography (TGIC) in separating the star-shaped polystyrenes. The motivation of this investigation stems from the need to comprehensively characterize the star-shaped PS in the coordinates of molar mass (SEC) and branching structure (SGIC, TGIC). From a fundamental point of view, the idea was to find out if SGIC or TGIC or both can separate the star samples having similar chemical compositions and molar masses according to the number of arms.

3.6.4 Solvent gradient interaction chromatography

In SGIC the retention is governed by either the interaction strength or solubility. One way of controlling solubility is to change the thermodynamic quality of the mobile phase. Figure 3.12 shows SGIC chromatograms of the crude six-arm, four-arm and three-arm star polystyrene using a reversed stationary phase (Nucleosil C18). A binary solvent gradient of acetonitrile (ACN) and dichloromethane (DCM) was used, where ACN is a poor solvent and DCM is a good solvent for PS. On the C18 column, at high concentration of ACN, the PS interaction with the stationary phase is strong and high molecular weight PS retention is stronger. As the concentration of DCM increases, the retention of PS becomes weak and lower molecular weight PS chains are eluted first. The experimental protocol started with an isocratic step for unretained material including unreacted RAFT agent to elute with the void peak.

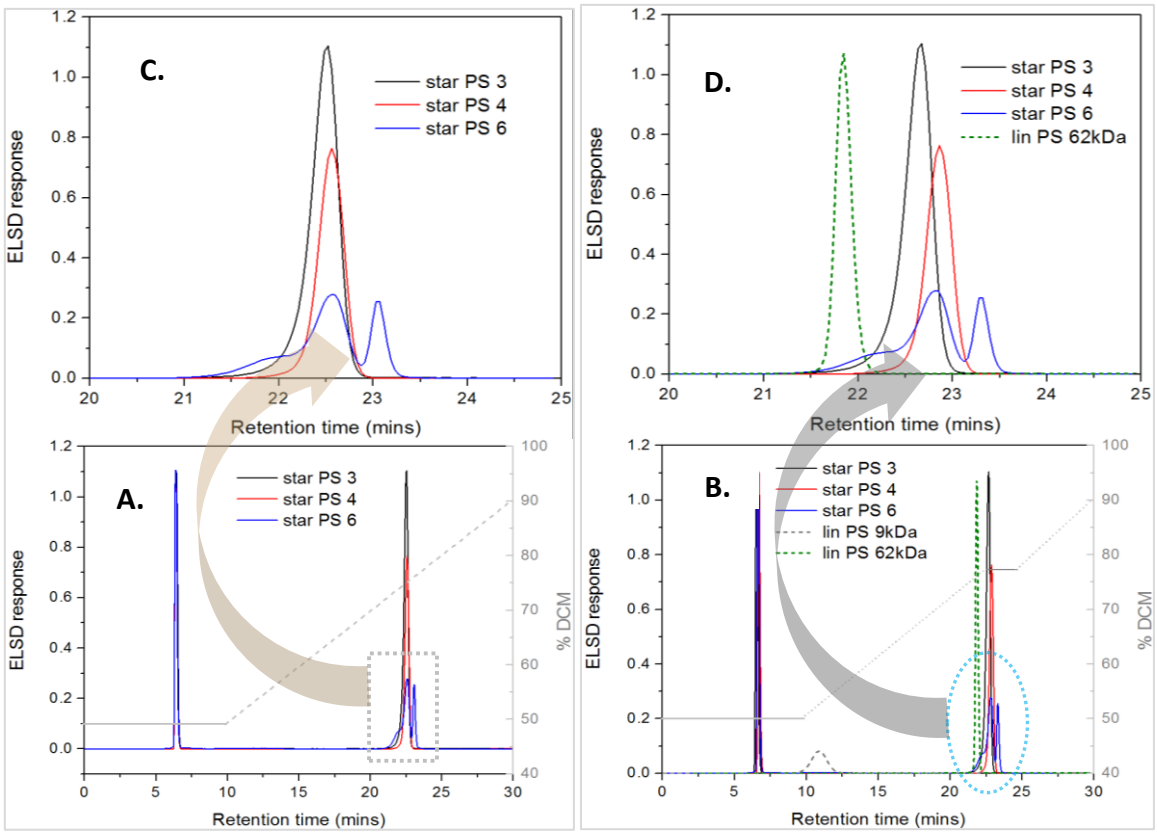

Figure 3.12: RP-SGIC analysis of star PS 3-arm, 4-arm and 6-arm using two different solvent gradients (A and B) and enlarged parts of the chromatograms (C and D).

The polymers were separated first using a linear gradient from 50% to 90% DCM as shown in Figure 3.12A. There was no significant separation between the 3-arm and the 4-arm stars, while the 6-arm star chromatogram displayed some multimodality that was not seen in the SEC chromatograms. This multimodality might indicate the presence of differently branched species as was assumed from the different Mark-Houwink parameters seen in the conformation plot (see Figure 3.9). To increase the resolution, an isocratic step was introduced at the midpoint of the chromatogram, see Figure 3.12B. As can be seen, there was an improvement in the separation between the 3-arm and the 4-arm stars. There was still noticeable peak overlapping between the 3-arm star, 4-arm star and some components of the 6-arm star. The fact that the 2nd peak of the 6-arm star sample co-elutes with the 3/4-arm stars suggests that 3/4-arm stars are formed as by-products in the synthesis of the 6-arm star. Accordingly, the last eluting peak would then be partly assigned to the pure 6-arm star fraction as well as to that of the high molar mass linear by-product in relation to the data obtained from the Mark-Houwink plot of the more complex 6-arm star sample. The application of SGIC as a sub-technique of LAC may still be associated with drawbacks such as co-elution of linear and branched species with similar molar mass. Following this logic, the early eluting fraction would correspond to low molar mass linear by-products. Finally, the

very first eluting peak at about 6.5min is due to unreacted RAFT agent and other low molar mass impurities carried over from synthesis of the polymer. This peak was not present in the standard reference sample.

These findings for the 6-arm star sample agree with the SEC results that indicated coelution of a high molar mass fraction (a_3=0.78) that is attributed to the linear species, a 6-arm fraction (a_2=0.36), and a 3/4-arm fraction a_1=0.48, (see Figure 3.12). The higher the molar mass and/or chain density (number of arms), the longer the sample is retained on the stationary phase. However, a SGIC fraction may still contain species with the same molecular weights but different molecular sizes in solution. According to the SGIC separation results, the complex 6-arm star sample has a composition of 21% of the low molar mass linear species, 46% of the 3 and 4-arm stars and 33% of the 6-arm star as shown in Figure 3.13 (composition based on peak area percentages). Linear polystyrene standards of known molar masses were used in order to identify and ascertain the linear by-products of the star polymers as evidenced in the crude six-arm sample shown in Figures 3.12B and 3.12D.

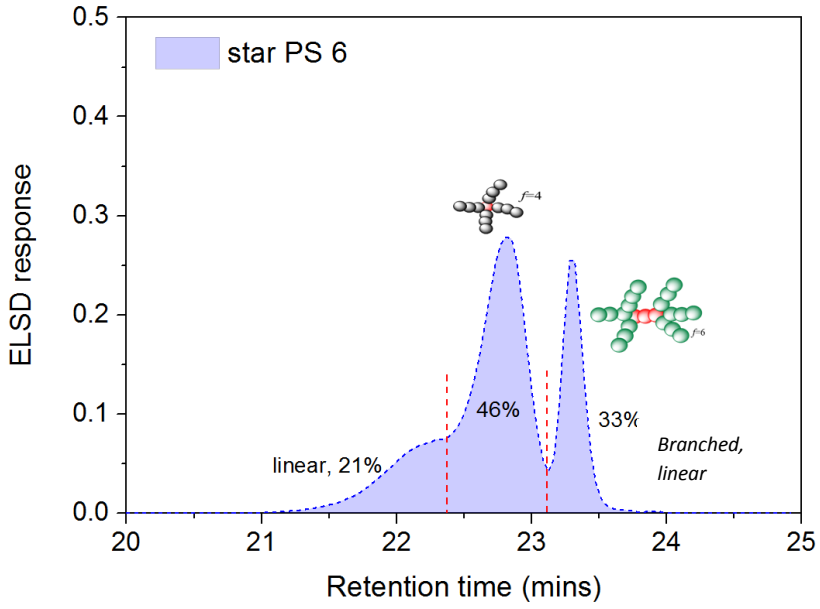

Figure 3.13: SGIC fractionation of six-arm star PS sample and peak area quantification of the individual fractions calculated via peak deconvolution.

The estimated percentages of the eluting species in the more complex 6-arm crude star in Figure 3.13 were solely based on the area under the curve. When using the ELSD detection method, it is difficult to base the signal intensities to structural or chemical composition differences since an ELSD is not an accurate quantitative detection method as would a concentration detector such as the RI or UV detector. In our work, both the SGIC and TGIC

set ups were coupled to the ELSD only, otherwise, it would have been great for comparison and validation had there been a RI or UV detector in the set-ups.

3.6.5 Temperature gradient interaction chromatography

Different from SGIC, retention in TGIC is controlled by adjusting the column temperature via a programmable temperature compartment. [46] The temperature of the column was raised by a ramp from 5 to 50 °C, as shown in the temperature reading for Figures 3.14 and 3.15. To explore all capabilities of TGIC, normal phase (NP) and reversed phase (RP) separations were tested.

Figure 3.14 (A-C) shows overlaid normal phase (NP)-TGIC chromatograms of crude six-arm, four-arm and three-arm star polystyrenes (Figure 3.14A) together with the enlarged parts of the chromatograms (Figure 3.14B). For a successful TGIC analysis of a complex mixture of polymers with a broad molar mass distribution in a single run, the polymer-stationary phase interactions must be weak, therefore, the mobile phase must be near critical conditions. Chang et al. investigated the characterization of various homopolymers by TGIC and established a wide range of critical conditions for different binary solvent systems.[61] For this study, the chosen mobile phase composition was a mixture of n-hexane and tetrahydrofuran at 57:43% by volume. The temperature program was varied in two linear gradients in order to achieve optimum separation of the branched polystyrenes. For comparison, individual injections of the RAFT cores were made under the same NP-TGIC conditions to ascertain the influence of the RAFT agent composition in separating the stars based on polarity (see Figure 3.14C). As can be seen, the unreacted RAFT agents elute at retention times of 8-12 min. In Figure 3.14B the RAFT agents can be detected in addition to the desired star-branched polystyrenes that elute after 15 min. It is also worthy to note that the ELSD signal intensities at the early eluting peaks might be a bit misleading, a case observed in Figure 3.12 for SGIC but more intense for Figure 3.14 and 3.15 for TGIC studies. To begin with, an ELSD as a method of detection is not a reliable source to base concentration information on signal intensities of a complex mixture in which the macromolecules vary regarding composition. In addition to that, during synthesis of the RAFT agents, the resultant products were not collected with 100% purity according to the NMR results. Due to the oily/viscous nature of these products, eliminating the impurities using the standard procedure without losing the integrity of the RAFT agents was difficult. Owing to that, these impurities were carried over into the polymerizations leading to complex crude products which were analysed as collected without further fractionation. There was no separation of the 3-arm and 4-arm stars even with the help of

isothermal steps or a much slower heating rate. This was largely due to the limitation of the interaction strength of the polar cores to the stationary phase.

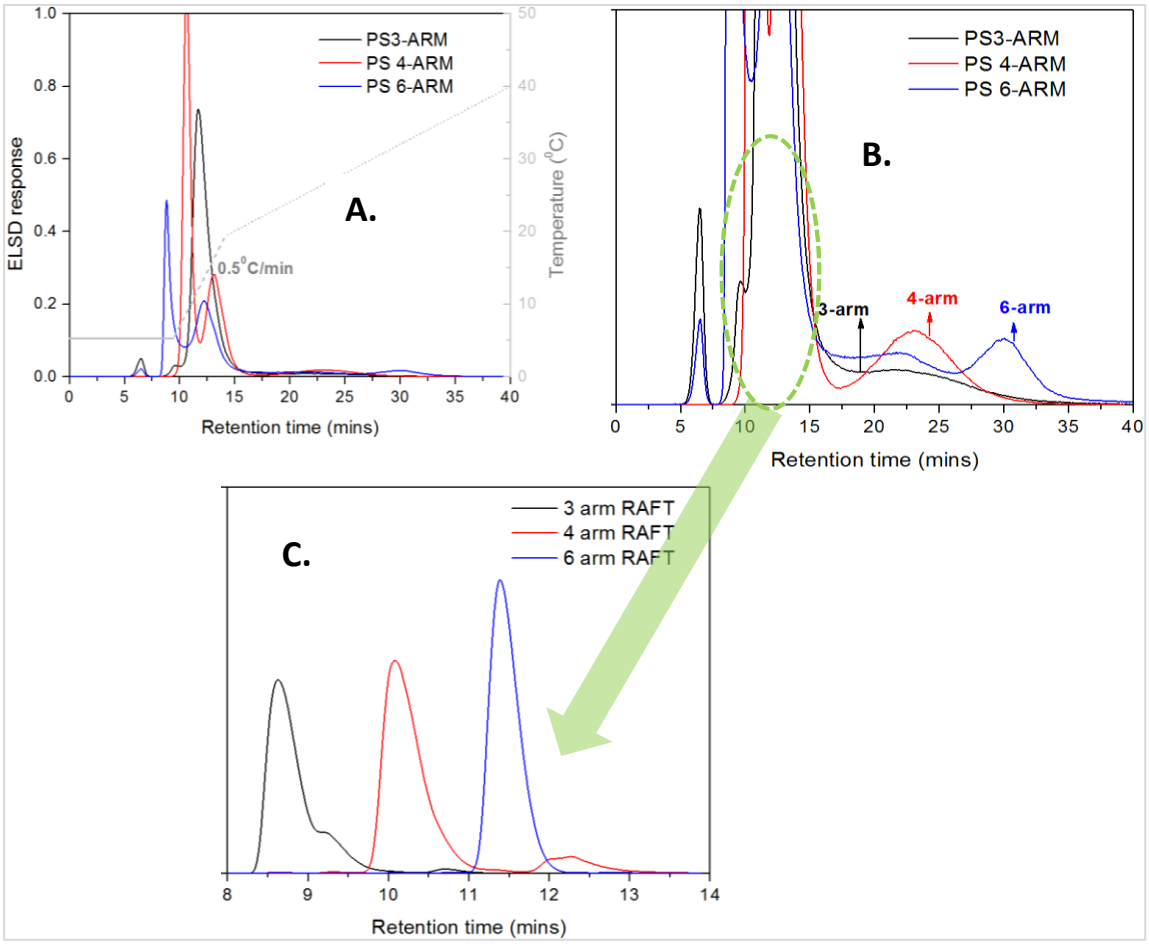

Figure 3.14: NP-TGIC of star-shaped polystyrenes using a linear temperature ramp profile (A) and enlarged parts of the chromatogram in A, (B). Chromatograms of the multiarmed RAFT agents under the same chromatographic conditions used in (A), (C).

The 6-arm star polystyrene eluted significantly later than the 3-arm and 4-arm due to a much more pronounced polarity effect of the larger 6-arm core as shown in Figure 3.14 B. However, the entire NP-TGIC separation was characterized by a rather low resolution of the star molecules. One of the important parameters to vary during a TGIC experiment is the temperature ramp rate. However, temperature alone cannot provide a large enough variation in the interaction strength since the range of temperature variation is limited due to polymer solubility and the boiling of the solvent system. It is, therefore, necessary to try other solvent systems and stationary phases for specific polymer systems of interest to increase the effect of temperature in controlling the retention of the polymers according to their molar mass. [45]

Figure 3.15A-C shows overlaid reversed phase (RP)-TGIC chromatograms of the crude six-arm, four-arm and three-arm star polystyrenes (Figure 3.15A) together with the enlarged parts

of the chromatograms (Figure 3.15B) using a C18 column. The column temperature was raised from 5 to 50 °C in two linear steps. The first step was set at a temperature ramp rate of 0.5 °C/min from 10 to 17 min after the initial isothermal step in order to isolate low molar mass species including the unreacted RAFT agent cores. The second step was set at a ramp rate of 0.3 °C/min to achieve optimum separation of the different star-shaped polymers. The mobile phase was a mixture of acetonitrile and dichloromethane at 43:57 % by volume. The RP-TGIC separation of the PS stars was characterized by broad elution profiles, particularly for the 3-arm and 4-arm star samples. A significant improvement in the separation of the 3-arm and 4-arm stars under the reversed phase conditions was observed, compared to the results that were obtained for NP-TGIC. Individual injections of the RAFT agent cores were also run under the same RP-TGIC conditions (see Figure 3.15C). From the chromatograms in Figure 3.15B, it became clear that the crude samples contain the desired functionalities of 3, 4 and 6 arms. However, as was found before, they were largely contaminated with by-products (RAFT agents) and species of lower functionality including linear macromolecules resulting in lower bulk functionalities of 2.48, 3.14 and 4.47 arms, respectively. These findings agree with the results obtained by ^{1}H-NMR (Section 3.6).

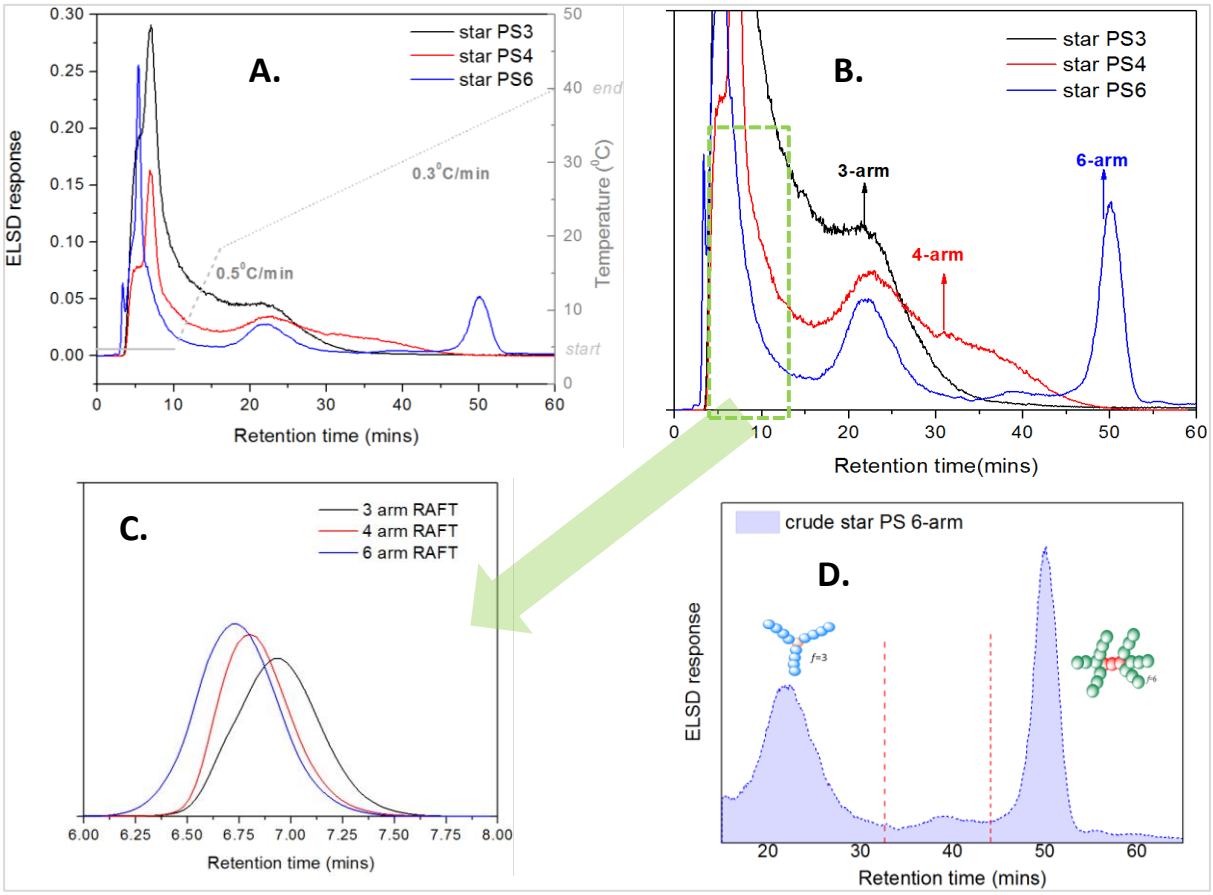

Figure 3.15: RP-TGIC chromatograms of star-shaped polystyrenes (A); enlarged parts of A chromatograms (B); traces of RAFT agents run under the same chromatographic conditions of A, (C); Insert of TGIC chromatogram of star PS 6-arm with peak assignment. (D)

In the TGIC chromatogram of the most complex 6-arm star in Figure 3.15D several peaks are detected that can be assigned to different species. Most obviously, the last eluting peak corresponds to the 6-arm and the peak eluting at roughly 20 min is tentatively assigned to the 3-arm. Between these two elution peaks, another component is seen that can be assigned to the 4-arm (based on the chromatograms of the 3-arm and 4-arm stars). In the 6-arm star sample, the remarkable isolation of the by-products of lower functionality (including the linear molecules) from the desired functionality correlates with what was obtained from the conformation plots in section 3.6.3, validating the merits of further fractionation.

It is worthy to mention that although the choice of Z-RAFT, core first method to prepare star polymers is not the ideal strategy to synthesize "model" and perfect star-branched polymers, our main goal was to prepare regular star polymers that we could use for HPLC (SGIC as well as TGIC) method development. Interestingly, the shortfalls of the Z-group core first approach translated to notable positives for the chromatographic methods employed, in which the by-products from the synthesis were exposed during the separation as well as fractionation steps.

In addition, this was ongoing research based on published works carried out in our research group which highlighted on the practical capabilities of a novel tetrafunctional RAFT agent to prepare star polymers, from which the analytical work of the resultant polymers had not been explored, forming part of the motivation of this current work

3.6.6 Online 2D-TGICxSEC

In principle, comprehensive 2D-LC is the ideal method to determine the molar mass distribution and chemical composition distributions simultaneously. [62-64] Gerber et al. and Radke et al. [65] studied the off-line 2D separations of mixtures of linear and star-shaped polymers using solvent gradient interaction chromatography (TGIC) in the first and SEC in the second dimension. In their work, the star-shaped polymers were mixtures of stars with different numbers of equal arms, hence different molar masses. Gorbunov et al. [66] investigated the theory of topological separation of pure linear and star-shaped polymers by two-dimensional chromatography. In their simulations, the stars were of the same molar mass, but they had different arm numbers. From their theoretical 2D plots there was a significant influence of branching on the adsorption interaction. To the best of our knowledge, the comprehensive HPLC/TGIC analysis of branched polymers has not been reported on extensively. In this present study, the crude stars are of comparable total molar masses and increasing numbers of arms of 3, 4 and 6 arms. Based on the findings in Sections 3.4 and 3.5, we aim to use the merits of 2D-chromatography in which TGIC is the 1st dimension and SEC the 2ndas neither SEC-TD nor another single mode of chromatography (SGIC or TGIC alone) could achieve a full separation of the complex polymers by molar mass and topology. Figure 3.16 A-C shows the 2D-chromatograms of the crude 3-arm, 4-arm and 6-arm stars.

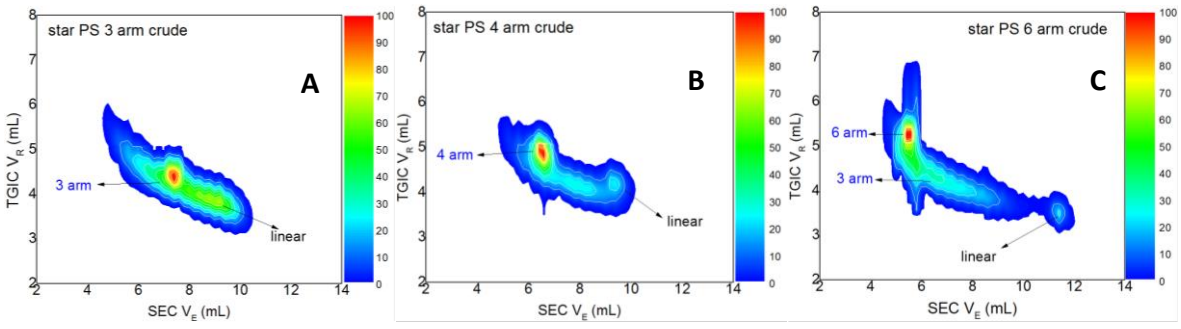

Figure 3.16: 2D RP-TGIC x SEC contour plots of the 3-arm (A),4-arm (B) and 6-arm (C) star-shaped polystyrenes with ELSD detector. Column: C18 250×4.6 Nucleosil 100Å, 5µ.; Mobile phase: DCM/ACN (57:43 %v/v). Temperature ramp rate: linear; 0.1 °C/minute

The 2D contour plots display the improved separation capabilities of the TGIC × SEC method in isolating the 3-arm (Figure 3.16A) star from the 4-arm (Figure 3.16B) and 6 arm stars

(Figure 3.16C) regarding both branching and molar mass. The more complex PS 6-arm crude star further highlighted the efficiency of the TGIC × SEC (2D-LC) method to isolate the by-products in the form of stars and linear molecules of different molar masses. The 2D method showed remarkable separation which correlates with the findings from the conformation plots and average branching data from NMR. The ELSD signals of the early-eluting peaks observed in the 1D-TGIC chromatograms were not the most intense in the 2D chromatograms as shown in Figure 3.16. This was attributed to the variation of the ELSD settings in addition to the sample dilution effects in the 2D experiments.

3.7 Conclusions

The aim of this study was to evaluate the capabilities of different liquid chromatographic methods for the comprehensive analysis of star-shaped polymers. As representative reference samples, star-shaped polystyrenes were prepared that theoretically should have 3, 4 and 6 arms and similar total molar masses. As has been shown, RAFT polymerization produced samples with average arm numbers of 2.8, 3.14 and 4.47, respectively, indicating that instead of pure and homogeneous polymers, very complex mixtures of different star topologies were obtained.

The complex mixtures were analyzed using different HPLC protocols including multidetector SEC, SGIC, TGIC and 2D-LC. The Mark-Houwink (conformation) plots obtained by triple detector SEC with RI-, MALLS- and viscometer detection showed that the slopes of the intrinsic viscosity versus. molar mass functions decreased with increasing numbers of arms signifying the increased polymer coil densities. Branching ratios and star functionalities that were obtained from triple detector SEC agreed with the average functionalities calculated from the NMR results. For the 6-arm star PS sample, at different molar masses Mark-Houwink exponents of 0.78, 0.48 and 0.36 obtained indicated coelution of linear and differently branched species in this complex sample.

SGIC and TGIC experiments proved that the 6-arm star PS sample comprised a significant linear portion in addition to 3-arm, 4-arm and 6-arm star molecules. Improvements in the selectivity of the SGIC and TGIC experiments will enable the strict quantification of these species. Comprehensive 2D-TGICxSEC has been demonstrated to be able to separate the samples according to molecular topology and molar mass and paves the way for more detailed investigations on the molecular composition of differently branched polymers that are prepared by various Reversible deactivation radical polymerization (RDRP) methodologies.

3.8 References

1. J. M. Ren; T. G. McKenzie; Q. Fu; E. H. H. Wong; J. Xu; Z. An; S. Shanmugam; T. P. Davis; C. Boyer; G. G. Qiao. *Chem. Rev.* 2016, **116**: 6743-6836.
2. J. Xu; Q.-y. Qian; J.-l. He; M.-z. Zhang; L.-x. Dai; P.-h. Ni. *Acta. Polym. Sin.* 2018: 356-365.
3. M.-P. Van Den Eede; J. De Winter; P. Gerbaux; J. Teyssandier; S. De Feyter; C. d. Van Goethem; I. F. Vankelecom; G. Koeckelberghs. *Macromolecules.* 2018.**21**, 8689-8697
4. A. Eibel; D. E. Fast; J. Sattelkow; M. Zalibera; J. Wang; A. Huber; G. Müller; D. Neshchadin; K. Dietliker; H. Plank. *Angew. Chem. Int. Ed.* 2017, **56**: 14306-14309.
5. P. Pahl; C. Schwarzenböck; F. A. Herz; B. S. Soller; C. Jandl; B. Rieger. *Macromolecules.* 2017, **50**: 6569-6576.
6. L. Mei; Y. Jiang; S.-S. Feng. *Nanomedicine.* 2014, **9**: 9-12.
7. K. Matyjaszewski; P. J. Miller; J. Pyun; G. Kickelbick; S. Diamanti. *Macromolecules.* 1999, **32**: 6526-6535.
8. A. Gregory; M. H. Stenzel. *Prog. Polym. Sci.* 2012, **37**: 38-105.
9. M. G. Mayadunne R. T. A., Rizzardo E. *Tetrahedron Lett.* 2002, **43**: 6811-6814.
10. R. K. O'Reilly; C. Hansell. *Polymers.* 2009, **1**: 3-15.
11. C. Zhang; Y. Zhou; Q. Liu; S. Li; S. b. Perrier; Y. Zhao. *Macromolecules.* 2011, **44**: 2034-2049.
12. W. Weber; H. Chirowodza; H. Pasch. *Tetrahedron.* 2013, **69**: 2017-2021.
13. T. G. Wright; W. Weber; H. Pfukwa; H. Pasch. *Macromolecules Chem. Phys.* 2015, **216**: 1562-1572.
14. D. Boschmann; P. Vana. *Macromolecules.* 2007, **40**: 2683-2693.
15. C. Barner-Kowollik; T. P. Davis; M. H. Stenzel. *Aust. J. Chem* .2006, **59**: 719-727.
16. Y. S. Ye; W. C. Shen; C. Y. Tseng; J. Rick; Y. J. Huang; F. C. Chang; B. J. Hwang. *Chem. Commun.* 2011, **47**: 10656-10658.
17. Q. Bian; Y. Xiao; M. Lang. *J. Polym. Sci. A: Polym. Chem.* 2012, **50**: 571-580.
18. M. H. Stenzel; L. Zhang; W. T. Huck. *Macromol. Rapid Commun.* 2006, **27**: 1121-1126.
19. D. Boschmann; R. Edam; P. J. Schoenmakers; P. Vana. *Macromol. Symp.* 2009, **275**: 184-196.
20. N. Förster; S. Schmidt; P. Vana. *Polymers.* 2015, **7**: 695-716.
21. N. Förster; A.-C. Pöppler; D. Stalke; P. Vana. *Polymers.* 2013, **5**: 706-729.
22. Y. H. Kim. *J. Polym. Sci. A: Polym. Chem.* 1998, **36**: 1685-1698.
23. N. Li; T. Yan; Z. Li; T. Thurn-Albrecht; W. H. Binder. *Energy Environ. Sci.* 2012, **5**: 7888-7892.
24. E. R. Gillies; J. M. Frechet. *Drug. Discov. Today.* 2005, **10**: 35-43.
25. E. Gungor; G. Cote; T. Erdogan; H. Durmaz; A. L. Demirel; G. Hizal; U. Tunca. *J. Polym. Sci. A: Polym. Chem.* 2007, **45**: 1055-1065.
26. H. Pasch In *New Developments in Polymer Analytics I*; Schmidt, M., Ed.; Springer Berlin Heidelberg: Berlin, Heidelberg, 2000, p 1-66.
27. H. Pasch In *Polymer Analysis Polymer Physics*; Springer Berlin Heidelberg: Berlin, Heidelberg, 1997, p 1-45.
28. D. M. Meunier; Y. Li; W. Gao In *Recent Progress in Separation of Macromolecules and Particulates*; American Chemical Society: 2018; Vol. 1281, p 89-109.
29. C. Gao; D. Yan. *Prog. Polym. Sci.* 2004, **29**: 183-275.
30. A. A. T. D. R. Robello, A. McCovick, A. Kraus, T. H. Mourey. *Macromolecules.* 2002, **35**: 9334.
31. R. Ma; L. Zhang. *J. App. Polym. Sci.* 2007, **103**: 1853-1859.
32. W. Radke; A. H. E. Müller. *Macromolecules.* 2005, **38**: 3949-3960.
33. T. Biela; A. Duda; K. Rode; H. Pasch. *Polymer.* 2003, **44**: 1851-1860.

34. Y. Wang In *Recent Progress in Separation of Macromolecules and Particulates*; American Chemical Society: 2018; Vol. 1281, p 19-30.
35. W. J. Wm.; D. J. F. *J. Chem. Educ.* 2017, **94**. 867-872.
36. A. de Villiers; P. Venter; H. Pasch. *J. Chromatogr. A.* 2016, **1430**: 16-78.
37. H. Maier; F. Malz; W. Radke. *Macromolecules Chem. Phys.* 2015, **216**: 228-234.
38. K. Maiko; H. Pasch. *Macromolecular rapid communications* 2015, **36**: 2137-2142.
39. J. Gerber; W. Radke. *e-Polymers* 2005, **5**. 474-486.
40. S. Lee; H. Lee; T. Chang; A. Hirao. *Macromolecules.* 2017, **50**: 2768-2776.
41. S. Lee; T. Chang. *Macromolecules Chem. Phys.* 2017, **218**: 1700087-97.
42. L. R. Hutchings; S. Agostini; M. E. Oti; J. Keth. *Eur. Polym. J.* 2015, **73**: 105-115.
43. T. Chang. *J. Polym. Sci. B: Polym. Phys.* 2005, **43**: 1591-1607.
44. T. Chang. 2003, In *Liquid Chromatography/FTIR Microspectroscopy/Microwave Assisted Synthesis*, Springer, Berlin, Heidelberg, **163**: p1-60.
45. H. C. Lee, Chang, T. *Polymer.* 1996, **37**: 5747-5749.
46. H. C. Lee, Chang, T. *Macromolecules.* 1998, **31**: 690-694.
47. H. C. Lee, Chang, T. *Polymer.* 2017, **112**: 71-75.
48. P. Kilz; R. Kruger; H. Much; G. Schulz. *Adv. Chem. Ser.*1995, **247**. 223-241.
49. J. Huang; L. Lin; H. Liang; J. Lu. *Polym. Chem.* 2015, **6**: 4020-4029.
50. D. J. Keddie; G. Moad; E. Rizzardo; S. H. Thang. *Macromolecules.* 2012, **45**: 5321-5342.
51. R. Nagarajan. In *Amphiphiles: Molecular Assembly and Applications*. American Chemical Society. 2011, **1070**: p1-22.
52. D. Ida. *React. Funct. Polym* 2018, **130**: 111-117.
53. B. H. Zimm; R. W. Kilb. *J. Polym. Sci.* 1996, **34**: 1367.1367
54. S. Podzimek; T. Vlcek. *J. App. Polym. Sci.* 2001, **82**: 454-460.
55. T. G. Scholte; N. Meijerink; H. Schoffeleers; A. Brands. *J. App. Polym. Sci.*1984, **29**: 3763-3782.
56. S. Ahn; H. Lee; S. Lee; T. Chang. *Macromolecules.* 2012, **45**: 3550-3556.
57. H. Lee; J. Yang; T. Chang. *Polymer.* 2017, **112**: 71-75.
58. J. Ryu; S. Park; T. Chang. *J. Chromatogr. A.* 2005, **1075**: 145-150.
59. H. Pasch. *Polym. Chem.* 2013, **4**: 2628-2650.
60. Y. Wang; A. Masur; Y. Zhu; J. Ziebarth. *J. Chromatogr. A.* 2010, **1217**: 6102-6109.
61. T. Chang; H. C. Lee; W. Lee; S. Park; C. Ko. *Macromol. Chem. Phys.* 1999, **200**: 2188-2204.
62. W. Radke. *J. Chromatogr. A.* 2014, **1335**: 62-79.
63. B. W. J. Pirok; D. R. Stoll; P. J. Schoenmakers. *Anal. Chem.* 2018: **91**240-263
64. F. Vilaplana; R. G. Gilbert. *Macromolecules.* 2010, **43**: 7321-7329.
65. J. Gerber; W. Radke. *Polymer.* 2005, **46**: 9224-9229.
66. A. A. Gorbunov; A. V. Vakhrushev. *Polymer.* 2009, **50**: 2727-2735.

4.

Multidimensional liquid chromatography analysis of highly branched and miktoarm star polymers prepared by Williamson coupling reactions[2]

Authors TBD

Abstract: A comprehensive analysis of branched block copolymers was accomplished using temperature gradient interaction chromatography (TGIC) and solvent gradient interaction chromatography (SGIC) to demonstrate and contrast the resolving potential of the two interactive modes of liquid chromatography and to evaluate their application in comprehensive two-dimensional liquid chromatography (2D-LC). Although branching has a notable effect on the size of macromolecules in solution, a significant characterization challenge for conventional size-sensitive methods such as size exclusion chromatography (SEC) arises from the fact that high molar mass branched macromolecules may co-elute with low molar mass linear macromolecules. This challenge can be overcome by using two-dimensional liquid chromatography which integrates interactive and size separation mechanisms in one analytical experiment. The comparison between TGIC and SGIC as the interactive modes was made using model star-branched polybutadiene, hyperbranched polybutadiene-polystyrene (PBd-PS) and mikto-arm star-branched polystyrene-polyisoprene. Each polymer system was characterized by both 2D SGIC x SEC and 2D TGIC x SEC. Fractions from the more complex hyperbranched PBd-PS were further analysed by ^{1}H-NMR for structural elucidation.

Keywords: Branching analysis. Multidimensional liquid chromatography. Miktoarm star polymers. Hyperbranched polymers. Polybutadiene. Polystyrene. Polyisoprene.

4.1 Introduction

Synthetic branched polymers are usually not molecularly homogeneous but often complex mixtures with distributions in molecular characteristics such as chemical composition, molar mass, degree of branching, and functionality.[1-6] These parameters strongly affect the bulk and solution properties of the resultant polymeric products and, therefore, understanding the structure-property relationships of these complex mixtures is vital for the polymer chemist.

[2] Manuscript to be submitted to Polymer Chemistry

To meet this aim, the synthesis of model polymers with controlled molecular characteristics that include chain branching is an area of ongoing interest. The design and characterization of various model branched polymers with well-defined molecular architectures such as star and miktoarm star[7,8], dendritic[6], comb-shaped[9] and hyperbranched polymers[10] has contributed much insight to the understanding of structure-property correlations of branched polymers. In particular, the synthesis and characterization of highly branched block copolymers has been an intense research subject due to the formation of ordered nanophases that can be used as templates for various applications in nanotechnology, in structural materials such as thermoplastic elastomers or high impact polymers.[11]

In this study, two branched block copolymer architectures were chosen to investigate the analytical capabilities of multidimensional liquid chromatography techniques, namely (i) a miktoarm star polymer comprising polystyrene and polyisoprene arms (miktoarm star PS-$(PI)_2$), and (ii) a complex long-chain hyperbranched copolymer (hyperbranched PBd-PS) prepared from a mixture of polystyrene and polybutadiene building blocks synthesized by living anionic polymerisation and coupled via a Williamson coupling reaction. Such materials are branched analogues of an industrially relevant class of synthetic rubbers based on triblock copolymers of styrene-butadiene-styrene (SBS) and styrene-isoprene-styrene (SIS). Such materials exhibit the elasticity and resilience of polybutadiene or polyisoprene along with the permanence of the fixed ends of polystyrene segments. SBS and SIS are easily processed and reprocessed owing to the thermoplastic properties of polystyrene, and they are remarkably strong at room temperature. These properties allow them to be used for applications that include injection-moulded parts, hot-melt adhesives or additives to improve the properties of bitumen. In addition to these model copolymers, homopolymer 3-arm and 4-arm star polybutadienes were characterised.

The current investigation based on “model” branched polymers to investigate the capabilities and limitations of multidimensional liquid chromatography shall contribute to providing more detailed information on the molecular heterogeneity of these complex structures and in turn support studies on structure-property correlations.

There is a variety of experimental protocols which are used for the synthesis of model branched polymers. These typically involve the use of living or controlled polymerisation techniques to produce linear polymer segments which are subsequently joined using different coupling strategies.[12-15] A number of key strategies have been summarised previously. [16] Briefly, the branched polymers studied in the current investigation are prepared using anionic

polymerisation, a truly living polymerisation which provides the gold standard in control over molar mass and molar mass dispersity. 3- and 4-arm polybutadiene star polymers are formed by reaction of the living polymer chain ends with an appropriate multifunctional chlorosilane according to previous reports.[17-20] The PS-$(PI)_2$ miktoarm star and polystyrene-polybutadiene hyperbranched polymers are prepared by the "macromonomer" approach in which linear polymer precursor chains – macromonomers – are produced by a living or controlled (preferably anionic) polymerisation. The macromonomers carry reactive functionalities either at the chain end or along the polymer chain, to allow the macromonomers to be linked together via a chosen coupling strategy, to produce the desired branched architecture. This approach has previously been used by Hutchings (and others) for the synthesis of a variety of branched architectures.[11,21-23] Typically, among the different synthetic approaches developed for the preparation of end-functionalized polymers with well-defined structures as described in the literature, [24-29] living ionic polymerization is still the leading standard method employed.[6,30-34] The resultant polymeric arms are usually end-functionalized with reactive groups such as azides, alcohols or halides and then efficiently coupled via azide coupling, click coupling or Williamson coupling reactions.[16,35,36]. Due to the simplicity of the reaction steps, the method is a versatile route to prepare model branched and highly branched polymers.[37]

Although the synthesis of complex branched (co)polymers is commonplace, there are still significant deficiencies in the characterization of complex branched polymers. The aim of this investigation is to design and develop a multidimensional analytical strategy of characterization which combines advanced liquid chromatographic methods for the fractionation of model regular star-branched, miktoarm star-branched and hyperbranched polymers. It is anticipated that only a multidimensional characterization approach can achieve the required comprehensive and accurate separation and characterization of complex polymer mixtures with a focus on composition, molar mass and degree of branching.

For the characterization of complex polymers with multivariate distributions, the separation of polymeric species with respect to one molecular parameter would be a great starting point. While size exclusion chromatography (SEC) is very effective in some cases, it is not sufficiently selective to isolate multiple branching distributions with similar molecular sizes. It is well known that SEC is unable to accurately and fully characterize the molar mass distribution (MMD) of copolymers or branched polymers since there is no simple correlation between the molecular size in solution and the molar mass of polymer chains which differ in chemical composition, functionality and/or chain architecture. Porous HPLC column packing

materials (e.g. porous silica) can be used for both SEC and interaction chromatography (IC) separations depending on the choice of separation conditions applied. Different mechanisms may be operative depending on whichever mode plays a dominant role (size exclusion or interaction). If the SEC mode is operative, the exclusion effect dominates over the interaction effect and polymers elute before the injection solvent peak in decreasing order of molecular size. When the exclusion effect is exactly balanced by the interaction effect, all polymers elute near the injection solvent peak independent of molecular size and this is known as the critical point of adsorption. If the IC mode plays a dominant role, the interaction effect exceeds the exclusion effect and polymers elute after the injection solvent peak and in increasing order of molar mass. Each of these separation mechanisms have their own merits and limitations. In many instances, a single separation mode cannot provide conclusive information and a coupling of two one-dimensional LC separation modes into an online two-dimensional LC (2D-LC) set-up with the appropriate characterization methods can give comprehensive analysis on the molecular heterogeneity of the sample, in a single run. Among the available chromatographic techniques used to isolate (by)products of complex polymer mixtures, IC has been used effectively to separate homopolymers from copolymers.[38-41]. The combination of various separation and characterization techniques in 1D and 2D separation modes in order to analyse complex mixtures based on different molecular heterogeneities has been well investigated.[42-47]. In an interesting example of the application of solvent gradient IC (SGIC) in both 1D and 2D modes, Maiko et al. isolated various polybutadiene samples based on their respective microstructures.[48]. More recently, Chang et al. and Lee et al. conducted significant work on the separation of various polymers by Temperature gradient IC (TGIC) in 1D and 2D separation modes according to different molecular heterogeneities including polymer block length and size.[49-53]

The focus of the present study is on the comparison between the separation capabilities of SGIC and TGIC in both 1D and 2D-modes. To the best of our knowledge, there is very little work done on the comprehensive analysis of branched polymers using liquid chromatographic techniques in combination with spectroscopic techniques. In a series of publications on polymer separations using hyphenated techniques, Hiller et al. and Hehn et al. reported extensive work on HPLC-NMR.[54-56] In the current study, normal-phase (NP) and reversed-phase (RP) IC is used for chemical composition separation. Fractions are collected and subjected to ^{1}H-NMR for structure elucidation. Depending on the specific sample, SGIC and TGIC might provide different results and, for the first time, a comprehensive investigation of SGIC and TGIC as the primary IC separation technique subsequently coupled to SEC in the

second dimension is presented for resolving the different molecular heterogeneities of complex branched copolymers.

4.2 Experimental

Materials

Isoprene (Sigma-Aldrich; 99%, contains <1000 ppm p-TBC), benzene (Aldrich, HPLC grade, ≥99%), styrene (Sigma–Aldrich, ≥99%), dichloromethane (DCM) (in-house solvent purification) and toluene (Sigma-Aldrich; 99%) were dried with calcium hydride (Acros; ca. 93%, 0-2 mm grain size), degassed by a series of freeze-pump-thaw cycles and stored under high vacuum. 1,3-Butadiene (Sigma-Aldrich, 99%) was dried and purified by passing successively through columns of Carbosorb (Sigma-Aldrich), to remove any inhibitor, and molecular sieves, to remove moisture. Tetrahydrofuran (THF) (Fisher ≥99.9 %) was dried and degassed over sodium (Fisher; metal sticks in liquid paraffin) and benzophenone (Sigma-Aldrich; ≥99%) by freeze-pump-thaw cycles until the solution turned purple. *Sec*-Butyllithium (*s*-BuLi) (1.4 M solution in cyclohexane), N, N, N'N'-tetramethyl ethylenediamine (TMEDA), 2-bromoethanol (95%), triphenylphosphine (PPh_3), cesium carbonate, triphenylphosphine, carbon tetrabromide (CBr_4) (99%), all Sigma–Aldrich, were used as received. Methanol (AR grade) and hydrochloric acid (HCl) (37 wt.%) (both Fisher Scientific) were used as received. Ethylene oxide (EO) (Sigma-Aldrich; ≥99.5%) was dried and purified by passing through columns of Carbosorb (Sigma-Aldrich) onto calcium hydride, before stirring at 0 °C for 30 minutes. Dimethyl formamide (DMF) (Sigma–Aldrich 99.8%) was stored over molecular sieves (Sigma–Aldrich) under inert atmosphere. 1,1-Bis(4-*tert*-butyldimethylsiloxyphenyl) ethylene (DPE-OSi) was synthesized in two steps from dihydroxy benzophenone (Sigma-Aldrich, 99%) according to the procedure of Quirk and Wang as shown in Figure 4.1.

The synthesis of all polymers (building blocks) was carried out via anionic polymerization using standard high vacuum techniques and trap-to-trap distillation by the co-authors in Professor Lian Hutchings' research group at the Centre for Soft Matter, University of Durham, United Kingdom. I prepared the hyperbranched block copolymers and the miktoarm star polymers via the Williamson coupling reactions, under the guide of one of the co-authors, then went on to do the rest of the analytical work.

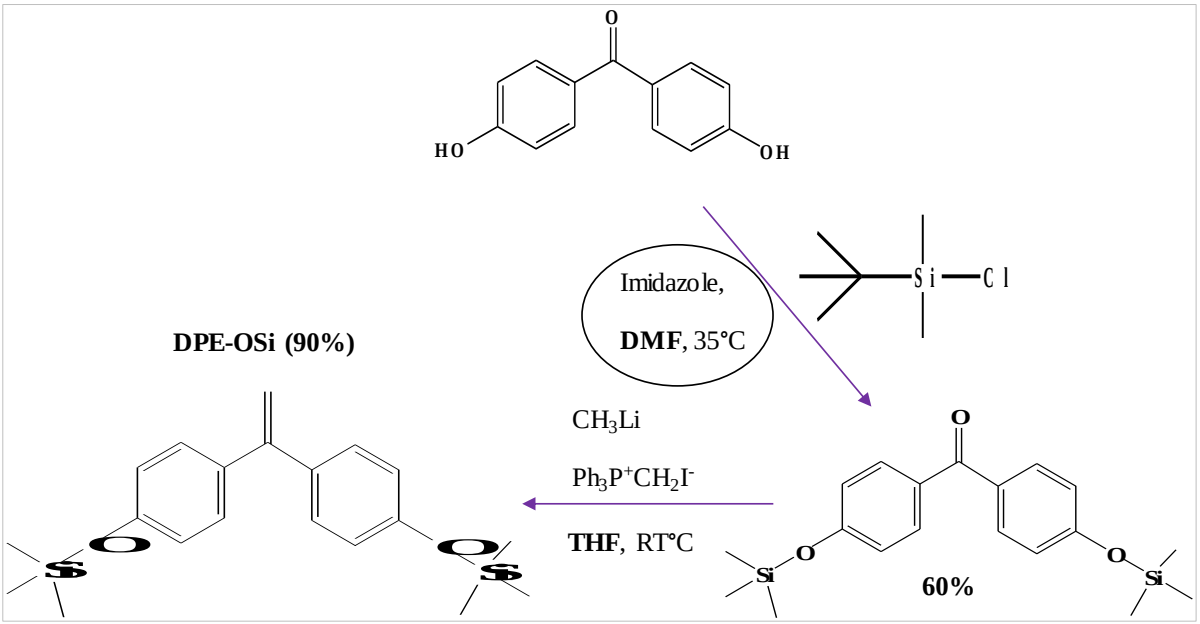

Figure. 4.1: Synthesis of bis(4-*tert*-butyldimethylsiloxyphenyl)ethylene (DPE-OSi) according to the procedure of Quirk and Wang. [57]

4.2.1 Synthesis of Polybutadiene Crossbars – PB-(OH)$_4$

DPE-OSi (0.69 g, 1.25 mmol) was added to the reaction vessel and azeotropically dried three times with benzene, then dissolved in freshly distilled benzene (250 mL) and the solution freeze-pump-thawed for further purification. The vessel was raised to atmospheric pressure with dry nitrogen. *s*-BuLi was added dropwise (to titrate out any residual impurities) until a red colour persisted and a final addition of 0.89 mL *s*-BuLi (1.25 mmol) was added by injection. The solution was stirred at room temperature for 24 hours before butadiene (24.03 g, 444 mmol) was distilled into the reaction vessel. The reaction was allowed to stir at 50 °C for 24 hours, after which a purified solution of DPE-OSi (0.83 g, 1.87 mmol) and TMEDA (0.38 mL, 2.5 mmol) in benzene (5 mL) was injected into the polymerisation mixture and the polymer solution stirred at 50 °C for a further 5 days before being terminated with nitrogen-sparged methanol. The polymer was precipitated into methanol, dissolved in THF, precipitated again into methanol, collected and dried under vacuum. The deprotection of the phenol groups was performed by dissolving the polymer (23.55g, 1.04mmol) in THF and adding HCl (4.2 ml, 41.7 mmol) in 10:1 ratio with respect to the phenol groups. Yield 96%. M_n 22 600 g mol^{-1}, M_w 23 500 g mol^{-1}, Đ 1.04; see Figure 4.3 for the reaction scheme.

PB-(OSi)$_4$: ^{1}H-NMR (400 MHz, $CDCl_3$, δ): 7.1–6.6 (16H, Ar **H**), 5.7−5.5 (−CH_2CHC**H**=CH_2), 5.5−5.3 (−CH_2C**H**=C**H**CH_2−), 5.1−4.9 (−CH_2CHCH=C**H**$_2$), 2.2−1.8 (−C**H**$_2CH$=CHC**H**$_2$−), 2.2−1.8 (−CH_2C**H**CH=CH_2), 1.4−1.2 (−C**H**$_2CHCH$=CH_2), 1.0–0.9 (36H, (C**H**$_3)_3$C-Si), 0.2–0.1 (24H, (C**H**$_3)_2$Si).

PB-$(OH)_4$: ^{1}H-NMR (400 MHz, $CDCl_3$, δ): 7.1–6.6 (16H, Ar **H**), 5.7−5.5 ($-CH_2CHC\mathbf{H}=CH_2$), 5.5−5.3 ($-CH_2C\mathbf{H}=C\mathbf{H}CH_2-$), 5.1−4.9 ($-CH_2CHCH=C\mathbf{H}_2$), 2.2−1.8 ($-C\mathbf{H}_2CH=CHC\mathbf{H}_2-$), 2.2−1.8 ($-CH_2C\mathbf{H}CH=CH_2$), 1.4−1.2 ($-C\mathbf{H}_2CHCH=CH_2$).

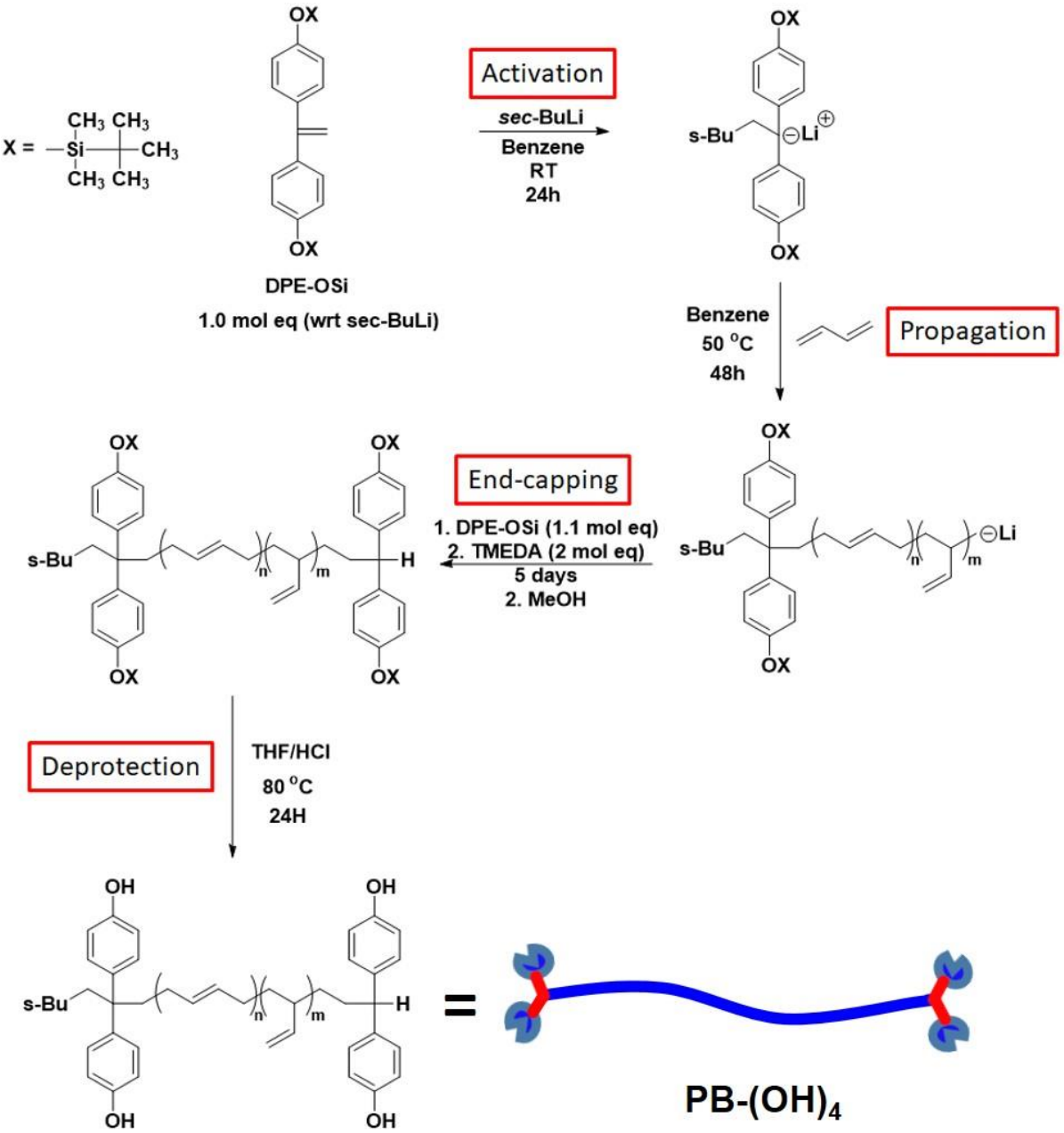

Figure 4.2: Synthesis of Polybutadiene "crossbar" macromonomer (PB-$(OH)_4$). [58]

The linear components (arms and macromonomers) of all the branched polymers and star polybutadienes studied in the current investigation were prepared by colleagues in Professor Lian Hutchings's research group at Durham University via living anionic polymerisation using standard high vacuum techniques. As part of my PhD exchange research work in

Professor Lian Hutchings' research group, I prepared the miktoarm star as well as hyperbranched block copolymers via classical coupling reactions.

4.2.2 Synthesis of 3 and 4-arm polybutadiene stars

Polybutadiene stars were prepared via the arm-first approach according to well-known procedures. [59,60] Briefly, the arms were prepared by living anionic polymerisation, initiated by butyllithium in benzene, and following complete conversion a suitable multifunctional chlorosilane – trichloromethylsilane and tetrachlorosilane for 3 and 4-arm stars, respectively – was added to couple the arms. Following recovery of the crude polymer, any unreacted arm was removed by fractionation using toluene and methanol as the solvent/non-solvent mixture. The molar masses of each arm and purified star are given in Table 4.1.

Table 4.1: SEC data for the linear arm precursors together with the 3-arm star (Star(3)150) and 4-arm star (Star(4)130) polybutadienes

Polymer	Target M_n ($x10^3$ g/mol)	M_n ($x10^3$ g/mol)	M_w ($x10^3$ g/mol)	Đ
Star(3)150_Arm	50	53	56	1.05
Star(3)150_Crude	150	123	142	1.16
Star(3)150_Pure	150	148	151	1.02
Star(4)130_Arm	30	33.6	34.6	1.03
Star(4)130_Crude	136	109.2	123.4	1.16
Star(4)130_Pure	136	134.2	138.4	1.03

4.2.3 Synthesis of PS-$(PI)_2$ miktoarm star

The term miktoarm star derives from the Greek word for *mixed* and was initially coined by Hadjichristidis to describe a star comprising of three chemically different polymer arms. [61] The term is now commonly associated with the synthesis of star-branched polymers comprising of arms of either different chemical composition or molar mass. In the current study a single miktoarm star polymer was investigated, which comprised of one polystyrene arm and two polyisoprene arms. Once again, the arms were prepared by living anionic polymerisation to produce macromonomers which were coupled via a Williamson coupling reaction as shown in Figure 4.4.

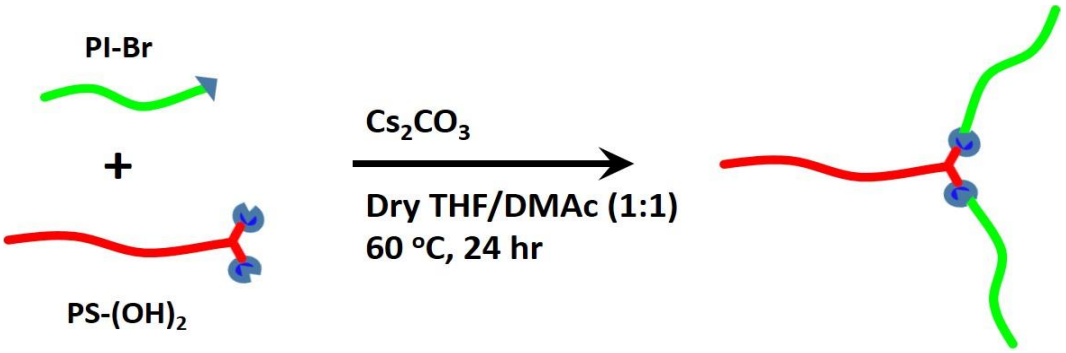

Figure 4.3: Reaction conditions for the synthesis of PS-$(PI)_2$ mikto arm star

4.2.4 Synthesis of PS-$(OH)_2$ and PI-Br_2 macromonomers

The polystyrene macromonomer (PS-$(OH)_2$) was prepared by end-capping living polystyryllithium with bis(4-*tert*-butyldimethylsiloxyphenyl) ethylene (DPE-OSi) followed by deprotection of the two phenol groups by mild acid hydrolysis, according to a previously published procedure (Figure 4.5; Yield 87%. M_n 6 200 g mol^{-1}, M_w 6 400 g mol^{-1}, Đ 1.03).[37] The polyisoprene macromonomer was prepared from living polyisoprenyl lithium in two steps. The living chain-end was firstly capped with excess ethylene oxide and quenched with methanol/HCl_{aq} and in a second step the resulting primary alcohol was converted into an alkyl bromide according to a procedure previously reported for the Bromination of an OH end-capped polystyrene macromonomer (Yield 93%. M_n = 4 000 g·mol^{-1}, M_w = 4 200 g·mol^{-1}; Đ = 1.05).[62]

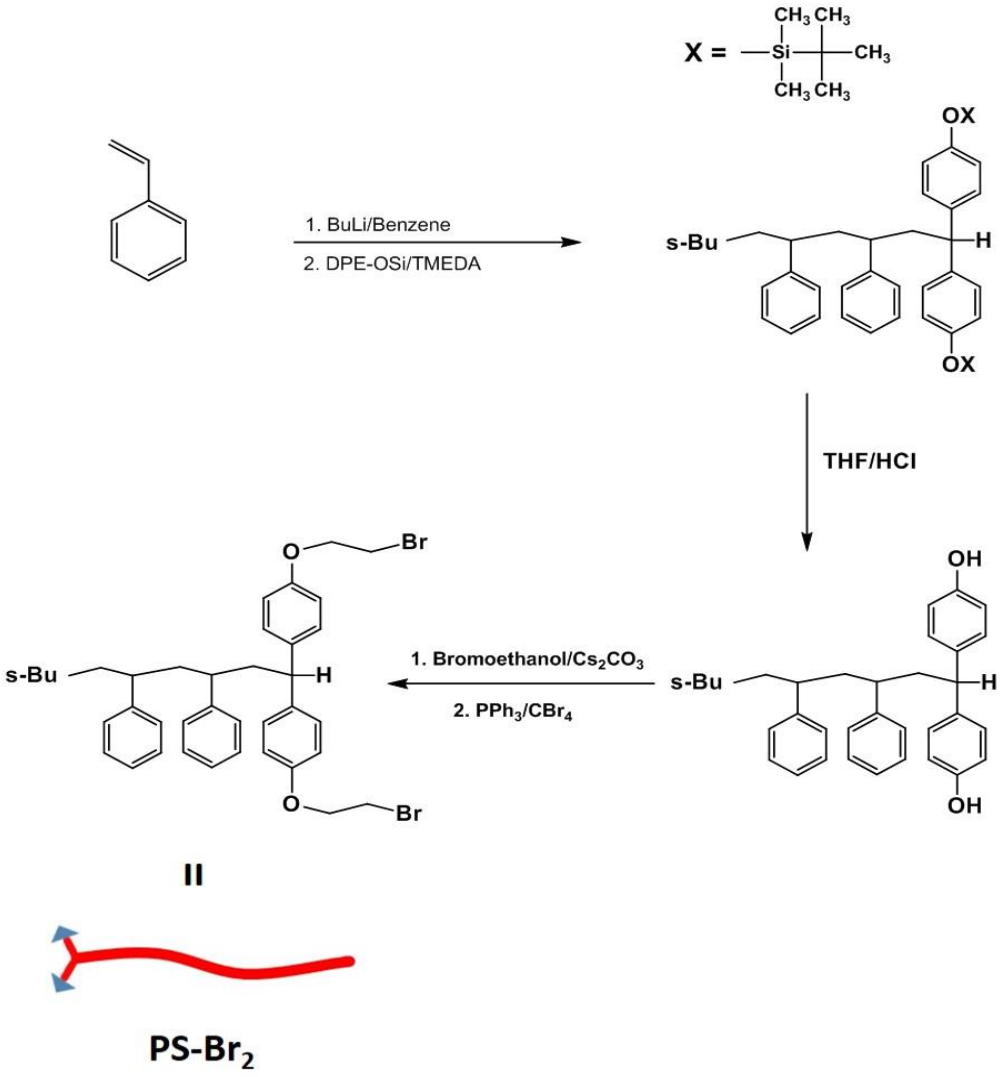

Figure 4.4: Synthesis of Polystyrene macromonomers (PS-$(OH)_2$ and conversion to PS-Br_2)

4.2.5 Synthesis of PS-PBd Hyperbranched Block Copolymer

A sample of hyperbranched block copolymer was prepared by the Williamson coupling of PB-$(OH)_4$, a polybutadiene macromonomer end-capped at each chain end with DPE-OSi and deprotected, and a polystyrene macromonomer PS-Br_2, see Figure 4.6. Reaction schemes illustrating the synthesis of both the macromonomers are reported in. Figure 4.3 and 4.5.

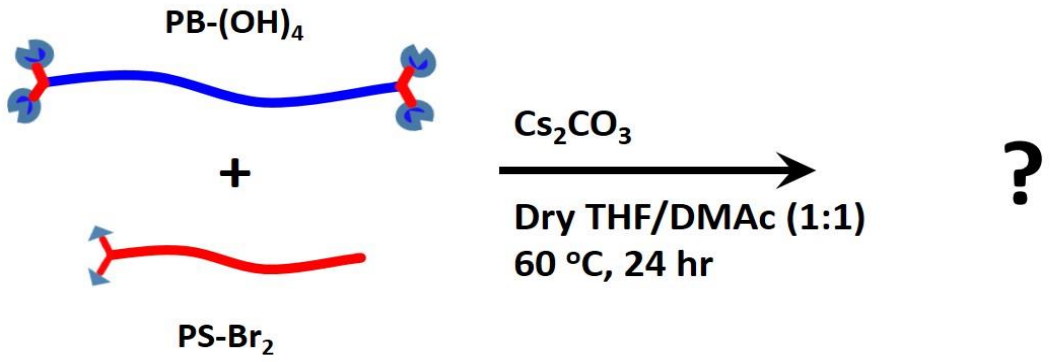

Figure 4.5: Synthesis of PS-PBd Hyperbranched Block Copolymer

4.3 Analytical techniques

4.3.1 ^{1}H-NMR

The dried samples were dissolved in deuterated chloroform ($CDCl_3$; Merck, Darmstadt, Germany ≥ 99.96% D). The signals were recorded on a Varian Unity INOVA 400 MHz spectrometer with a 5mm Dual broadband PFG probe (Agilent Technologies, Santa Clara, USA) by averaging 32 scans with a 0.5 μsec pulse delay.

4.3.2 Size exclusion chromatography (SEC)

Triple detection size exclusion chromatography (SEC) with refractive index (DRI), viscosity, and right-angle light scattering (RALS) detectors was used for the analysis of molar mass and molar mass distributions of the macromonomers, using a Viscotek TDA 302 system (Malvern PANalytical, Royston, United Kingdom). Tetrahydrofuran was used as the eluent at a flow rate of 1.0 mL/min and at a temperature of 35 °C. Separations were achieved using 2 × 300 mm PLgel 5 μm mixed C-columns (Agilent Technologies, Waldbronn, Germany). A value of 0.185 mL/g was used as the dn/dc of polystyrene, 0.130 mL/g for polyisoprene and 0.124 mL/g (measured in house) was used as the dn/dc of polybutadiene. Each solution contained 3 mg/mL of the sample in order to obtain a good signal-to-noise ratio. Molar mass analysis was carried out with OmniSEC software (Malvern PANalytical, Royston, United Kingdom).

4.3.3 Temperature gradient interaction chromatography (TGIC) and solvent gradient interaction chromatography (SGIC)

1D-TGIC and 1D-SGIC experiments were carried out on an Agilent 1200 HPLC instrument (Agilent Technologies, Waldbronn, Germany) comprising the following: autosampler, on-line degasser, quaternary pump unit and a thermostated column compartment. The HPLC system

was equipped with a C18 bonded silica column (Macherey-Nagel, Nucleosil C18, 100 Å pore size, 250 × 4.6 mm I.D, 5 µm particle size) for reversed phase IC and a bare silica column (Macherey-Nagel, Nucleosil, 100 Å pore size, 250 × 4.6 mm I.D, 5 µm particle size) for normal phase IC. The polymer samples were dissolved in a portion of the mixed eluent at a concentration of 2 and 0.5 mg/mL and an injection volume of 100 and 30 µL for TGIC and SGIC, respectively. The column temperature was controlled via a programmable heated bath circulator through home-made fluid column jackets for the TGIC set-up. The chromatograms were recorded and processed on the PSS WinGPC Unichrom software (8.2). An ELSD (Agilent 1260 Infinity; Agilent Technologies, Les Ulis, France) was used as the detector at a temperature of 100 °C and a gain of 8.

4.3.4 2D Liquid chromatography analysis (2D-LC)

For 2D RP-SGIC or 2D RP-TGIC experiments, the IC first dimension separation with respect to chemical composition or topology was carried out on the Nucleosil bare silica and Nucleosil C18 bonded columns, respectively, with the specifications mentioned above (see section 4.3.3) at varying flow rates and linear solvent gradient ramp rates depending on the sample batch under study. The SEC second dimension separated according to hydrodynamic volume using THF as the eluent on a styrene-divinylbenzene (SDVB; PSS Polymer Standards Service GmbH, Mainz, Germany) stationary phase with the following dimensions: 5 µm particle size, 50 mm length and 20 mm internal diameter, also with varying flow rates. An evaporative light scattering detector (ELSD, Agilent 1260 Infinity, Agilent Technologies, Les Ulis, France) was used as the detector at a temperature of 100 °C and a gain of 8 for all runs. The coupling of SGIC or TGIC and SEC was achieved by an electronically controlled eight-port valve EC8 W (VICI VALCO instruments, Texas, USA) equipped with two 200 µL loops. After the initial injection (100 µL), fractions from the first dimension were transferred into the second dimension at specific times in order to inject 200 µL of eluent from the first dimension into the second dimension. The sample concentration for the 2D-LC experiments was ≈ 3mg/mL for all runs.

4.4 Results and discussion

Although some of the attempted reactions are novel – specifically the synthesis of the hyperbranched block copolymer – the general approaches have been reported previously.[59,60]

TGIC and SGIC have both been widely used to separate and characterise various complex polymeric mixtures. Both separation techniques have demonstrated potential advantages as

well as disadvantages depending on the specific polymer structures to be fractionated. For the comprehensive analysis of complex polymers, however, the use of either TGIC or SGIC as stand-alone methods may not be sufficient for some samples and 2D liquid chromatography shall be employed as was highlighted in a previous review.[64] In this work, the aim is at using both TGIC and SGIC in 1D- and 2D-modes to separate the branched samples with regard to molar mass, block composition and size (branching), and to contrast the resolution capabilities of both methods.

4.4.1 Star polybutadiene

Size Exclusion Chromatography

The SEC chromatograms for the 3-arm and 4-arm star polybutadienes before and after fractionation cycles are shown in Figure 4.7. Both stars contain traces of the arm still present before fractionation, with the small arm peaks visible at 12.8 mL for the 3-arm star (Figure 4.7A) and at 13.2 mL for the 4-arm star (Figure 4.7C). After three cycles of fractionation for both crude polymers using a RI detector, SEC analysis indicated the total removal of excess arm polymer and the purification of the crude star polymer was completed (Figure 4.7B and 4.7D).

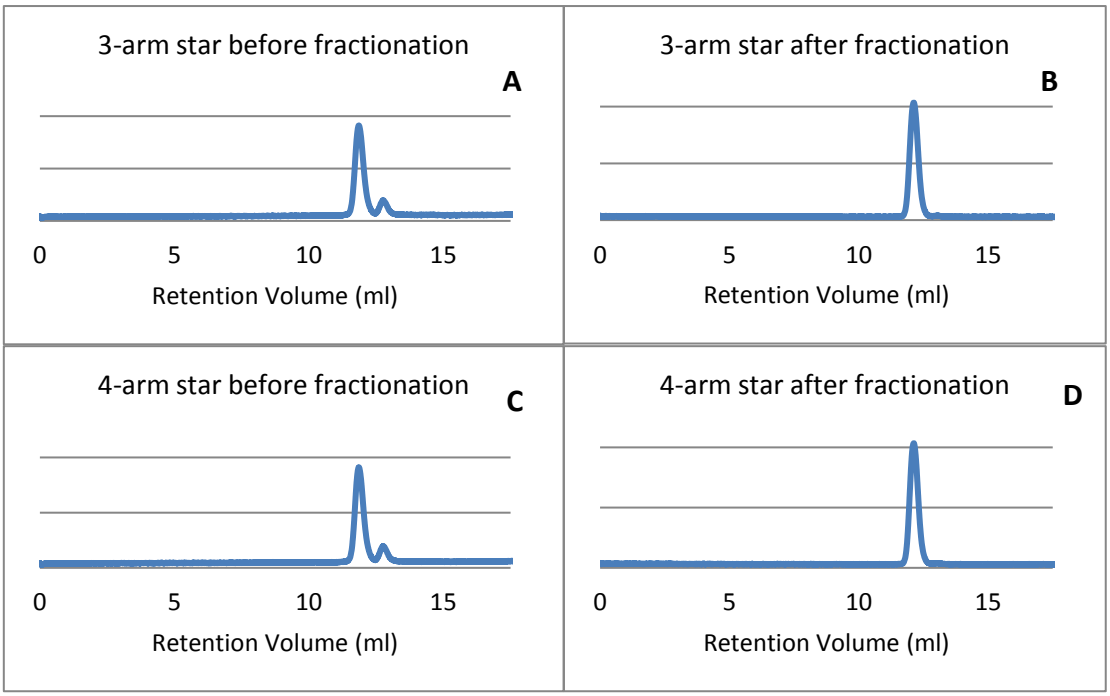

Figure 4.6: Fractionation of 3-arm (A and B) and 4-arm (C and D) star polybutadiene.; 3-arm star before fractionation (A) and after fractionation (B); 4-arm star before fractionation (C) and after fractionation (D)

The molar masses and dispersity values (obtained by SEC) of the precursor arms, crude sample and purified samples of the 3-arm and 4-arm star polybutadienes are summarised in Table 4.2. Purification by fractionation was carried out on the crude samples of each star polymer to remove the excess linear arm and obtain the purified samples. The linear precursor arms had molar mass values in excellent agreement with the target. The functionality of the star gives an indication of the efficiency of the linking reaction, i.e. the number of arms per star. This is calculated simply by the ratio of the M_n (star)/M_n (arm), which for Star(3)150 gave a value of 2.32 for the unfractionated crude star, and a value of 2.79 for the purified star, indicating that coupling had been highly efficient. For the 4-arm star, functionality was calculated to be 3.25 for the crude sample, and 3.99 for the purified sample, again showing that coupling was very efficient.

Table 4.2: Theoretical and experimental SEC and star functionality data for the linear arm precursors together with the 3-arm star (Star(3)150) and 4-arm star (Star(4)130) polybutadienes

Polymer	Target M_n ($x10^3$ g/mol)	M_n ($x10^3$ g/mol)	M_w ($x10^3$ g/mol)	Đ	Star functionality
Star(3)150_Crude	150	123	142	1.16	2.32
Star(3)150_Pure	150	148	151	1.02	2.79
Star(4)130_Crude	136	109.2	123.4	1.16	3.25
Star(4)130_Pure	136	134.2	138.4	1.03	3.99

1D Solvent gradient interaction chromatography (SGIC) and temperature gradient interaction chromatography (TGIC)

As another type of complex branched polymer structures, PBd star polymers were investigated using different liquid chromatographic approaches, including RP-TGIC and RP-SGIC. RP-TGIC was carried out on Star(3)150 (three-arm PBd) and Star(4)130 (four-arm PBd) samples before and after purification by fractionation. For RP-TGIC, a Nucleosil C18 stationary phase was used with 1,4-dioxane (a theta solvent for PBd)[67] as the eluent. The temperature was varied during the elution run and the flow rate kept constant at 0.4 mL/min. The RP-TGIC chromatograms for the crude polymers and the purified materials are presented in Figure 4.8. For Star(3)150_crude, three major peaks are detected in the TGIC chromatogram (Figure 4.8A.1), the first large peak at 3.2 mL is the solvent peak, confirming that elution is in IC mode. The next peak (1) at 5.0 mL corresponds to the excess unreacted arm still present in the crude sample. This is not seen in the star(3)150_pure sample as shown in Figure 4.8A. Then there is a peak (2) at 9.3 mL that corresponds to the "two-arm" incomplete star which was undetected in SEC experiments. The major peak (3) around 13.2

mL is representative of the three-arm star molecule. A similar result can be seen in Star(4)130 (Figure 4.8B1) with peaks 1-3, corresponding to the unreacted arm not visible in the purified star(4)130 in Figure 4.8B, the incomplete "two-arm" product and the major four-arm star.

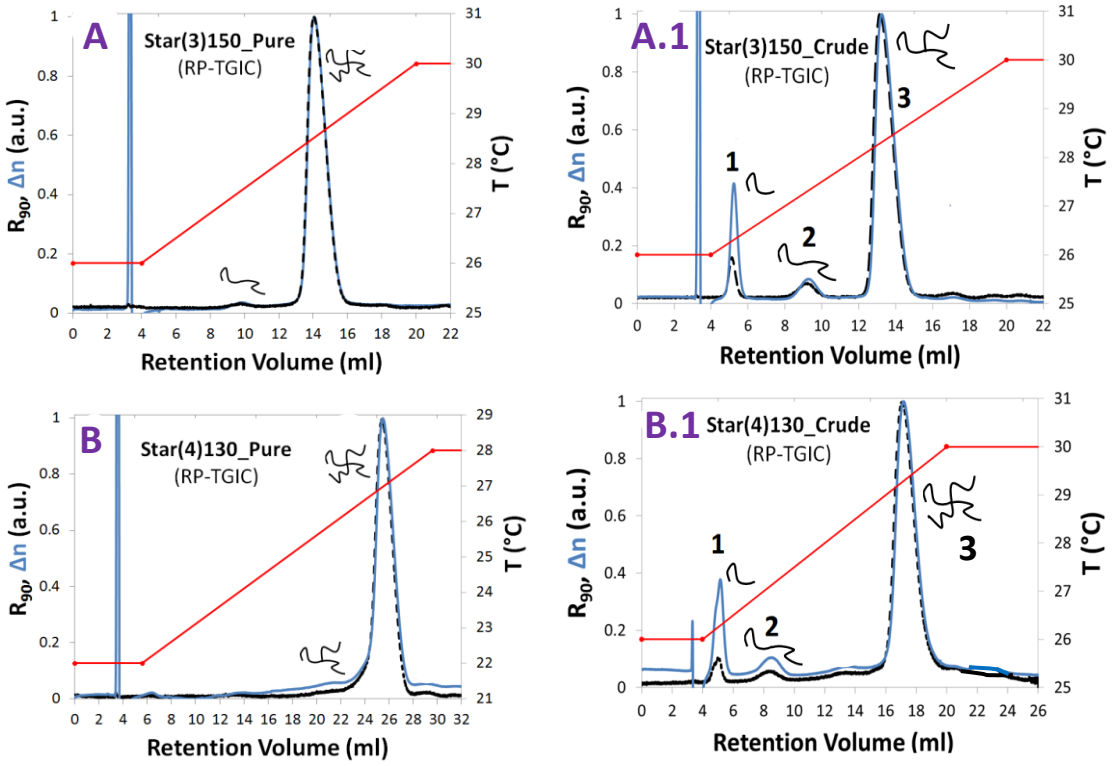

Figure 4.7 RP-TGIC chromatograms of the pure three arm (A), pure four arm (B), crude three arm (A.1) and crude four arm (B.1) polybutadiene stars recorded with an RI detector (Δn) and RALS detector (R_{90}).

It should be noted that in comparison to SEC, molar mass data obtained by TGIC-RALS may be of slightly lower accuracy. The refractive index detector is very sensitive to changes in temperature and this can result in unstable baselines, which in turn effects the accuracy of any molar mass analysis. However, results obtained by TGIC are often indicative and accurate enough to assign the separated polymer peaks. The molar masses for the different components listed in Table 4.4 correspond to the peaks presented in Figure 4.8. For Star(3)150_crude molar mass (M_n) values were calculated for every peak present in its TGIC chromatogram. Peak 1 has a M_n of 42 000 g mol^{-1}, which is in reasonable agreement with the value calculated by SEC (53 000 g mol^{-1}). Peak 2 has a M_n of 85 000 g mol^{-1}, in good agreement with the theoretical value that would be expected for an incomplete "two-arm" star (84 000 g mol^{-1}), and peak 3 has a value of 133 000 g mol^{-1}, again in agreement with the number expected for a three-arm star. In the case of Star(4)130_crude, analysis was only possible for peaks 1 and 3, with peak 1 having a M_n of 26 800 g mol^{-1}, and peak 3 having a M_n of 110 900 g mol^{-1} close to four times of that of peak 1. Although there are some discrepancies between the molar

mass measurements based on TGIC and SEC, the data help to confirm the identity of each component of the crude materials.

Table 4.3 Molar mass (M_n) values for crude star polybutadienes obtained by TGIC analysis

	Peak Molar Mass (M_n) (g mol^{-1})		
Sample Code	Peak 1	Peak 2	Peak 3
Star(3)150_crude	42 000	85 000	133 000
Star(4)130_crude	26 800	…	110 900

The SGIC separation of the 3-arm and 4-arm star polybutadienes was done at reversed phase conditions on a Nucleosil C18 bonded silica column. In this case the method development aimed at separating the stars regarding the number of arms (branches). A binary solvent system comprising of acetone and n-hexane was used as the mobile phase; where acetone is a poor solvent for polybutadiene and n-hexane is a good solvent. Figure 4.9 shows the RP-SGIC chromatograms of the crude 3-arm and 4-arm star PBd's (Figure 4.9A and Figure 4.9A1), together with the RP-SGIC chromatograms of the purified 3-arm and 4-arm star materials (Figure 4.9B and Figure 4.9B1). As the amount of n-hexane increased, the interaction of the PBd chains with the stationary phase became weak and some low molar mass species assigned to the linear PBd precursors that were used as the building blocks to form the stars were seen eluting at around 16.2 and 18.7 min. The solvent gradient program for all runs followed linear ramps with an isocratic step at the mid-point of the first eluting peak for the 3-arm star PBd around 21.6 min shown in Figure 4.9A and 4.9B. The unretained material shown in Figure 4.9A around 3.25 min which eluted early together with the solvent peak was attributed to the presence of low molar mass impurities in the crude 3-arm and 4-arm star PBd's. Although there was a peak shift during attempts to resolve the pure 3-arm and 4-arm stars after introduction of the isocratic step, there still was co-elution and no significant resolution regarding the number of arms as shown in Figure 4.9B1. A possible explanation is that under the 1D-SGIC conditions, the difference between the 3 and 4-arm stars is too small to achieve a significant resolution based on branching considering that the chemical composition is the same and the molar masses are comparable.

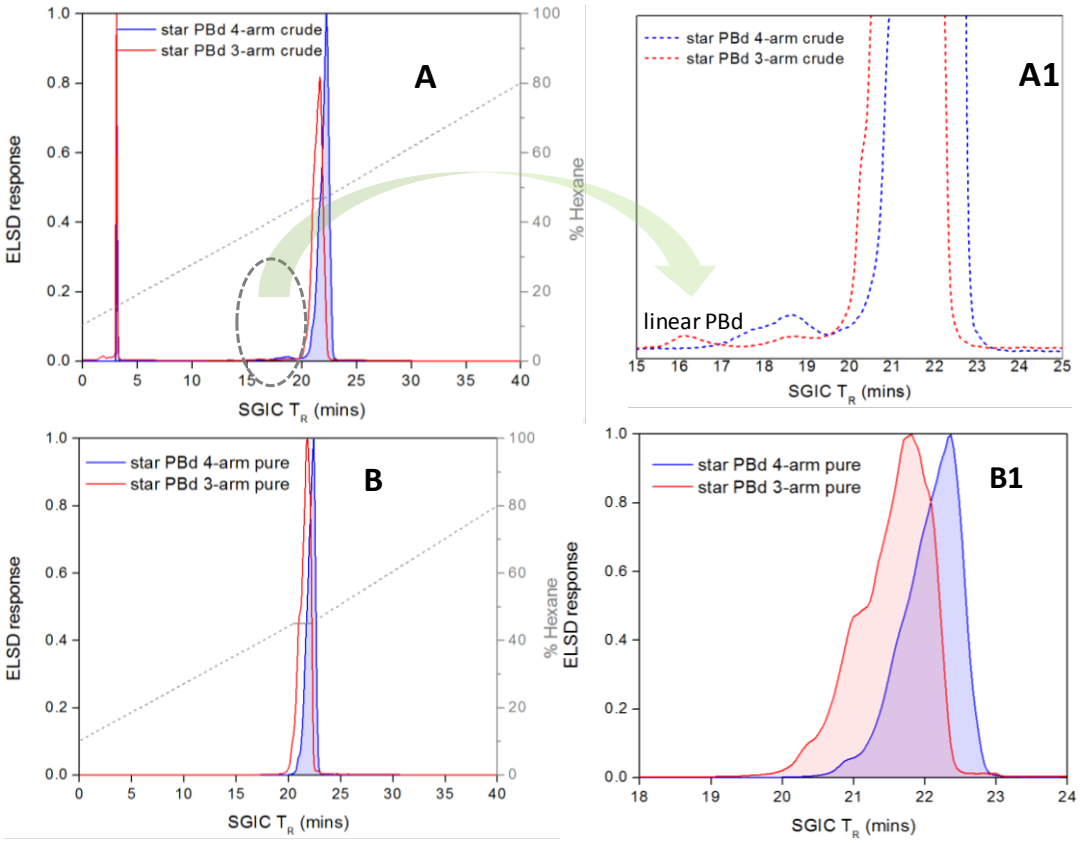

Figure 4.8 RP-SGIC chromatograms of the crude 3-arm and 4-arm star polybutadienes (A) and enlarged parts of the chromatograms (A1). RP-SGIC chromatogram of the pure 3-arm and 4-arm star polybutadienes (B) and enlarged parts of the chromatograms (B1).

In comparison to the 1D-SGIC and SEC separations, 1D-TGIC is superior in separation with the ability to separate each by-product present in the star polymers far beyond what is possible when using SEC. For the analysis of polymers before fractionation, TGIC was able to show the presence of incomplete, partially coupled products, in contrast to SEC that was only able to show the fully coupled product as well as any excess precursor still present in the crude samples. SGIC was not able to achieve significant baseline separation between products. For the purified samples, TGIC was also able to detect and quantify the amounts of impurities still present after fractionation, where SEC analysis had indicated complete purity and SGIC was unable to resolve any products from the major peak. However, for an all-inclusive analysis based on molar mass, chemical composition and degree of branching of all samples, 2D-LC should provide an even more comprehensive approach.

2D-LC analysis (RP-SGIC × SEC and RP-TGIC × SEC)

2D-LC is a combination of two orthogonal chromatographic separations that has a larger peak capacity compared to 1D-LC. When the conditions of the 1st and 2nd dimensions are optimized carefully, 2D-LC can show features that are otherwise impossible to obtain from

two stand-alone 1D-LC separation methods. In the present applications the 1st dimension was optimized to separate the polymer species present in the complex mixtures according to chemical composition or branching, while the 2nd dimension separated the 1st dimension fractions according to hydrodynamic volume/molar mass of the polymer species present in that specific fraction. In extension of the results obtained from the 1D-SGIC/TGIC experiments elsewhere in this chapter, a comparative study to assess the resolving power of the two IC techniques to comprehensively analyse complex polymer mixtures regarding the multivariate distributions in 2D mode was conducted.

Based on the 1D-SGIC and 1D-TGIC findings reported elsewhere in this chapter, the sets of star PBd were analysed in which the molar masses were comparable, and the chemical compositions were similar. The focus was on optimizing the 2D-LC analysis to separate the star PBd's based on the number of arms. The sample sets were unfractionated (crude) 3-arm and 4-arm star PBd's, as well as fractionated (pure) 3-arm and 4-arm star PBd's. For 2D RP-SGIC, the experiments were carried out on a Nucleosil C18 column, the mobile phase for the 1st dimension RP-SGIC separations being a binary solvent system comprising acetone and n-hexane. The solvent gradient was like the one employed for the 1D RP-SGIC analysis except that the flow rate was 0.1mL/min in the 1st dimension of the 2D-LC analysis. The mobile phase for the 2nd dimension was THF at a flow rate of 2mL/min. Figure 4.10A, C, E and G show the 2D RP-SGIC × SEC separations of the crude and pure 3- and 4-arm star polybutadienes. Like what has been seen in the 1D-SGIC separations, the linear PBd precursors are well separated from the crude stars in all cases. The crude 4-arm PBd eluted slightly later in the 1st dimension separation (≈ 15 mL, Figure 4.10C) than the crude 3-arm PBd (≈ 14.5 mL, Figure 4.10A). A much-improved resolution in the 1st dimension was achieved between the pure 3-arm PBd (≈15 mL, Figure 4.10E) and the pure 4-arm PBd (≈16.3 mL, Figure 4.10G). From the 2nd dimension SEC separation, the pure 3-arm PBd eluting around 3.3 mL (Fig 4.10E) while the more compact pure 4-arm PBd eluted later around 3.5mL (Figure 4.10G).

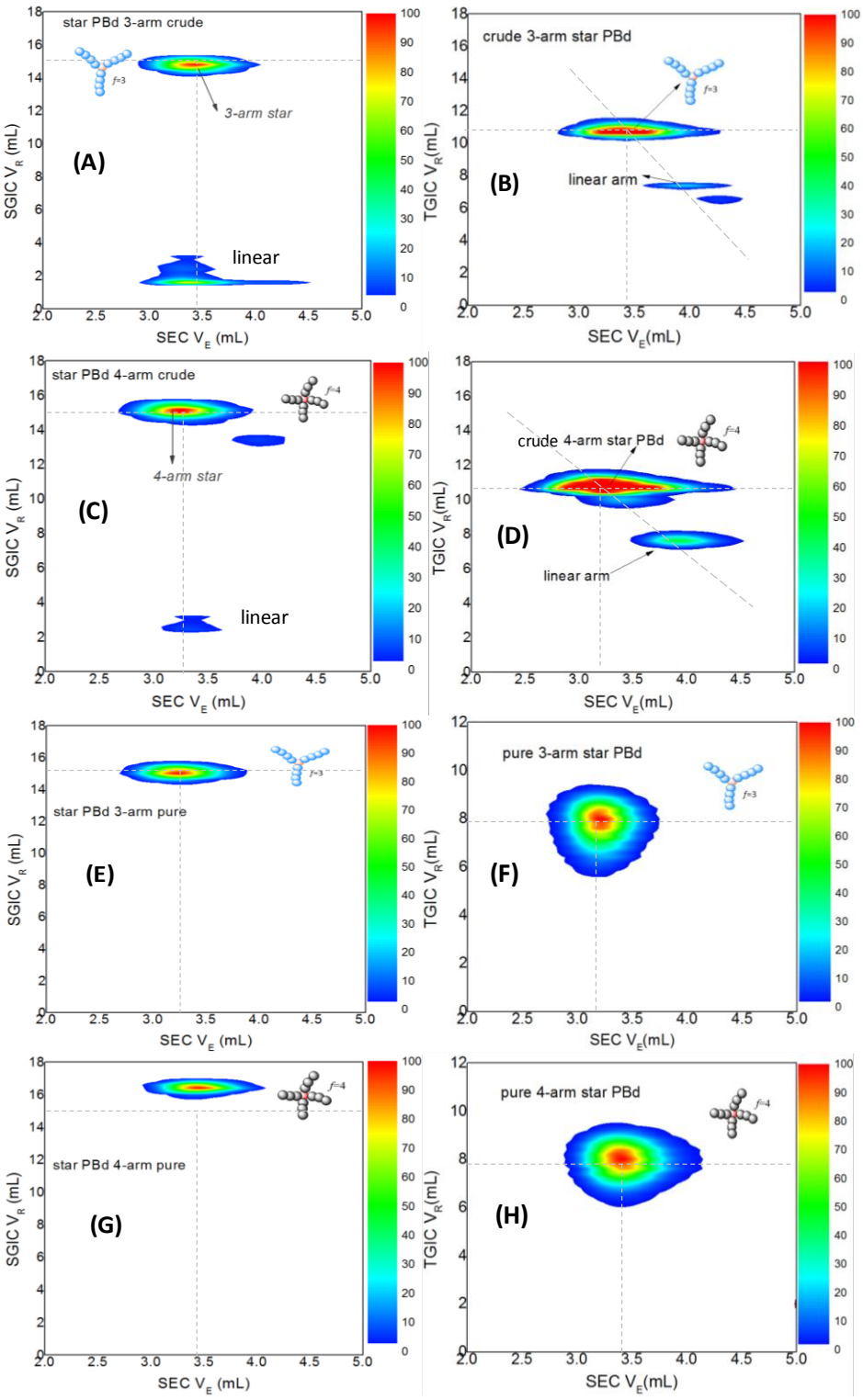

Figure 4.9 2D RP-SGIC x SEC contour plots of the crude 3-arm (A), crude 4-arm (C), pure 3-arm (E) and pure 4-arm (G) star polybutadienes. 2D RP-TGIC x SEC contour plots of the crude 3-arm (B), crude 4-arm (D), pure 3-arm (F) and pure 4-arm (H) star polybutadienes.

In a comparative study**,** 2D RP-TGIC experiments were also carried out on a Nucleosil C18 column with a mobile phase of 1,4-dioxane. The flow rate for the 1st dimension was 0.08mL/min, while that of the 2nd dimension was 2.5mL/min using THF as the mobile phase. Figure 4.10B, D, F and H show the 2D RP-TGIC × SEC separation of the crude samples

together with the pure 3- and 4-arm star polybutadienes. In 1st D TGIC separation of the crude mixtures, the 3-arm PBd eluted around 11 mL (Figure 4.10B) while the 4-arm eluted around 11.5 mL (Figure 4.1D). The 2nd D SEC separation of the purified stars showed notable differences between the 3-arm PBd which eluted around 3.2 mL (Figure 4.10F), while the more compact 4-arm PBd eluted around 3.5 mL (Figure 4.10H). From the findings above, the separation efficiency of 2D RP-SGIC × SEC in separating the purified 3-arm and 4-arm star polybutadienes based on the number of arms was superior to that of 2D RP-TGIC × SEC. The RP-TGIC resolution increased with molar mass. However, 2D RP-TGIC × SEC was more sensitive in isolating the desired 3-arm and 4-arm star polybutadienes from the linear by-products in the crude mixtures.

4.4.2 Miktoarm star polystyrene-polyisoprene (PS-PI$_2$)

Size Exclusion Chromatography

Figure 4.11 shows the RI detector response versus the elution time plots of the crude miktoarm star-branched PS-(PI)$_2$ compared to the linear polystyrene and polyisoprene blend before the coupling reactions. The Williamson coupling reaction between the di-hydroxyl terminated polystyrene and the bromine end-capped polyisoprene was carried out in caesium carbonate as the base and dry DMF as the solvent (good solvent for Williamson coupling when using bromine as the leaving group) to afford the miktoarm star-branched polymer. The SEC chromatogram in Figure 4.11 shows a significant peak shift towards the lower retention time region. The peak around 15.4 min at the start of the reaction was attributed to possible minor coupling to form PS-PI upon combining the starting materials, while the peak shift around 14.9 min after the reaction was assigned to possible mixture of the desired miktoarm star-branched PI-PS-PI and incompletely coupled PS-PI. From the SEC trace of the crude polymer mixture after the reaction, there was evidence of unreacted starting material in the resultant crude mixture after the coupling reaction around 16 min.

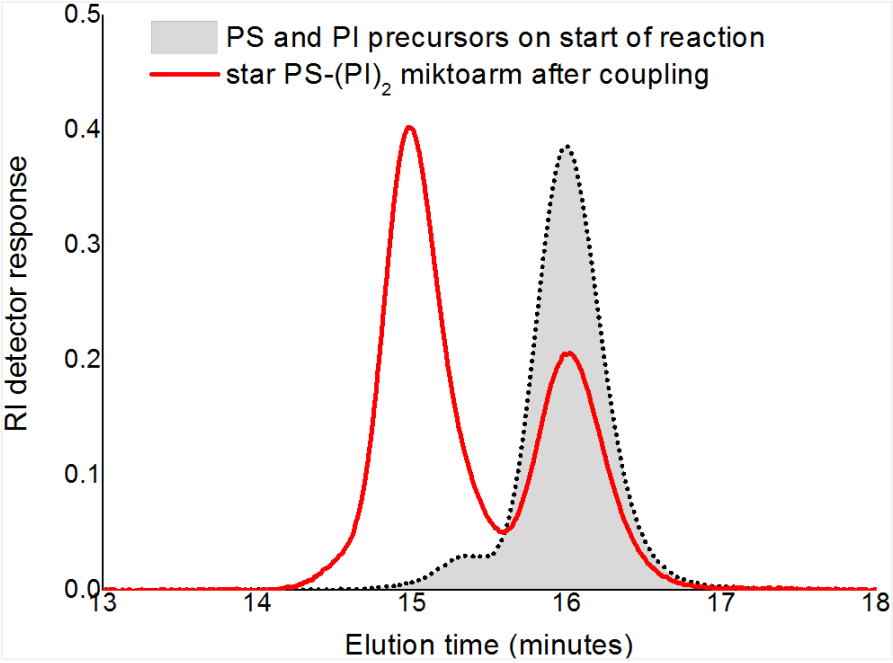

Figure 4.10 Overlaid SEC chromatograms of polystyrene and polyisoprene blend at the start of the coupling reaction (black dotted line); together with the crude PS-PI_2 after coupling (red curve). Detector: RI.

It is also possible that there was some incompletely coupled PS-PI together with the desired miktoarm star-branched PI-PS-PI in the final product. This can be attributed to the inefficiency of the Williamson coupling reactions to completely favour formation of the desired miktoarm stars under the conditions they were carried out. [63] The SEC results for the crude miktoarm star-branched PS-$(PI)_2$ are summarised in Table 4.5. The molar masses of the individual macromonomers were 6 200 $g.mol^{-1}$ (PS) and 4 000 $g.mol^{-1}$ (PI) respectively (see Section 4.2.3). Although it is common knowledge that the fraction of high molar mass will grow with increasing number of PI arms during a successful Williamson coupling reaction, the analysis of polymers comprising of chemically differing chains using SEC is a challenge because the samples constitute a molar mass distribution in addition to the chemical composition distribution. This is because conventional SEC separates according to the polymer chain size in a good solvent. While the chain size is dependent on the molar mass, it is also affected by the polymer chain chemical composition, architecture and so on.

Table 4.4 Molar mass (M_n, M_w) and dispersity values of the blended PS and PI starting materials before coupling reaction and PS-$(PI)_2$ after the coupling reaction.

	Blend before coupling reaction	**After coupling reaction**	
Elution Time (min)	**16.0**	**15.1**	**16.0**
M_n - (x10^3 g/mol)	5.5	12.6	5.6
M_w - (x10^3 g/mol)	5.8	13.1	5.9
Đ	1.05	1.03	1.05

1D Solvent gradient interaction chromatography (SGIC) and temperature gradient interaction chromatography (TGIC)

One possible way to circumvent the limitations of conventional SEC in characterising complex polymers is to make use of multidetector setups that include molar mass and/or chemical composition sensitive detectors. Another alternative is the use of non-SEC chromatographic techniques such as interaction chromatography (IC) in solvent or temperature gradient modes (SGIC or TGIC). Figure 4.12 shows 1D-SGIC and 1D-TGIC chromatograms of the crude miktoarm star PS-PI_2 using a reversed stationary phase Nucleosil C18. A binary mobile phase of acetonitrile (ACN) and dichloromethane (DCM) was used for RP-SGIC, where ACN is a poor solvent for PS and a non-solvent for PI, while DCM is a good solvent for both PS and PI. In previous work, Lee et al. used a combination of liquid chromatographic techniques to characterize a PS-*graft*-PI copolymer that consisted of varying amounts of PI branches on a PS backbone. In their work, they made use of TGIC and LCCC to highlight the shortcomings of SEC in characterizing branched and highly branched polymers.[65]

On the C18 column, at high concentrations of ACN, the PS and PI interaction with the stationary phase is strong, and an elution time of ≈ 25 min is obtained for both PS and PI, see Figure 4.12A (upper chromatogram). As the concentration of DCM in the mobile phase increases, the retention of PS and PI becomes weaker and lower molar mass PS, PI and PS-PI species are eluted at lower elution times. In order to improve the resolution between the PS and PI species, isocratic steps were introduced at the midpoint of each chromatogram as shown in Figure 4.12A1. Initially, the coupled PS-PI and desired miktoarm star PS-PI_2 co-eluted at around 27.3 min. After introduction of the isocratic step at the midpoint of the

corresponding elution peak, a bimodal distribution could be seen and a new peak emerged at around 27.8 min as shown in Figure 4.12A2. This was due to increased retention from the additional PI arm forming the miktoarm star PS-PI_2.

In order to compare the resolution capabilities and get more information about the molecular composition of the sample, the crude miktoarm star PS-PI_2 was also separated by TGIC. In order to confirm the peak assignments for the early eluting species, linear PS (Mw = 6 460 $g.mol^{-1}$; PSS) and PI (Mw = 4 250 $g.mol^{-1}$; PSS) standards were also run under the same SGIC and TGIC conditions as shown in Figure 4.12A and 4.12B. TGIC experiments are conducted under isocratic solvent conditions, and they are usually carried out at near critical conditions for the polymer species under study. Typically, critical conditions are established using a combination of two or more solvents, however, such critical conditions are not easily reproducible since the preferential sorption of the polymer species critically depends on the solvent purity and composition.[66] Accordingly, if the polymer sample under study permits, the use of a single solvent system is preferred.

Figure 4.12B shows the 1D RP-TGIC chromatograms of the crude miktoarm star PS-PI_2 using 1,4-dioxane as the mobile phase. An isothermal step at 5 °C for the first 10 min was introduced along the temperature profile to ensure that if present, non-retaining species will elute before the actual Temperature gradient. The unreacted PS chains were detected at around 14 min while the unreacted PI chains were retained for longer with the help of an isothermal step and eluted at around 18 min as shown in Figure 4.12B1. A shoulder at the main elution peak assigned to PS-PI was seen eluting at around 21.5 min while the component eluting at around 22.9 min was assigned to the desired miktoarm star PS-PI_2 as shown in Figure 4.12B2.

Based on the 1D SGIC and TGIC experiments in this work, it appears that TGIC has a gradually better resolution. However, even the use of isocratic steps in SGIC or isothermal steps and varying temperature ramp rates in TGIC did not achieve a full resolution regarding both the chemical composition and molar mass heterogeneities in a single run. Due to time constraints, we could not manage to vary more parameters in order to assess their effects on the resolution. From the chromatograms obtained in the SGIC as well as TGIC analyses, it would be recommended to vary the solvent composition, or use a different solvent choice altogether in order to delve into a more exhaustive study. Although the use of a single solvent system would be advantageous for TGIC analyses due to the flexibility of detector/detector train choices, the application of a co-solvent might have enhanced the resolution between PS-

PI and PS-PI. To overcome the limitations of the 1D IC techniques, 2D liquid chromatography approaches might be useful. Still, both techniques achieved remarkable resolution compared to the SEC separations.

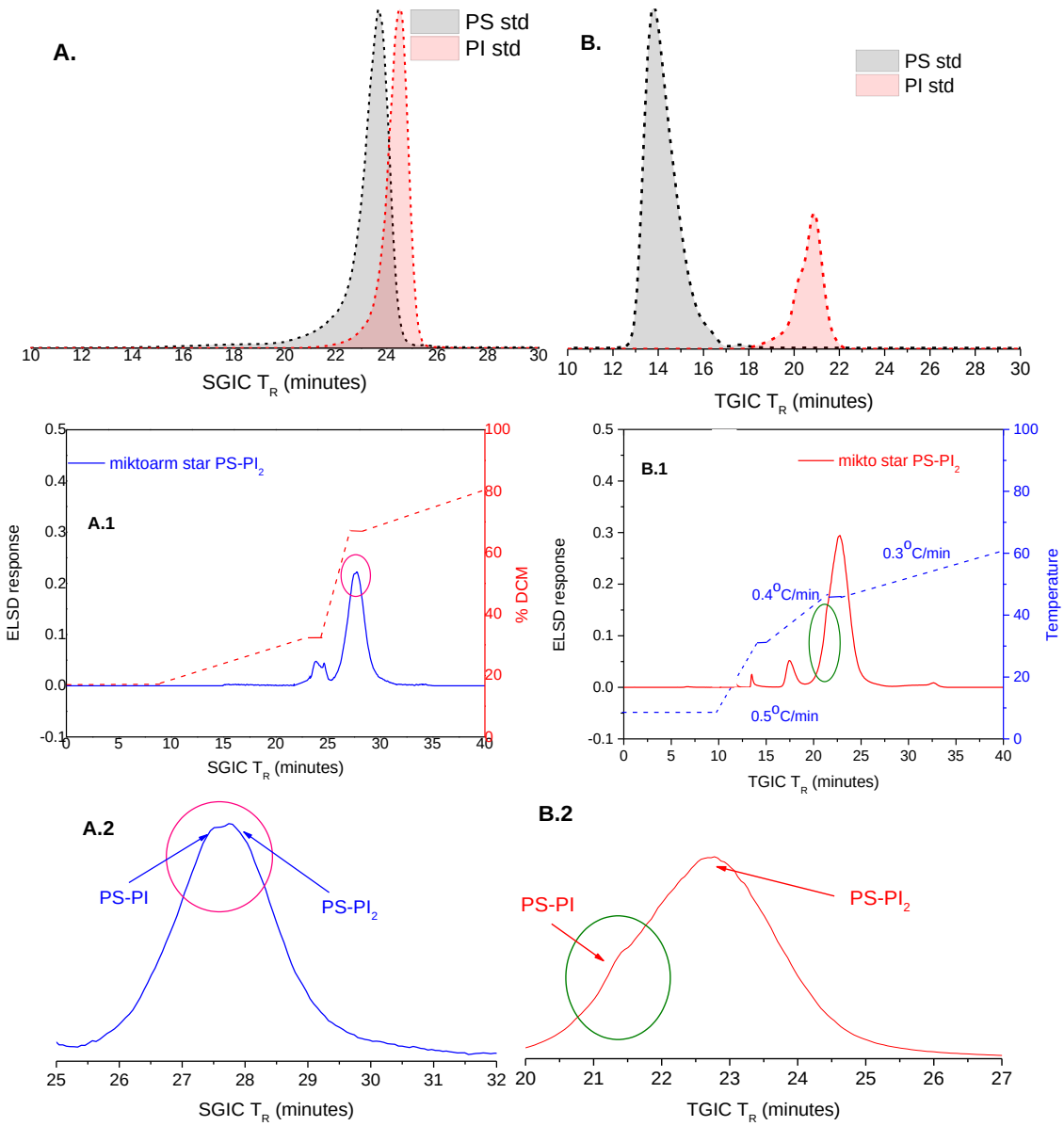

Figure 4.11 RP-SGIC chromatogram of the PS and PI linear standards (A), miktoarm star-branched PS-PI$_2$ (A1); enlarged parts of the chromatogram A, (A2). RP-TGIC chromatogram of the PS and PI linear standards (B), miktoarm star-branched PS-PI$_2$ (B1); enlarged parts of the chromatogram in B, (B2).

2D-LC analysis (RP-SGIC × SEC and RP-TGIC × SEC)

In order to complement the 1D-SGIC and 1D-TGIC findings, these IC methods were combined with SEC in an online 2D-LC set-up. Figure 4.13A and 4.13B shows the 2D RP-SGIC × SEC and 2D RP-TGIC × SEC contour plots of the crude miktoarm star PS-PI$_2$. The

1st dimension SGIC separations were carried out on a Nucleosil C18 column using a binary solvent composed of acetonitrile (ACN) and dichloromethane (DCM). The flow rate for the 1st dimension was 0.065 mL/min. An isocratic step with ACN/DCM 80:20 % v/v was introduced for the first 40 min and then the solvent gradient was run for 180 min using a linear ramp up to ACN/DCM 20:80 % v/v. The flow rate for the 2nd dimension SEC separation of the RP-SGIC fractions was 3 mL/min using THF as the mobile phase.

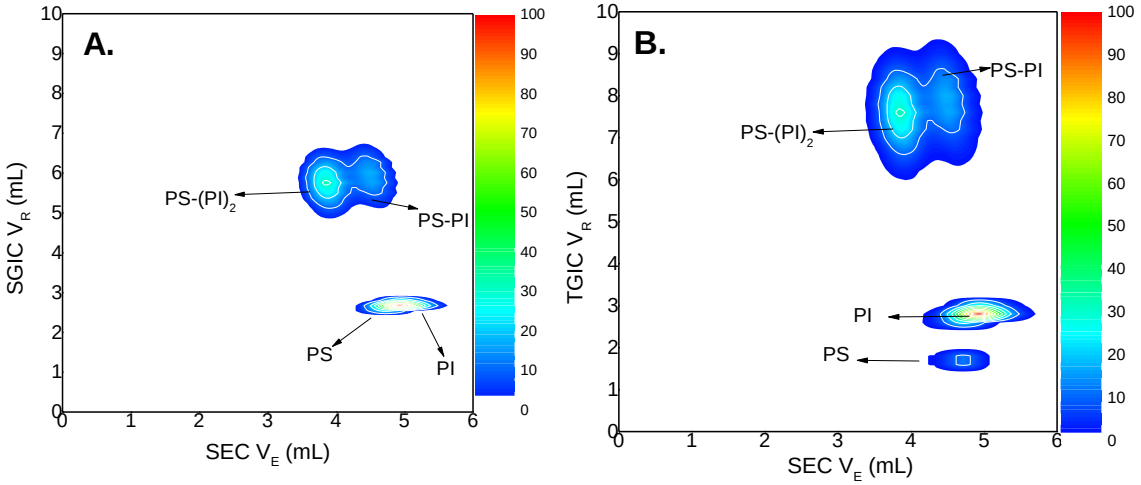

Figure 4.12 2D RP-SGIC x SEC contour plots of the crude miktoarm star PS-PI_2 (A). 2D RP-TGIC contour plots of the crude miktoarm star PS-PI_2 (B).. Temperature gradient 5-60 °C with a linear ramp rate of 0.1 °C/min from the start of the gradient.

The 2D-LC experiments confirm the findings of 1D-LC. Neither TGIC nor SGIC alone can separate the miktoarm stars from the PS-PI by-products. Regarding the starting blocks the separation of PS and PI is very poor in SGIC but good in TGIC. The shortcomings of the 1D-LC methods, however, are very nicely compensated by adding the 2nd dimension. Due to the molar mass differences between PS-PI_2 and PS-PI, SEC can resolve these two components. The separation of the starting blocks is also enhanced by the 2nd dimension due to the fact that both homopolymers had slightly different molar masses which would be a significant factor in the 1st dimension, in addition to chemical composition differences (therefore, different solution behaviours). This was not too surprising considering the fact that from these findings, SGIC separation was more sensitive to chemical composition while TGIC analyses were more sensitive to molar mass. Comparing the SGIC and TGIC analyses for the present samples, TGIC x SEC may be the better technique to explore and vary the separation conditions to improve the resolution. This was because the relevant components were significantly separated and with further experiments can, ideally, be comprehensively quantified.

4.4.3 Hyperbranched PBd-PS

Size Exclusion Chromatography

Using the scope of preparing the simpler miktoarm star PS-$(PI)_2$, an attempt was made to prepare a more complex polymer and obtain hyperbranched PBd-PS via Williamson coupling reactions. Figure 4.14 shows the SEC traces of the OH-terminated polybutadiene crossbar (PBd-$(OH)_4$) and the dibromo-functionalized polystyrene (PS-$(Br)_2$) starting materials at the beginning of the coupling reaction and the crude hyperbranched PBd-PS. There was evidence of unreacted starting material species around 13.8 and 16.1 min for the PBd-$(OH)_4$ and PS-$(Br)_2$, respectively. However, from the SEC chromatogram in Figure 4.14 and the molar mass data presented in Table 4.6 the coupling reaction was a success to an extent. At the start of the reaction the mixture showed two distinct peaks around 13.6 and 16.1 min while the resultant product had a new broad peak from around 11–13 min which may be attributed to the presence of the high molar mass hyperbranched species. The molar masses and dispersities for the SEC traces of the crude hyperbranched PBd-PS displayed in Figure 4.14 are summarised in Table 4.6 for both the initial materials (at the beginning of the coupling reaction) and SEC traces of the hyperbranched PBd-PS (after the coupling reaction).

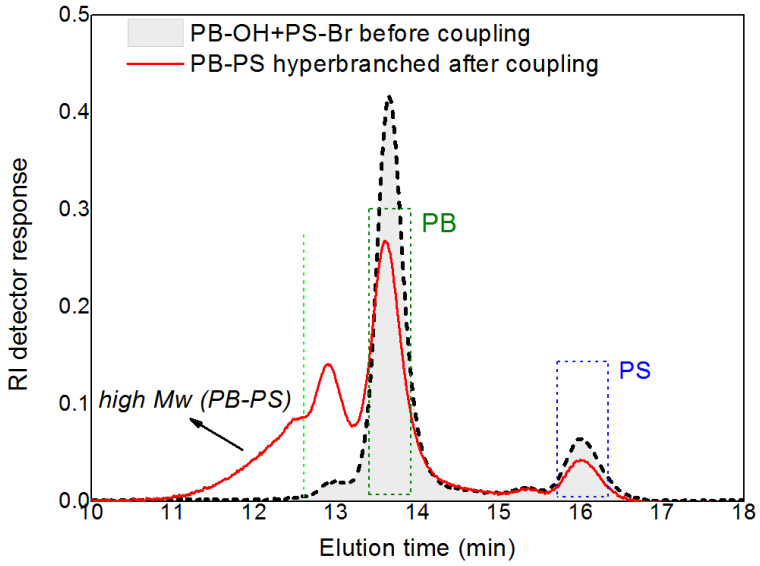

Figure 4.13 Overlaid SEC chromatograms of polybutadiene crossbars and polystyrene arms at the beginning of the coupling reaction (black-dashed curve) with hyperbranched polybutadiene-polystyrene after coupling (red solid curve). Detector: RI

Due to the limitation of conventional SEC to separate only according to hydrodynamic size which is influenced by parameters that include molar mass, chemical composition and chain architecture, there was no resolution amongst the different species present in this complex polymer mixture particularly in the high molar mass regime. This proves the necessity of

further fractionation techniques and characterization methods that will separate and distinguish the highly branched polymers regarding chemical composition, molar mass and branching distribution.

Table 4.5 Molar mass (M_n, M_w) and dispersity values of the PBd and PS precursors before and after the coupling reaction.

Elution time (min)	**12.0**	**13.0**	**13.8**	**16.1**
Before coupling				
M_n - (× 10^3 g/mol)		54.5	23.8	5.3
M_w - (× 10^3 g/mol)		56.9	24.5	5.6
Đ		1.02	1.03	1.05
After coupling				
M_n - (× 10^3 g/mol)	133.4	63.6	23.3	5.4
M_w - (× 10^3 g/mol)	166.1	64.6	24.3	5.7
Đ	1.25	1.02	1.04	1.05

1D Solvent gradient interaction chromatography (SGIC) and temperature gradient interaction chromatography (TGIC)

Having assessed the capabilities of both 1D-SGIC and 1D-TGIC in separating the simpler crude miktoarm star PS-PI_2 from its by-products to the extend discussed in Figure 4.12, the same principles were applied to fractionate a more complex crude mixture of hyperbranched PBd-PS and its by-products. Figure 4.15 shows the 1D-SGIC and 1D-TGIC chromatograms of the hyperbranched PBd-PS. For RP-SGIC experiments of the hyperbranched PBd-PS, a mixed mobile phase of ACN/THF was used to perform solvent gradient elution where ACN is a poor solvent for both PS and PBd while THF is a good solvent for both polymer species. An isocratic step of 100% ACN was introduced at the start of the gradient and then maintained for 7 min to ensure that both the PS precursor and the unreacted PBd were retained as shown in Figure 4.15A. As the amount of THF increased, the retention of the low molar mass PS precursor became weak and eluted first just after the beginning of the gradient at around 7.5 min. The later eluting components in the chromatogram in Figure 4.15A showed a rather complex elution profile which, even with the introduction of isocratic steps between the eluting peaks, could not be fully resolved according to chemical composition, molar mass and branching under the 1D RP-SGIC experimental conditions employed.

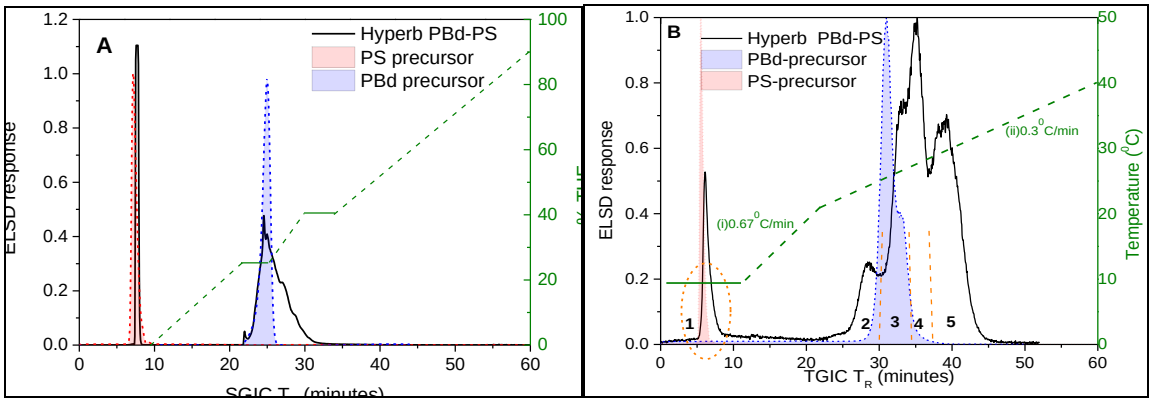

Figure 4.14 RP-SGIC chromatogram of the hyperbranched PBd-PS (A).. RP-TGIC chromatogram of the hyperbranched PBd-PS (B).. Temperature gradient 10-40 °C with varying ramp rates of 0.67 °C/min and 0.3 °C/min, respectively, along the linear temperature program.

To evaluate the capabilities of the RP-SGIC technique, RP-TGIC was employed as a complementary technique. Figure 4.15B shows the RP-TGIC of the hyperbranched PBd-PS. A single mobile phase of 1,4-dioxane was used to simplify the experimental conditions. An isothermal step at 10 °C was introduced at the start of the temperature program and maintained for 10 min via a temperature programmed column compartment. The early eluting peak was ascribed to unreacted low molar mass PS precursor, which eluted with the void peak under these conditions. A closer look at these findings is advantageous in the sense that since one assumes the SEC separation mode for PS chains. However, the uncoupled low molar mass PS entities effectively elutes under critical conditions which makes the resolution of the branched polymer solely governed by the PBd blocks. The PS (Mw = 6 200 g.mol^{-1}) and PBd (Mw = 23 000 g.mol^{-1}) precursors were also run under the same temperature gradient conditions and their chromatograms were overlaid with that of the hyperbranched PBd-PS chromatogram as shown in Figure 4.15B, and the observation was in agreement to the RP-SGIC findings of the earlier eluting species assignment in Figure 4.15A. Owing to molecular weight differences of the PS and PBd building blocks, it is helpful keeping in mind that the separation was partly due to molecular weight and molecular weight distribution. The temperature ramp rate was programmed to change to 0.67 °C/min after the isothermal step, then maintained for a further 15 min. When the next peak started eluting at around 25 min, the ramp rate was reduced to 0.3 °C/min to improve the resolution. It is worth noting that 1,4-dioxane is a theta solvent for PBd (theta temperature ≈ 26 °C). Therefore, at the start of the temperature ramp (10 °C) the solvent is a poor solvent for PBd but becomes a good solvent as the temperature increases, precisely at the point where the polymers begin to elute. Figure 4.16 shows the ^{1}H-NMR spectra of the RP-TGIC fractions of the hyperbranched PBd-PS. The

fractions were collected at various times by means of an automated fraction collector coupled online with the rest of the HPLC setup.

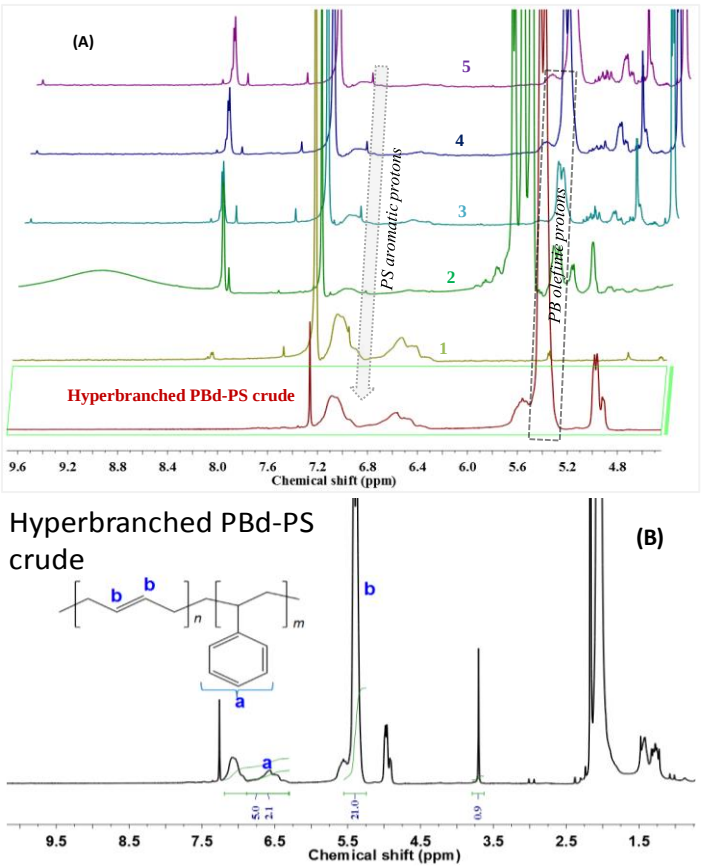

Figure 4.15 ^{1}H-NMR spectra RP-TGIC fractions (1-5) of PBd-PS, solvent $CDCl_3$ (A). ^{1}H-NMR of the crude hyperbranched PBd-PS with main signal assignments (B).

The styrene/butadiene (S/Bd) ratios were calculated via NMR analysis based on the integral ratios of the styrene aromatic protons and the butadiene methine protons. The S/Bd compositions are displayed in Table 4.6.

Table 4.6 RP-TGIC Styrene/Butadiene data for the offline NMR fractions

Fraction #	Styrene (mol %)	Butadiene (mol %)
1	97.3	2.70
2	2.50	97.5
3	5.40	94.6
4	7.30	92.7
5	8.20	91.8

The early eluting fraction (#1) composed of predominantly PS entities assigned to the unreacted PS building blocks from the Williamson coupling reactions. The second and third fractions (#2 and 3) comprised of mostly PBd blocks while the PS entities increased in the

preceding fractions (#4 and 5) as illustrated in the structural assignments in figure 4.17. However, the chemical compositions of the collected fractions may have still been clouded by co-elution of different entities of the hyperbranched PBd-PS and the unreacted PBd building block, thereby generally making it challenging to determine compositions of the eluting species based on molecular weight of the individual blocks. Therefore, the reported chemical composition data for the collected fractions are only the averages determined by NMR analyses.

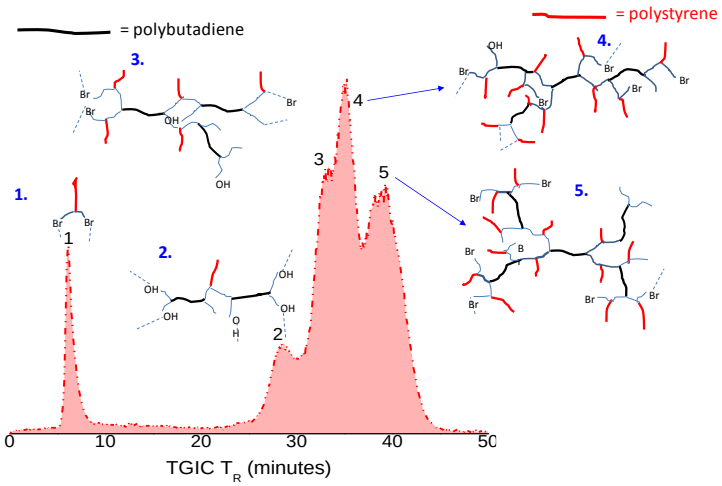

Figure 4.16 Tentative structural assignments of the collected fractions 1-5 based on S/Bd compositions.

As RP-TGIC is known to be a molar mass sensitive technique in addition to the molecular weight discrepancies between the PBd and PS blocks themselves, it was concluded that the eluting species were separated according to molecular weight and/or branching density in the order of increasing amounts of the polybutadiene entities in the hyperbranched sample with peak maxima around 29, 33, 35 and 40 min, respectively (see Figure 4.17).

In order to gain more molecular information based on TGIC fractionation and capitalise on its unique resolving power compared to SGIC, NP-TGIC was also used to collect fractions of the hyperbranched PBd-PS sample. A bare silica stationary phase was used to perform the fractionation. The sample was dissolved in a mixed mobile-phase of n-hexane/THF 62:38% v/v at a concentration of 2 mg/mL. A linear Temperature gradient running from 5-50 °C with a ramp rate of 0.4 °C/min was used while ELSD was employed as the method of detection. Figure 4.18 shows the NP-TGIC chromatogram of the hyperbranched PBd-PS. From the Williamson coupling reaction scheme shown in Figure 4.6, two building blocks PS and PBd constitute the different components forming the complex hyperbranched PBd-PS crude mixture. One type of structures was presumed to have mostly the PBd crossbar precursors at

the end of the growing branches while the other would mostly bear PS precursor blocks. Based on these considerations, RP-TGIC fractionation was compared to NP-TGIC fractionation in order to assess the extent of the effect of the polar uncoupled OH and Br moieties on the polybutadiene and polystyrene chains on the fractionation, respectively. The NP-TGIC fractions numbered 1-4 were collected at different set-times with an automated fraction collector attached to the HPLC set-up based on the peak maxima of the fractions eluting at ≈ 5, 10, 12.5 and 20 min, respectively, as shown in Figure 4.18.

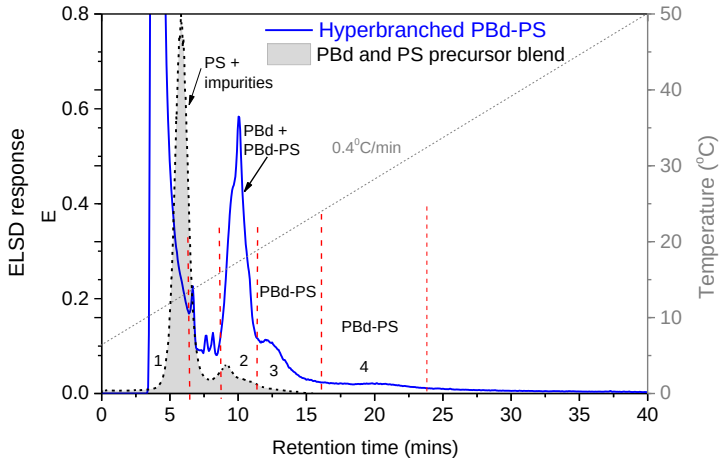

Figure 4.17 NP-TGIC chromatogram of hyperbranched PBd-PS. Mobile Phase: n-Hexane/THF (62/38 %v/v).

Based on the number of separated peaks, the separation of the hyperbranched PBd-PS on the bare silica stationary phase was not as good as the separation on the C18 bonded silica shown in Figure 4.15.However, due to complex nature and poor resolution of the hyperbranched PBd-PS chromatogram, generic slices of the chromatogram were collected at different times and analysed with offline ^{1}H-NMR for structural elucidation. The ^{1}H-NMR spectra of the collected fractions are displayed in Figure 4.19.

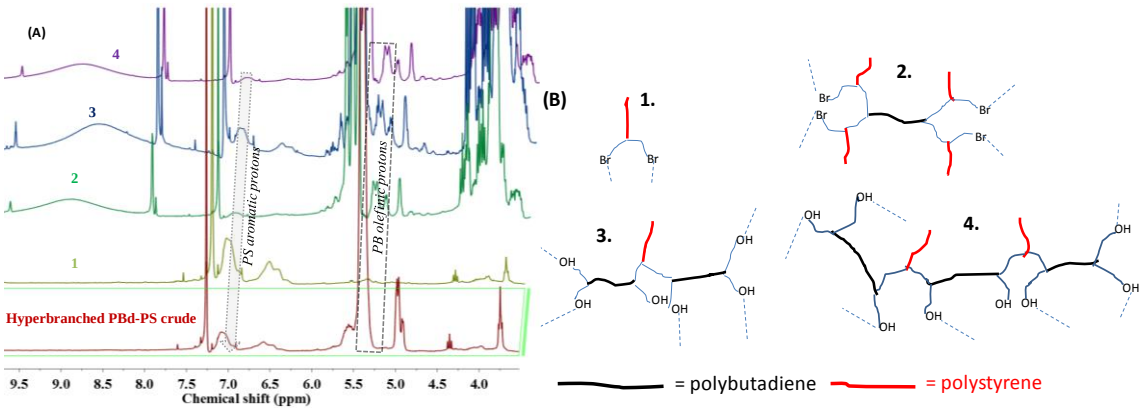

Figure 4.18 Offline ^{1}H-NMR of PBd-PS NP-TGIC fractions, 300MHz, $CDCl_3$ (A). Tentative structural assignments of the fractions based on the PBd/PS compositions (B).

The separation condition is the IC mode for PS and SEC mode for PBd hence the polymer species *would be expected* to be resolved mainly based on the PS molar mass. Based on the NMR analysis of the collected fractions, the first eluting peak could be assigned to unreacted PS chains. Accordingly, the second fraction would be assigned to uncoupled PBd block as well as hyperbranched PBd-PS with PBd blocks in the centre of the molecule and a comparable ratio by mass, of the PS blocks (less free polar OH groups) at the terminal ends of the complex branched block copolymer species. This observation was due to a synergistic effect of the low polarity of the Br end groups as well as the IC separation mode for the PS blocks and SEC separation mode for the PBd entities. Different from these findings, the RP-TGIC fractionation in Figure 4.15B was less sensitive to the polar OH groups on the PBd blocks and these were seen eluting in the early part of the chromatogram (Fraction 2).

The poor NP-TGIC resolution of the hyperbranched PBd-PS made it even more challenging to assign tentative structures due to gross co-elution. The PBd and PS compositions of the collected fractions were calculated based on the ratios of the styrene aromatic protons and the butadiene methine protons. The structural assignments were estimated from the NMR integral ratio of the butadiene –C**H**= proton signal (chemical shift around 5.5 ppm), with that of the styrene aromatic proton signal (chemical shift around 6.5 – 7.25 ppm), see Table 4.7.

Table 4.7 NP-TGIC Styrene/Butadiene data for the offline NMR fractions

Fraction #	**Styrene (mol %)**	**Butadiene (mol %)**
1	97.3	2.70
2	47.5	52.5
3	14.40	85.6
4	21.30	78.7

However, from results of the NP-TGIC fractionation in Figure 4.18 it can be concluded that the fractionation is mainly based on the interaction of the relative number of free OH groups of the PBd blocks with the stationary phase, that is with increasing numbers of incompletely coupled PBd blocks. To summarize, although RP-SGIC, RP-TGIC and NP-TGIC provide complementary separations, neither of the techniques afforded comprehensive information regarding the chemical composition and molar mass. For future exhaustive studies, a change in the separation condition such as variation in solvent choice and composition may give better resolution therefore make it easier to identify and assign structures to the collected fractions.

2D-LC analysis (RP-SGIC × SEC and RP-TGIC × SEC)

Figure 4.20 shows the 2D RP-SGIC × SEC and 2D RP-TGIC × SEC analysis of the crude hyperbranched PBd-PS. From the Williamson coupling reactions in Figure 4.6 and branching assessment in Figure 4.17 it was seen that the resultant heterogenous product was a very complex polymer sample containing polymeric species of different chemical composition, chain architecture and molar mass. Using the 1D-SGIC and 1D-TGIC approaches, there was co-elution of polymer species with different molecular compositions.

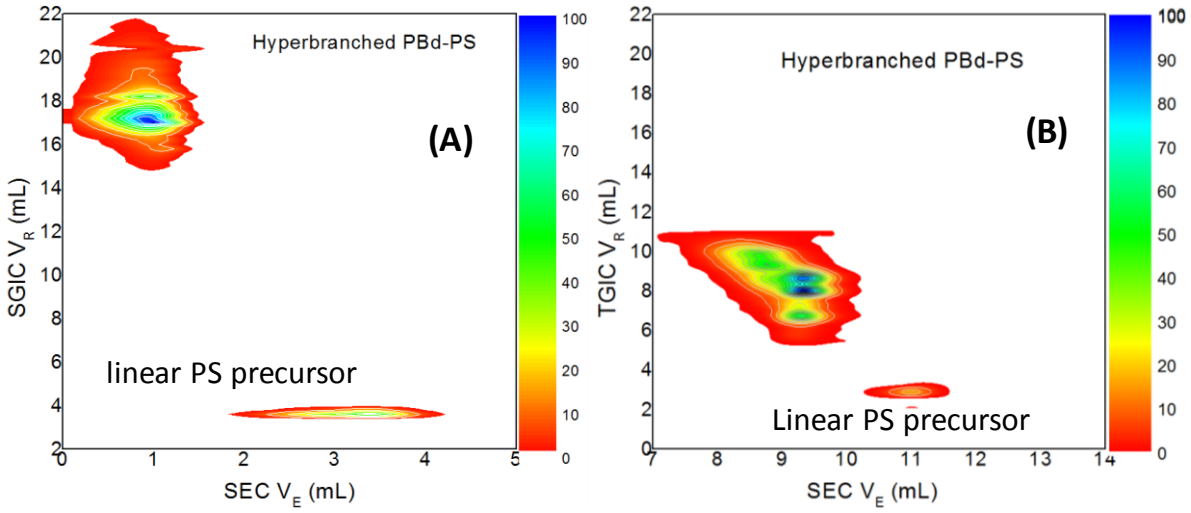

Figure 4.19 2D RP-SGIC × SEC contour plot of the crude hyperbranched PBd-PS (A).. 2D RP-TGIC × SEC contour plot of the hyperbranched PBd-PS (B).. Temperature gradient 10-40 °C with a linear ramp rate of 0.1 °C/min

Based on the 1D-LC separations of the hyperbranched PBd-PS sample, the PBd precursor co-eluted with the hyperbranched PBd-PS. The rest of the components in SGIC and TGIC can be identified as the hyperbranched copolymers. Based on the TGIC/SGIC set-up, one has to remember that when using the ELSD detection method, it is difficult to base the signal intensities to structural or chemical composition differences since an ELSD is not an accurate quantitative detection method as would a concentration detector such as the RI or UV detector used. It is interesting now to compare the substructures that can be seen in the contour plots for the hyperbranched material. Very similar to the 1D RP-SGIC separation in Figure 4.15A in which the linear PBd precursor co-eluted with the hyperbranched PBd-PS block copolymer, only 2-3 components with different chemical compositions can be identified, see SGIC elution volumes of about 16, 17 and 18 mL. Due to the low SGIC resolution, the assignment of these components to specific structures is rather challenging. In contrast to the SGIC separation, the TGIC separation shows at least 5 different substructures, see Figure 4.15B, that belong to different components of the hyperbranched material. The substructures

1-3 apparently have rather similar molar masses while the substructures 4 and 5 exhibit lower SEC elution volumes that indicate higher molar masses. These fractions might tentatively be assigned to fractions 4 and 5 in Figure 4.17 that are expected to have higher molar masses. Additionally, the linear PBd uncoupled starting material co-eluted with some of the hyperbranched PBd-PS species. However, a clear assignment of the substructures is only possible when the individual TGIC fractions 1-5 seen in Figure 4.17 can be collected and analysed by 2D-LC. From the results obtained in this work, although the RP-2D-LC showed a better picture regarding resolution of the hyperbranched it still is challenging to assign substructures of the complex branched block copolymer to the contour plots from fractionation of the crude hyperbranched PBd-PS alone. A more conclusive approach would involve collecting fractions with enough material (≈3 mg/mL per fraction!) to perform separate 2D-LC on each of the individual fractions then contrast them to the 2D-LC of the bulk crude material as well as NMR of the individual fractions.

In conclusion, TGIC seems to be better suited for the present separation task compared to SGIC due to the flexibility of the technique to manipulate temperature in influencing retention while holding the eluent composition constant.

4.5 Conclusions

Miktoarm star polystyrene-polyisoprene and hyperbranched polybutadiene-polystyrene were successfully prepared via Williamson coupling reactions. These complex polymer samples with multivariate distributions in molar mass, architecture and chemical composition of the constituting building blocks were successfully separated using a combination of SGIC and TGIC fractionation techniques. Star polybutadienes varying in number of arms and purity were also successfully characterised by TGIC and SGIC. By carefully optimising the separation conditions, both 1D-SGIC and 1D-TGIC can achieve significant resolution and provide complementary information when characterizing complex branched polymers. Compared to SEC, both SGIC and TGIC are more selective to changes in topology, chemical composition or molar mass, all of which affect the polymer chain size in solution. Although they are more superior than SEC in this regard, fractions from either SGIC or TGIC may well be resolved based on one molecular distribution but could still contain polymer species which vary in other molecular distributions. Based on the findings of this comparative study, we can conclude that depending on the type of sample under study, and the separation conditions thereto, a combination of SGIC and TGIC will provide complementary information of the complex polymer mixture. For a more exhaustive study on both TGIC and SGIC analyses, it

would be recommendable to assess the effect of varying the solvent composition, or the use of a different solvent choice altogether, on the resolution of the branched species. This would allow for a systematic study for example in TGIC fractionation, where one can directly compare the structural assignments calculated from H-NMR analysis. For the present samples in this work, TGIC is a more flexible IC technique and provides more alternatives of probing into the multiple molecular heterogeneities. The fractions from TGIC analysis of the more complex hyperbranched PBd-PS were collected and successfully analysed by offline ^{1}H-NMR and tentative structures were assigned to the collected fractions.

Based on the 1D SGIC and TGIC results and in order to identify exactly the multiple distributions present in the complex polymers analysed in this work, 2D-LC separation methods were also modelled. The 2D-LC separations were carried out by combining RP-SGIC × SEC and RP-TGIC × SEC and a remarkable contrast of the results was established.

4.6 References

1. B. Voit. *Journal of J. Polym. Sci. A: Polym. Chem.* 2000, **38**: 2505-2525.
2. B. I. Voit; A. Lederer. *Chem. Rev.* 2009, **109**: 5924-5973.
3. Q. Qiu; G. Liu; Z. An. *Chem.Commun.* 2011, **47**: 12685-12687.
4. G. Wang; X. Li; D. Yang; Y. Gao; H. Li. *Des. Monomers. Polym.* 2013, **17**: 132-139.
5. W. Sun; G. Zhang; L. Pan; H. Li; A. Shi. *Int. J. Polym. Sci*. 2013, **2013**: 1-10.
6. A. Hirao; K. Sugiyama; Y. Tsunoda; A. Matsuo; T. Watanabe. *J. Polym. Sci. A: Polym. Chem.* 2006, **44**: 6659-6687.
7. T. G. M. J. M. Ren, Q. Fu, E. H. H. wong, J. Xu, Z. An, S. Shanmugam, T. P. Davis, C. Boyer, G. G. Qiao. *Chem. Rev.* 2016, **116**: 6743-6836.
8. K. Matyjaszewski; P. J. Miller; J. Pyun; G. Kickelbick; S. Diamanti. *Macromolecules.* 1999, **32**: 6526-6535.
9. W. Radke; A. H. E. Müller. *Macromolecules.* 2005, **38**: 3949-3960.
10. N. Hadjichristidis; H. Iatrou; M. Pitsikalis; J. Mays. *Prog. Polym. Sci.* 2006, **31**: 1068-1132.
11. L. R. Hutchings; J. M. Dodds; D. Rees; S. M. Kimani; J. J. Wu; E. Smith. *Macromolecules.* 2009, **42**: 8675-8687.
12. S. M. Grayson; J. M. Frechet. *Chem. Rev.* 2001, **101**: 3819-3868.
13. B. M. Rosen; G. Lligadas; C. Hahn; V. Percec. *J. Polym. Sci. A: Polym. Chem.* 2009, **47**: 3931-3939.
14. Q. Fu; G. Wang; W. Lin; J. Huang. *J. Polym. Sci. A: Polym. Chem.*2009, **47**: 986-990.
15. M. A. Harvison; A. B. Lowe. *Macromol. Rapid. Commun.* 2011, **32**: 779-800.
16. L. R. Hutchings; S. J. Roberts-Bleming. *Macromolecules.* 2006, **39**: 2144-2152.
17. B. Bauer; L. Fetters. *Rubber Chem. Technol.* 1978, **51**: 406-436.
18. L. Zhou; N. Hadjichristidis; P. Toporowski; J. Roovers. *Rubber. Chem. Technol.* 1992, **65**: 303-314.
19. N. Hadjichristidis. *J. Polym. Sci. A: Polym. Chem.* 1999, **37**: 857-871.
20. A. B. Burns; R. A. Register. *Macromolecules.* 2016, **49**: 2063-2070.
21. L. R. Hutchings; J. M. Dodds; S. J. Roberts-Bleming. *Macromolecules.* 2005, **38**: 5970-5980.
22. F. J. López-Villanueva; F. Wurm; A. F. Kilbinger; H. Frey. *Macromol. Rapid. Commun.* 2007, **28**: 704-709.
23. U. Yolsal; L. R. Hutchings. *Eur. Polym. J.* 2019, **113**: 254-259.

24. K. Min; H. Gao. *J. Am. Chem. Soc.* 2012, **134**: 15680-15683.
25. B. Liu; A. Kazlauciunas; J. T. Guthrie; S. Perrier. *Macromolecules.* 2005, **38**: 2131-2136.
26. D. Konkolewicz; A. Gray-Weale; S. b. Perrier. *J. Am. Chem. Soc.* 2009, **131**: 18075-18077.
27. A. H. Müller; D. Yan; M. Wulkow. *Macromolecules.* 1997, **30**: 7015-7023.
28. S. G. Gaynor; S. Edelman; K. Matyjaszewski. *Macromolecules.* 1996, **29**: 1079-1081.
29. K. Matyjaszewski. *Macromolecules.* 2012, **45**: 4015-4039.
30. N. Hadjichristidis; M. Pitsikalis; S. Pispas; H. Iatrou. *Chem. Rev.* 2001, **101**: 3747-3792.
31. M. Hayashi; K. Kojima; A. Hirao. *Macromolecules.* 1999, **32**: 2425-2433.
32. A. Hirao; M. Hayashi; N. Haraguchi. *Macromol. Rapid. Commun.* 2000, **21**: 1171-1184.
33. T. Higashihara; M. Hayashi; A. Hirao. *Prog. Polym. Sci* 2011, **36**: 323-375.
34. D. M. Knauss; H. A. Al-Muallem; T. Huang; D. T. Wu. *Macromolecules.* 2000, **33**: 3557-3568.
35. N. V. Tsarevsky; B. S. Sumerlin; K. Matyjaszewski. *Macromolecules.* 2005, **38**: 3558-3561.
36. D. Fournier; R. Hoogenboom; U. S. Schubert. *Chem. Soc. Rev.* 2007, **36**: 1369-1380.
37. A. Pagliarulo; L. R. Hutchings. *Macromol. Chem. Phys.* 2018, **219**: 1700386.
38. H. Pasch In *Polymer Analysis Polymer Physics*; Springer, Berlin: 1997, p 1-45.
39. B. Trathnigg; M. I. Malik; N. Pircher; S. Hayden. *J. Sep. Sci.* 2010, **33**: 2052-2059.
40. Y. Brun. *J. Liq. Chrom. Relat. Tech.* 1999, **22**: 3027-3065.
41. W. Radke. *J. Chromatogr. A.* 2014, **1335**: 62-79.
42. H. Pasch In *New Developments in Polymer Analytics I*; Schmidt, M., Ed.; Springer Berlin Heidelberg: Berlin, Heidelberg, 2000, p 1-66.
43. H. Pasch. *Polym. Chem.* 2013, **4**: 2628.
44. P. Kilz; R. Kruger; H. Much; G. Schulz. *Adv. Chem. Ser.* 1995, **247**.223-241
45. J. Gerber; W. Radke. *Polymer* 2005, **46**: 9224-9229.
46. P. Schoenmakers; P. Aarnoutse. *Anal. Chem.* 2014, **86**: 6172-6179.
47. B. W. J. Pirok; D. R. Stoll; P. J. Schoenmakers. *Anal. Chem.* 2019, **91**, 240-263.
48. K. Maiko; H. Pasch. *Macromol. Rapid. Commun.* 2015, **36**: 2137-2142.
49. T. Chang; H. C. Lee; W. Lee; S. Park; C. Ko. *Macromol. Chem. Phys.* 1999, **200**: 2188-2204.
50. T. Chang. In *Liquid Chromatography/FTIR Microspectroscopy/Microwave Assisted Synthesis*, Springer, Berlin, Heidelberg, **163**: p1-60.
51. H. C. Lee, Chang, T. *Polymer.* 1996, **37**: 5747-5749
52. S. Lee; H. Lee; L. Thieu; Y. Jeong; T. Chang; C. Fu; Y. Zhu; Y. Wang. *Macromolecules.* 2013, **46**: 9114-9121.
53. S. Lee; H. Choi; T. Chang; B. Staal. *Anal. Chem.* 2018, **90**: 6259-6266.
54. W. Hiller; P. Sinha; H. Pasch. *Macromolecules Chem. Phys.* 2007, **208**: 1965-1978.
55. W. Hiller; H. Pasch; P. Sinha; T. Wagner; J. r. Thiel; M. Wagner; K. Müllen. *Macromolecules.* 2010, **43**: 4853-4863.
56. M. Hehn; W. Hiller; T. Wagner; J. Thiel; H. Pasch. *Macromol. Chem. Phys.*2012, **213**: 401-410.
57. R. P. Quirk; Y. Wang. *Polym. Int.* 1993, **31**: 51-59.
58. L. R. Hutchings. *Macromolecules.* 2012, **45**: 5621-5639.
59. C. Adams; L. Hutchings; P. Klein; T. McLeish; R. Richards. *Macromolecules.* 1996, **29**: 5717-5722.
60. C. Adams; M. Brereton; L. Hutchings; P. Klein; T. McLeish; R. Richards; M. Ries. *Macromolecules.* 2000, **33**: 7101-7106.
61. H. Iatrou; N. Hadjichristidis. *Macromolecules.* 1992, **25**: 4649-4651.
62. S. Agostini; L. R. Hutchings. *Eur. Polym. J.* 2013, **49**: 2769-2784.
63. J. M. Dodds; L. R. Hutchings. *Macromol. Symp.*2010; **291**: 26-35.
64. D. Murima; H. Pasch. *Anal.Bioanal. Chem.* 2019, **411**: 1-16.
65. S. Lee; H. Lee; T. Chang; A. Hirao. *Macromolecules.* 2017, **50**: 2768-2776.
66. W. Lee; S. Park; T. Chang. *Anal. Chem.* 2001, **73**: 3884-3889.

67. J. Roovers; P. Toporowski; J. Martin. *Macromolecules.* 1989, **22**: 1897-1903.

5.

Characterization of complex branched polymers using multidetector Thermal field-flow fractionation (ThFFF): A complementary technique to 2D-LC [3]

Douglas Murima, Harald Pasch *

Correspondence to: Harald Pasch, email:hpasch@sun.ac.za

Abstract: The unique features of Thermal field-flow fractionation (ThFFF) in combination with multiple detection methods make it a versatile alternative to the commonly employed column-based techniques to fractionate and characterize the solution behavior of low and highly branched polymers based on a set of different molecular distributions including size (molar mass and branching) and chemical composition. In this study, for the first time, the application of multidetector ThFFF was demonstrated for determining polymer conformations from Mark-Houwink plots and the degree of branching using functionality plots for a set of 3-, 4-, and 6-arm star polystyrenes, and a more complex hyperbranched polybutadiene-polystyrene (PBd-PS) copolymer in a single experiment. Also discussed is the application of multidetector ThFFF for the analysis of the radius of gyration (R_g), the hydrodynamic radius (R_h) and the hydrodynamic diameter (D_h) that are measured by static light scattering, viscometry and dynamic light scattering, respectively. The shape factors (R_g/R_h) are evaluated as influenced by branching where reasonably narrow star-branched polystyrenes with varying numbers of arms (3, 4 and 6 arms) provided "model" systems for the analysis of the more complex hyperbranched PBd-PS.

Key words: hyperbranched copolymer, star polystyrene, branched polymer conformations, Multidetector Thermal field-flow fractionation

5.1 Introduction

The innovations in the synthesis of polymeric materials with desirable bulk and solution properties continue to add to the limitations of existing analytical methods, hence the growing need to develop state-of-the-art analytical techniques with advanced capabilities. This is due to the fact that polymers exist as complex macromolecules with multiple distributions that

[3] Murima, D.; Pasch, H. *Macromol. Rapid Commun.* **2019** (**DOI: 10.1002/marc.201900556)**

include molar mass, chemical composition, functionality, and branching.[1-4] It is known that polymer features such as double bonds, cyclic structures and branches affect the ability of polymer chains to form random coils in solution resulting in specific viscosity changes.[5] However, the presence of branches also affects the interaction of the polymer chains with the solvent.[6] Since the solvation of a polymer chain has a direct influence on the coil expansion, the polymer-solvent interactions and, therefore, the intrinsic viscosity, these parameters are affected by a change in the thermodynamic quality of the solvent. In one instance, an increase in temperature may increase the chain flexibility due to the lower potential barrier of the transition from one conformation to another.[7] On the other hand, an increase in temperature may increase the thermodynamic quality of the solvent. It is worth noting that the intrinsic viscosity of a polymer chain changes with solvent quality and the coil dimensions in a good solvent are different from those in a theta solvent.[8] Figure 5.1 illustrates some general conformations adopted by a polymer under different solvent conditions.

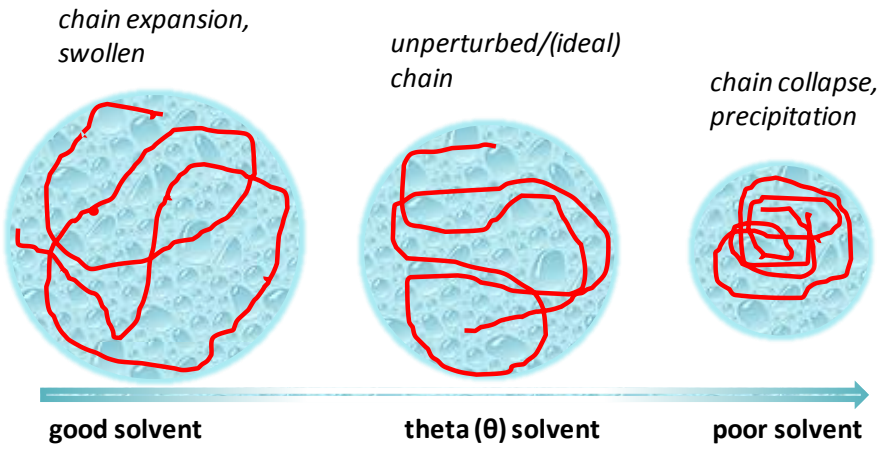

Figure 5.1 Polymer chain conformations under good, theta and poor solvent conditions.

The variance of the intrinsic viscosity in different solvents and at different temperatures produces important applications for some branched polymer systems as additives or rheology modifiers for lubricants and flocculants.[9,10] In addition, the properties of rheology modifiers for lubricants in fluid mechanical processes i.e. mixing and transport, are directly governed by particle size distribution. As such, an exhaustive quantitative account of the size and shape of the polymeric particles is required for process optimization and design of both the starting materials and the final products.[11] On this basis, from a polymer scientist's and industrial perspective, there is an increased urge for comprehensive information on the various

distributions which influence the properties of products made from branched polymeric systems.

Over the years, size exclusion chromatography (SEC) has become a benchmark for the characterization of polymers and a number of experimental variables have been modelled in order to achieve characterization of branched polymers, with the most useful being triple detection SEC. The separation of branched polymers by SEC can lead to the well-known phenomenon of abnormal SEC elution where linear and branched polymers of similar hydrodynamic sizes but different molar masses co-elute. Interaction chromatography (IC) has been widely employed as the column-based alternative to SEC for separation of complex polymer mixtures according to chemical composition. For fast separation, the mobile phase strength in IC is often increased over the duration of the experimental run which can be achieved by applying gradients of the eluent (solvent gradient interaction chromatography, SGIC)[12-15] or temperature (temperature gradient interaction chromatography, TGIC)[16-21] as well as online two-dimensional LC (2D-LC).[22-31] These separation techniques are often used in combination with multiple detection systems such as concentration detectors (refractive index-dRI or UV-detector), molar mass sensitive detectors (light scattering-MALS) and size or architecture sensitive detectors (viscometer).

Despite these advanced approaches, the inherent limitations of column-based liquid chromatography in addition to the increasing complex nature of new materials clearly show that there is a growing need for alternative separation technologies that can address some of the limitations associated with column-based techniques. Recently, open channel-based techniques that include Temperature field-flow fractionation (ThFFF) have received great attention in separation technology.[32-34] ThFFF is a sub-technique of the field-flow fractionation (FFF) family that applies a temperature drop perpendicular to a carrier liquid flowing through an open, ribbon-like channel.[35,36]

The free diffusion of a macromolecule in solution depends on both the hydrodynamic and thermodynamic polymer-solvent interactions. Hydrodynamic diameters (D_h) calculated from the diffusion coefficient (D) can be measured from batch dynamic light scattering (DLS) according to the Stokes−Einstein equation 16.

$$\mathbf{D_h = \frac{k_B T}{3\pi\eta D}} \qquad \textbf{[16]}$$

where k_B, T, and η represent Boltzmann's constant, temperature, and solvent viscosity, respectively. When analytes are introduced to a Temperature gradient, they migrate away from the hot wall towards the cold wall of the ThFFF channel. This temperature-induced migration is termed Temperature diffusion and is characterized by the Temperature diffusion coefficient (D_T), which is influenced by chemical composition. Furthermore, due to the concentration build-up at the cold wall, the analyte molecules diffuse back towards the center of the channel and this diffusion is characterized by the normal diffusion coefficient, D, which is determined by the analyte's size in solution. Thus, analytes are separated based on the interplay between D_T and D. This interplay between the two mass transport processes introduces the ability to separate based on a combination of polymer size and chemical composition because separation occurs on the basis of the Soret coefficient (S_T), the ratio of D_T to that of D.[37]

In the present contribution, an online DLS detector was added to the fractionation set-up with the aim of determining the hydrodynamic sizes (R_h) and diffusion coefficients (D) of the branched polymers, which would then be used to calculate D_T according to Equation 17.[38]

$$\mathbf{D_T = \frac{6Dt_R}{\Delta T t_o}} \qquad \textbf{[17]}$$

where ΔT is the Temperature gradient - the temperature difference between the hot and cold wall -, while t_R and t_o denote the retention and void times, respectively. Elution occurs with polymers of lower S_T eluting earlier and polymers of greater S_T eluting later. For composition distribution analysis, UV absorbance (UV) or differential refractive index (dRI) detector signals may be used to provide the composition of the polymer components eluting at a given time. In this work, ThFFF analysis was carried out using a detector train comprising of MALS, dRI, differential viscometer and online-DLS (as illustrated in Figure 5.2).

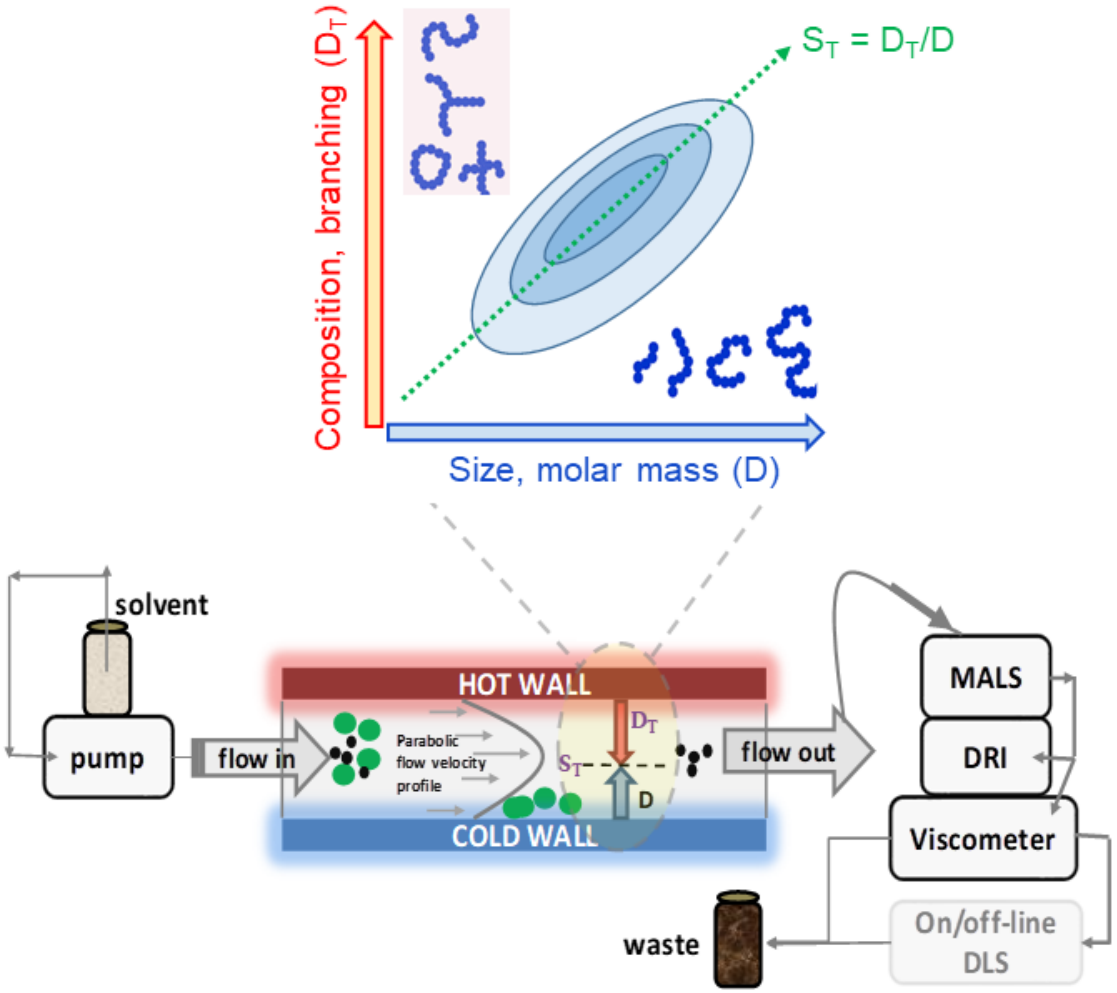

Figure 5.2 Schematic illustration of the multidetector ThFFF separation set-up illustratin the separation of a complex polymer mixture based on different molecular heterogeneities due to S_T.

Molecular size can also be determined from M_W measurements by static light scattering (i.e. MALS) combined with an online viscometer (to provide intrinsic viscosity, IV). This method helps to obtain size parameters in the form of radius of gyration (R_g) and hydrodynamic radius (R_h). It is important to note that R_h is different from R_g (see Figure 5.3).

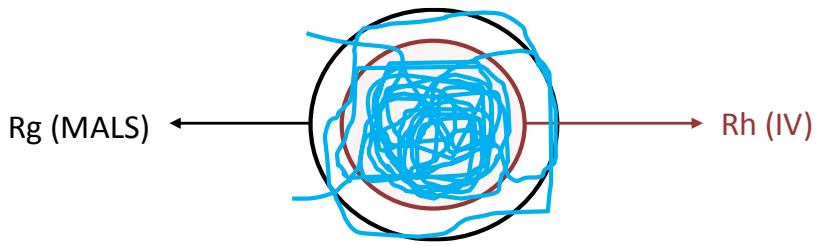

Figure 5.3 Differences between the size parameters measured by multiangle light scattering (R_g) and by viscometry (R_h)

The R_h is the radius of a hard sphere that diffuses at the same rate as the coil of an analyte under observation, while R_g is defined as the mass weighted average distance from the core of a molecule to each mass element in the molecule.[39,40] A more precise and accurate method of obtaining R_h is through the use of on-line MALS and viscometer detectors using the relationship shown in Equation 18.

$$[\eta]M = \frac{10}{3}\pi R_h^3 \quad \textbf{[18]}$$

where η is the intrinsic viscosity (from the viscometer) and M is the molar mass (from the MALS). Direct determination of R_g is obtained by measuring the change in scattered light intensity with change of observation angle.

The aim of this work was to experimentally investigate the effects of the degree of branching on polymer conformation relative to the thermodynamic quality of the solvent using multidetector ThFFF.[41] The first objective was to determine the polymer structures (from Mark-Houwink plots) and the degrees of branching (functionality plots) for a set of 3-, 4-, and 6-arm star PSs and a more complex hyperbranched PBd-PS. The second objective was to measure R_g (MALS), R_h (dVisc) and D_h (DLS) and then evaluate the shape factor (R_g/R_h) as influenced by branching. Monodisperse star-branched polystyrenes with varying numbers of arms (3, 4 and 6 arms) provided a model system for the analysis of the more complex hyperbranched PBd-PS. M_w was calculated from MALS and RI; the intrinsic viscosity (IV) and the Mark-Houwink plot were derived from the online viscometer and RI detection.[42] Branching ratios (g´ plots) and functionalities (f plots) were derived from the molecular weight and intrinsic viscosity relationships using models for determining star functionality and branching ratios outlined in chapter 3.[43]

5.2 Experimental Section

5.2.1 Materials

The linear polybutadiene (PBd) was purchased from PSS GmbH (Mainz, Germany) and the linear polystyrene (PS) standard sample was supplied by Postnova Analytics GmbH, Germany. All sample solutions were prepared in 3 $mg.mL^{-1}$ concentrations using HPLC grade THF (99.8%) and cyclohexane (CH, 99.9%) purchased from Sigma-Aldrich.

5.2.2 Polymer synthesis

Details of all the synthetic work related to the samples are described in chapters 3 and 4. Table 5.1 shows a summarized list of the polymer samples that were used in this current work. The molar masses and molar mass dispersities are also listed.

Table 5.1: List of polymer samples that were used to conduct in this study

Polymer sample	**M_w (kg/mol)**	**Đ**
Star PS 3-arm	67.2	1.50
Star PS 4-arm	58.1	1.40
Star PS 6-arm	62.0	1.50
Hyperbranched PBd-PS crude	166	1.25
PS-standard	138	1.80
PS-precursor	6.42	1.03
PBd-standard	86.0	1.07
PBd precursor	23.5	1.04

5.3 Analytical techniques

5.3.1 Multidetector ThFFF

All measurements were carried out using a TF2000 instrument (Postnova Analytics, Landsberg, Germany) coupled to the following detectors: MALLS (PN3621), capillary bridge viscometer (PN3310), and refractive index dRI (PN 3140), all from Postnova Analytics, Landsberg, Germany. A Zetasizer Nano series (Malvern Instruments, Worcestershire, UK) with built-in data-processing software was used for DLS detection at a back-scattering detection angle of 175°. The TF2000 channel had a tip-to-tip length of 45.6 cm, breadth of 2 cm, thickness of 127 μm, and void volume of 1.14 mL. The temperature of the cold wall was ≈ 23 °C, maintained via an externally controlled chiller (Uber Unichiller, Monitoring and Control Laboratories, South Africa). A constant ΔT of 80 °C was used to achieve fractionation. The analytes were introduced into the channel via a Rheodyne manual injection valve and carrier flow was generated by an isocratic pump (PN 1130, Postnova Analytics). THF and cyclohexane (Sigma-Aldrich, South Africa) were used as carrier liquids with a flow rate of 0.4 mL·min^{-1}. The analytes were injected through a 100 μL capillary sample loop, and triplicate analysis of each sample was performed without overloading the channel.

5.3.2 Offline DLS analysis

Triplicate runs were performed per sample measurement using a glass cuvette with an open round aperture at a temperature of 30 °C and using 1 mL sample volumes at respective concentrations of ≈ 2 mg/mL. The measurements were recorded using the Zetasizer software (version 7.11, Malvern Instruments, Worcestershire, UK). Five-minute equilibrium times were programmed before each measurement.

5.4 Results and discussion

Based on the findings presented in chapters 3 and 4, the method development for the analysis of complex branched polymers was carried forward moving from column-based techniques to channel-based techniques, in the present case ThFFF. Here, the idea was extended to explore the effects of low to extreme branching on polymer conformation, where monodisperse star-branched polystyrenes with varying numbers of arms (3, 4, and 6 arms) provided a suitable model system for this investigation. The potential of ThFFF with a multiple detection system to separate and characterize model star-branched homopolymers and complex highly branched block copolymers is highlighted.

5.4.1 Triple detector ThFFF and DLS conformation analysis of star polystyrene

Triple detector ThFFF analysis of polystyrene stars whose functionalities and conformations had been confirmed in chapter 3 using triple detector SEC was carried out with the aim of evaluating how the star functionality (number of arms) affects the macromolecular dimensions and the separation thereof, in a good solvent (THF) versus a theta solvent (cyclohexane) as a pilot study for the fractionation of a more complex hyperbranched polymer. Figure 5.4 shows the superimposed MALS, dRI and viscometer (DP) fractograms for star 3-,4- and 6-arm polystyrene together with the linear analogue in THF (A, C, E; void time ≈ 4.3 min) and cyclohexane (B, D, F; void time ≈ 2.5 min). From Figure 5.4 it was observed that the star-branched PSs had weak retention in THF (A, C, E) and very poor retention in cyclohexane (B, D, F). This is due to the fact that the star polystyrenes have relatively low molecular weights. It is important to point out here that the star polystyrenes had very similar molecular weights and polydispersities, see Table 5.2.

Based on the peak maxima of the fractograms, the elution times of the star-branched PSs in THF were in the order 3-arm (6.3 min) < 4-arm (7.6 min) < 6-arm (9.85 min). In cyclohexane, the elution profiles of all samples overlapped indicating that under these conditions a separation according to molecular topology is not obtained.

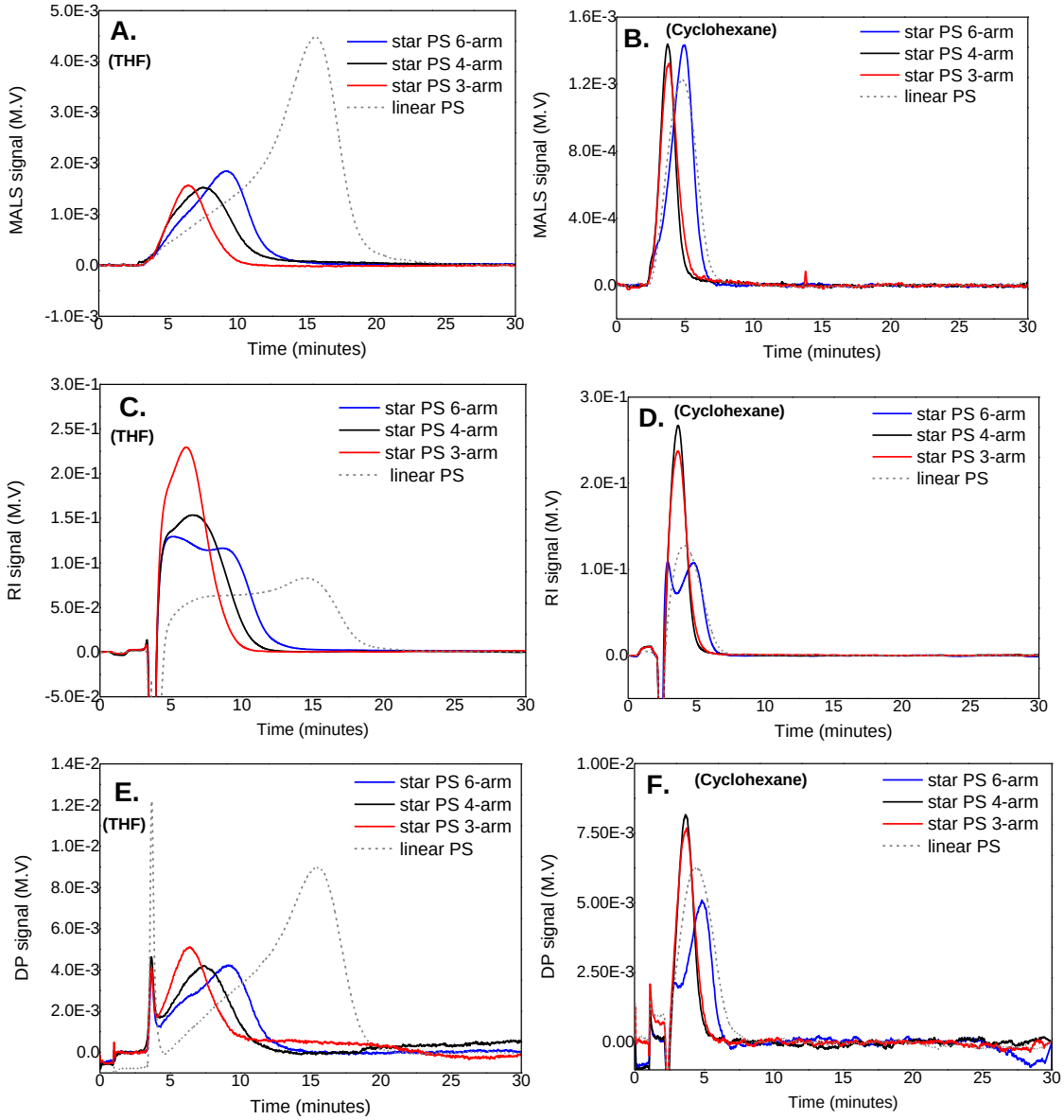

Figure 5.4 Overlaid MALS, dRI and viscometer (DP) fractograms for star 3-,4- and 6-arm polystyrene together with the linear reference in THF (A, C, E) and cyclohexane (B, D, F)

Previous studies have proven that normal diffusion (D) is dependent on size related parameters (in the present case molecular weight and branching) while Temperature diffusion (D_T) is influenced by the chemical composition distribution and the polymer-solvent interactions.[44,45] Unfortunately, because of the low retention times observed, the D_T values could not be accurately calculated. A similar finding has been reported before.[46] Since the star polystyrenes in this study had similar chemical compositions and comparable molecular weights, the separation must be size-based due to differences in star functionalities. The molecular weights as a function of elution volume as obtained by ThFFF-MALS are shown in Figure 5.5.

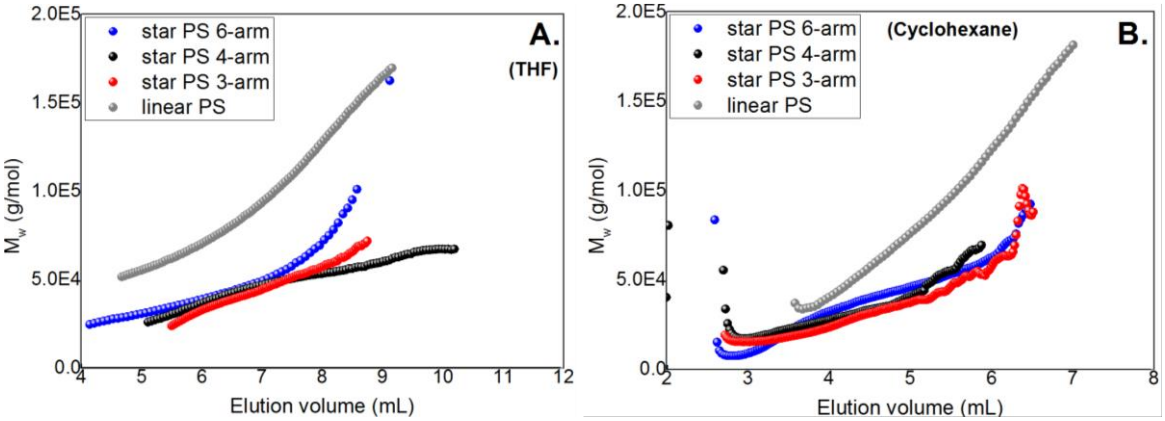

Figure 5.5 Overlaid molecular weight plots as a function of ThFFF elution volume for the star 3-, 4- and 6-arm polystyrenes together with the linear reference in THF (A) and in cyclohexane (B).

The results clearly prove that the star polystyrenes have a significantly more compact topology compared to the linear reference. The behavior in THF is distinctively different from that in cyclohexane. Since cyclohexane is a theta-solvent for PS, the star polystyrenes form quite compact coil structures. The effect of the number of arms is very low and there is only a small difference seen between the 3-arm and the 6-arm sample. In THF being a good solvent for PS the effect of the number of arms is more pronounced. At low elution volumes (5-6 mL) it can be seen clearly that at similar elution volumes the molecular weight increases from the 3- to the 6-arm sample. At higher elution volumes corresponding to higher molecular weights the behavior of the samples is more complex. This is due to the fact that the samples are not strictly 3-, 4- and 6-arm but mixtures of different topologies. This has been documented in the previous chapters.

Intrinsic viscosity (IV), obtained from online viscometry, relates molecular size directly to M_W for any polymer. IV is an inverse measure of molecular density. Polymers that are less compact have considerably high IV values at similar molecular weights, while the more compact ones have lower IV values.[47,48] In the present study, the intrinsic viscosity decreased with an increase in the star functionalities and coil compactness for both solvent systems. The intrinsic viscosity values were much smaller for the star-branched polymers relative to the linear reference as was expected. Table 5.2 summarizes the intrinsic viscosities (IV), normal diffusion coefficients (D) and molecular weights (M_w) of the star PSs in THF and cyclohexane together with the linear reference, as determined by the viscometer, DLS and MALS detection, respectively.

Table 5.2 Multidetector ThFFF molecular weights (M_w), intrinsic viscosities (IV) and diffusion coefficients (D) of the star-branched polystyrenes measured at 30°C.

Sample	IV^{THF} (dL/g),	$IV^{C\text{-}Hex}$ (dL/g),	D^{THF} ($\times 10^{-8}$ cm^2/s)	$D^{C\text{-}Hex}$ ($\times 10^{-8}$ cm^2/s)	M_w (kg/mol) MALS
Linear PS	0.642	0.364	3.88	6.47	138
Star PS 3-arm	0.318	0.143	4.72	5.69	67.0
Star PS 4-arm	0.224	0.117	4.41	5.53	58.0
Star PS 6-arm	0.205	0.098	4.18	6.61	62.0

In a theta solvent, it is expected that the polymer will exhibit a smaller coil size compared to a good solvent.[49] This is the case indeed as can be seen from Table 5.2. The smaller dimensions will result in greater diffusion and thus reduced retention. In addition to the increasing molecular density (i.e. increase in the number of arms attached to a fixed central linking point), the 3-arm (938 $g.mol^{-1}$), 4-arm (1210 $g.mol^{-1}$) and 6-arm (1780 $g.mol^{-1}$) cores differed in molecular weight which may have contributed to variations in the solution viscosity (an inverse function of density) for the star PSs, thereby affecting the normal diffusion rates.[50-52]

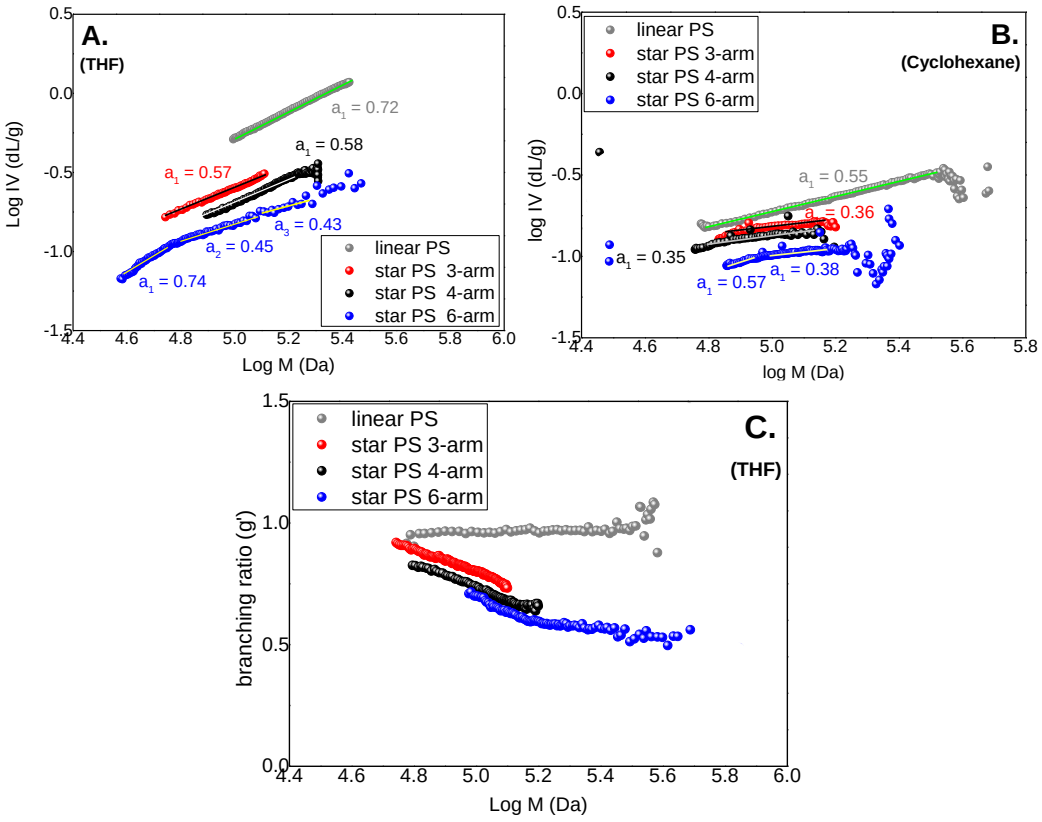

Figure 5.6 Superimposed Mark-Houwink and branching ratio *(g´)* plots as a function of molar mass for the star 3-, 4-, and 6-arm polystyrene together with the linear analogue in THF (A, C) and Mark-Houwink plots for the star PSs in cyclohexane (B).

Figure 5.6 shows the Mark-Houwink (A, B) and branching ratio (g´; C) plots determined from online viscometry as a function of molecular weight for the star-branched PSs. The Mark-Houwink exponent decreases from α = 0.72 for the linear PS (which is in agreement with literature data) to α = 0.57/0.58 for the 3/4-arm star PSs, respectively, in THF and from α = 0.55 for linear PS to α = 0.36/0.35 for the 3/4-arm star PSs in cyclohexane. The more complex 6-arm PS showed a mixture of linear (α = 0.74) and star functionalities (α = 0.45 and 0.43) in THF, as well as a mixture of linear (α = 0.57) and higher functionalities (α = 0.38) in cyclohexane. Although there were similar trends in THF and cyclohexane for the Mark-Houwink and branching ratio (g´) plots, the differences between the samples are more clearly seen in THF and only these plots are presented in Figure 5.6. The synergistic effect of both the molar mass and average functionality (both of which affect the molecular size in solution according to the Stokes-Einstein relationship) on the measured D are clearly seen in Table 5.2.[45]

A dimensionless parameter ρ, which is the ratio of the radius of gyration to the hydrodynamic radius ($\rho = R_g/R_h$), provides information on the shape and conformation of linear and branched polymers in solution. ρ is expected to exhibit values of 1.2–1.5 for linear random coils, and around 0.7 for a hard spheres.[53-55] In this work, R_g/R_h^{IV}, and R_g/R_h^{DLS} were calculated, where R_h^{IV} and R_h^{DLS} are the hydrodynamic radii of the polymer measured using both the viscometer (IV) and dynamic light scattering (DLS), respectively.

Table 5.3 Multidetector ThFFF size parameters and shape factors of the star-branched polystyrenes measured at 30°C.

Sample	R_g (nm)	MALS	R_h (nm)	IV	R_h (nm)	DLS	$\rho = (R_g/R_h^{IV})$	$\rho = (R_g/R_h^{DLS})$
	THF	C-Hex	THF	C-Hex	THF	C-Hex	THF	THF
Linear PS	17.5	14.2	12.6	10.2	13.8	11.3	1.39	1.26
Star PS 3-arm	9.53	7.94	8.16	7.58	10.4	8.32	1.16	0.91
Star PS 4-arm	7.22	6.44	7.36	6.73	9.03	8.21	0.98	0.80
Star PS 6-arm	6.01	5.97	6.31	6.22	7.71	7.63	0.96	0.78

Table 5.3 shows the size parameters and shape factors for the star-branched PSs and the linear reference in both THF and cyclohexane. The ρ-values for linear PS were within the anticipated range and decreased as the branching density of the star PSs increased. As a batch

technique, DLS allowed determination of the average size of the whole analyte, while the use of on-line MALS and viscometer enabled precise and accurate measurement of R_h. Owing to that, the R_h values from the DLS were slightly higher than those from the on-line MALS and viscometer as expected. To extend the capabilities of DLS in addition to the conformations derived from ρ, (R_g/R_h^{DLS}), size distributions for linear PS and the star-branched PSs were presented as a function of elution time. Figure 5.7 shows the size distributions as determined from online DLS in THF (A, C, E, G) and in cyclohexane (B, D, F, H).

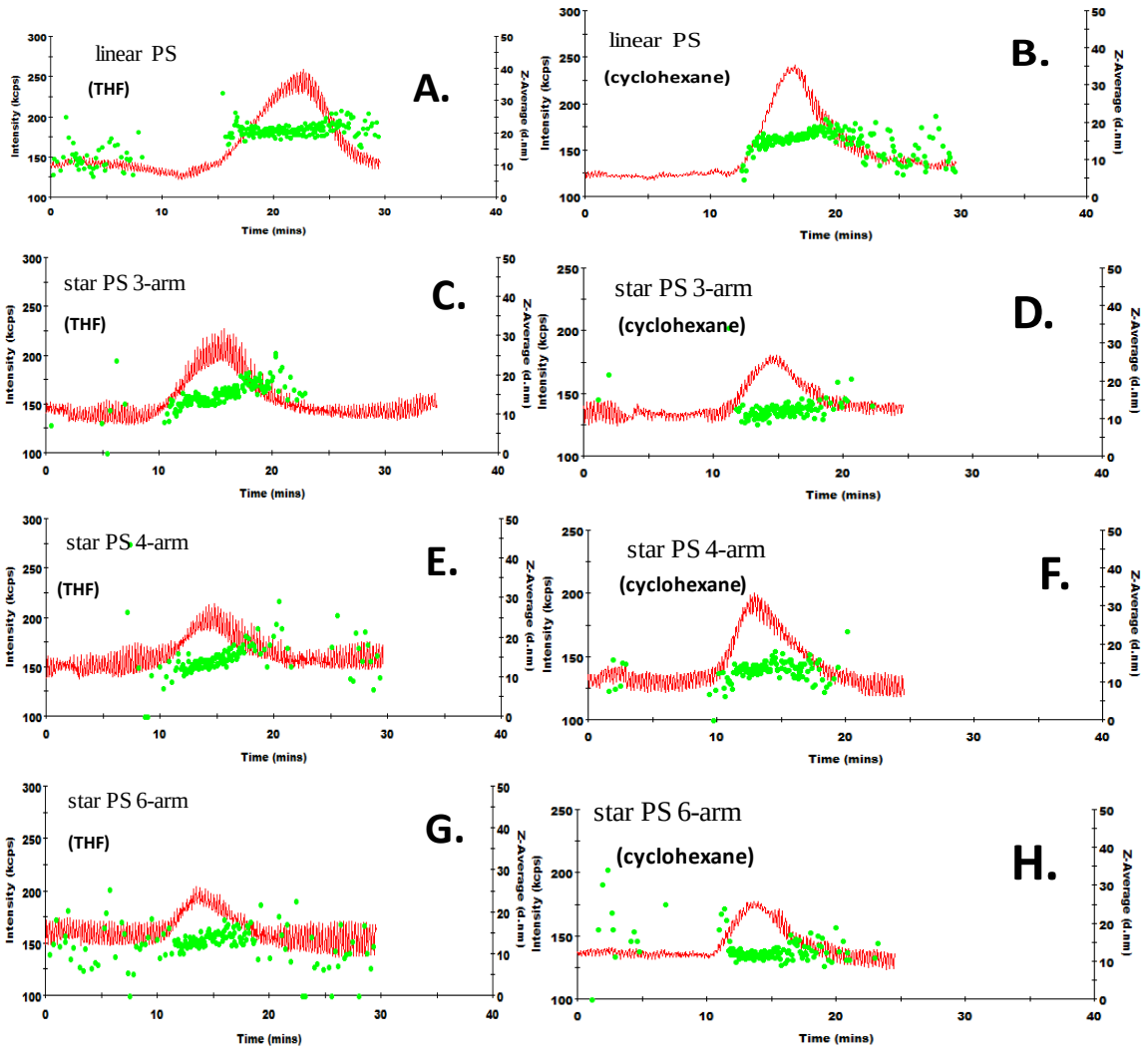

Figure 5.7 Online DLS data collected for star-branched polystyrenes together with the linear reference in THF (A, C, E, G) and in cyclohexane (B, D, F, H) at 30 °C.

In THF we see a clear size increase with increasing retention time. In C-Hex this is not clearly seen due to the theta solvent effect. Additionally, the Z-average data were recorded from offline DLS as mean average values from the triplicate measurements per every sample analyzed and plotted as a function of temperature. Figure 5.8 shows the variation of the

offline DLS measurements at isothermal 10 °C increment steps, from 20 – 60 °C for the star-branched PSs together with the linear PS reference in THF (Figure 5.8A) and cyclohexane (Figure 5.8B). From the offline DLS analyses, we observed that in the good solvent conditions (THF), the Z-average values increased above 30 °C due to thermally induced coil expansion, then were constant at 50 – 60 °C.[56] This phenomenon was more pronounced in the linear PS from 30 – 40 °C when compared to the stars since thermally induced coil expansion is restricted for branched polymers. In the theta solvent (cyclohexane), the Z-average values increased with increasing temperature for the linear PS until 50 °C, while they were relatively stable for the star-branched PSs across the temperature range owing to the thermodynamic quality differences of the solvents and the resulting lower coil expansion.[57]

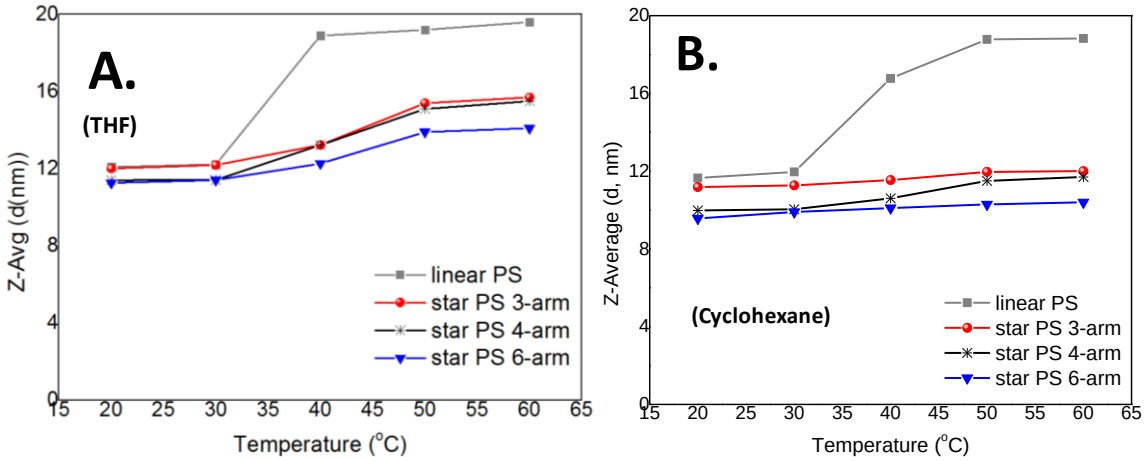

Figure 5.8 Offline DLS data for the linear and star-branched PSs measured at various isothermal steps from 20 – 60 °C in THF (A) and cyclohexane (B).

5.4.2 Triple detector ThFFF and DLS conformation analysis of hyperbranched PBd-PS

It is particularly challenging to characterize the complexity of polymers consisting of three or more molecular distributions. Therefore, it is important in polymer characterization to have readily available and robust techniques that enable the separation and comprehensive characterization of polymer mixtures based on their multimodality for structure-property correlations.[58-62] Multidetector ThFFF introduces the possibility to fractionate and detect the architecture and composition distributions of complex branched polymer samples in a single run since separation occurs based on the Soret coefficient (S_T), the ratio of the Temperature diffusion coefficient (D_T, which is dependent on the polymer and the solvent composition) to the translational diffusion coefficient (D, which is a polymer or particle size-dependent parameter).[63-68] The polymer species with lower S_T elute earlier while polymers with higher S_T will elute later. In this study, a hyperbranched PBd-PS block copolymer sample is analyzed

using the same model discussed for star-branched PSs. The mobile phase is THF which is a good solvent for both the polybutadiene (PBd) and polystyrene (PS) blocks. Figure 5.9 shows the superimposed dRI (A) and MALS fractograms (B) for the hyperbranched PBd-PS sample together with the PBd and PS precursors. From Figure 5.9A it can be seen, that there are early eluting species that might indicate the presence of the low molar mass precursor PS block (6 400 g/mol) as confirmed by fractograms of the PS and PBd precursors, and the experimental conditions used (constant ΔT = 80 °C). Since the hyperbranched PBd-PS sample consists of different species such as highly branched and incompletely coupled precursors, the dRI signal shows high intensity at low elution times and lower intensities at higher elution times indicating lower concentrations of these species. The molecular heterogeneity of the sample was more suitably observed in Figure 5.9B from the multiangle light scattering detector that shows more intense signals for the larger species.

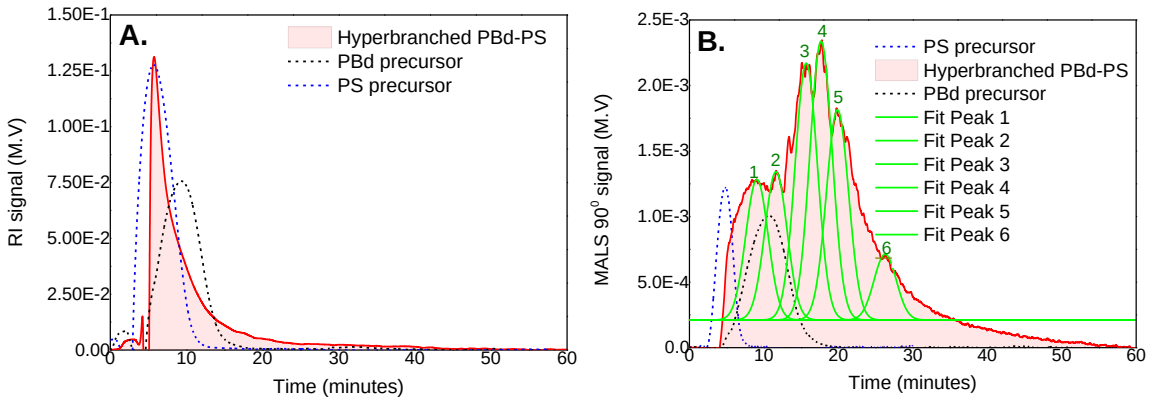

Figure 5.9 Overlaid dRI (A) and MALS (B) fractograms as a function of elution time for the hyperbranched PBd-PS together with the PS and PBd precursors in THF**.**

As can be seen, ThFFF was able to separate differently branched block copolymer species. Due to the weak retention of the early eluting species, a Gaussian model was used to carry out peak deconvolution of the complex fractogram so as to highlight the different eluting species as shown in Figure 5.9B.[69] Conclusive experimental data on the composition of these peaks would involve collecting fractions from the individual slices of the complex fractogram and then do a parallel ThFFF analysis to generate the diffusion coefficients to determine the D_T and S_T data based on the highlighted retention times.

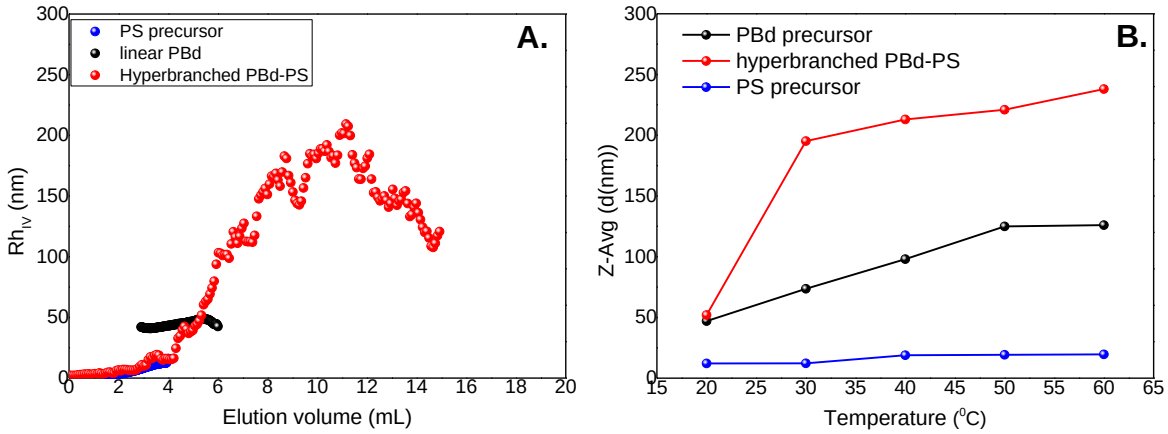

Figure 5.10 Superimposed online viscometer R_h data measured at 30 °C (A) and overlaid offline DLS data collected over isothermal steps from 20-60 °C (B) for the hyperbranched PBd-PS together with the PS and PBd precursors in THF**.**

Although the individual D, D_T and S_T values for the eluting species could not be calculated based on the experimental data obtained, it was apparent from the complex fractogram as evidenced by peak deconvolution that the eluting species varied in size as well as composition.[70] Figure 5.10A shows the overlaid R_h as a function of elution volume for the hyperbranched PBd-PS together with the PS and PBd precursors as determined by online viscometry at 30 °C. The variation in size distribution in Figure 5.10A in addition to the complex fractogram from the MALS analysis supports the notion that the eluting species vary in both composition and size (in this case, branching and molar mass). Offline DLS size data in the form of Z-average measurements for the hyperbranched PBd-PS and the PBd as well as PS precursors at different isothermal steps in 10 °C increments from 20 - 60 °C are also presented in Figure 5.10B. The hyperbranched PBd-PS showed more size-dependent thermoresponsive behaviour when compared to the linear PBd and PS precursors and such is typical of branched polymers due to thermally induced conformation changes of the polymer chains in solution.[46]

Unlike dendrimers which exhibit Mark-Houwink plots that have a maximum, hyperbranched polymers still show linear dependency of intrinsic viscosity on molecular weight with low exponents typically within the range 0.3-0.4 in a good solvent.[71,72]. For this work, in order to understand the dependency of intrinsic viscosity on the molecular weight for the hyperbranched PBd-PS, Mark-Houwink plots of the linear PBd and PS precursors were superimposed with that of the hyperbranched sample (see Figure 5.11).

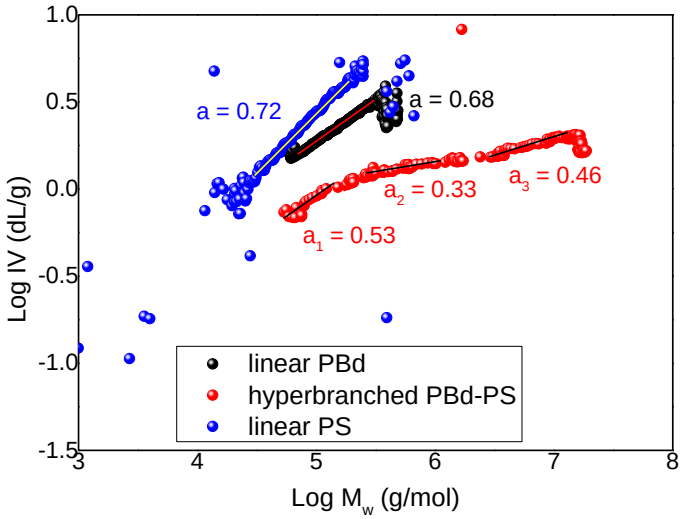

Figure 5.11 Overlaid ThFFF-online viscometry derived Mark-Houwink plot for the hyperbranched PBd-PS with linear PS and liner PBd standard references in THF.

The Mark-Houwink plot of the hyperbranched PBd-PS highlights the compactness differences in the structures present in this sample. Accordingly, the Mark-Houwink exponents of the hyperbranched PBd-PS structures were considerably lower ($\alpha = 0.53$ for low M_w species, and $\alpha = 0.33$ and $\alpha = 0.46$ for the high molar mass species) than those for the linear PS ($\alpha = 0.72$) and linear PBd ($\alpha = 0.68$). The relatively low α values observed are consistent with highly branched, compact structures.[73,74]

5.5 Conclusions

In this study the shape factors (ρ) and Mark-Houwink plots (intrinsic viscosity as a function of molecular weight) were generated via multidetector ThFFF for model star polystyrenes in both a thermodynamically good solvent (tetrahydrofuran) and a theta solvent (cyclohexane). A hyperbranched polybutadiene-polystyrene block copolymer was also analysed in THF, a good solvent for both polymer blocks. The results allowed a comparison of the various methods unattainable by SEC, SGIC or TGIC for deriving branching information by investigating several different parameters. Where classical characterization of dilute solution properties demands fractionation in order to obtain narrow molecular weight fractions with which to explore solution properties, the combination of light scattering and viscometry with ThFFF allows for the various fractions of a polydisperse sample to be characterized in a single injection provided there is sufficient retention to determine the Soret coefficient, which characterizes the interplay between the thermal diffusion coefficient and the translational/normal diffusion coefficient. For this study, the translational diffusion coefficients for star-branched polystyrenes were determined by online DLS measurements.

Unfortunately, the samples showed only weak retention and, therefore, the thermal diffusion coefficients as well as the Soret coefficients could not be calculated based on the Stokes-Einstein relationship. However, since the star-branched polystyrenes were chemically rather homogeneous, the fractionation was concluded to be solely size-based owing to the differences in the branching density of the star 3-, 4-, and 6-arm polystyrenes. For the offline DLS analyses of the star PSs in the good solvent (THF), the Z-average values increased above 30 °C due to thermally induced coil expansion, then were constant at 50 – 60 °C. This observation was more notable in the linear PS from 30 – 40 °C when compared to the stars since thermally induced coil expansion is restricted for branched polymers. Another more important point was that the multidetector ThFFF separation of the more complex hyperbranched PBd-PS block copolymer revealed the dependency of the branching density and chemical composition distribution on the fractionation of the sample.

5.6 References

1. T. H. Barrows. In *High performance biomaterials* Technol Publishing Company, Pennsylvania, U.S.A, 1991: pp 243-257.
2. J. H. Scrivens; A. T. Jackson. *Int. J. Mass. Spectrom.* 2000, **200**: 261-276.
3. T. Chang In *Liquid Chromatography/FTIR Microspectroscopy/Microwave Assisted Synthesis*; Springer: 2003, p 1-60.
4. P. Schoenmakers In *Encyclopedia of Separation Science*; Wilson, I. D., Ed.; Academic Press: Oxford, 2007, p 1-8.
5. P. Small. *J. Appl. Chem.* 1953, **3**: 71-80.
6. X. Zhu; Y. Zhou; D. Yan. *J. Polym. Sci. B* 2011, **49**: 1277-1286.
7. A. E. Tonelli. *Macromolecules.* 1972, **5**: 558-562.
8. N. Hoda; R. G. Larson. *J. Rheol.* 2010, **54**: 1061-1081.
9. J. M. Fréchet; C. J. Hawker. *React. Funct. Polym.* 1995, **26**: 127-136.
10. J. H. Barajas; C. Wandrey; D. Hunkeler; *Polymer flocculants with improved dewatering characteristics*. U.S. Patent 6,294,622.: 2001.
11. A. V. Shenoy *Rheology of filled polymer systems*; Springer Science & Business Media, 2013
12. A. de Villiers; P. Venter; H. Pasch. *J. Chromatogr. A.* 2016, **1430**: 16-78.
13. H. Maier; F. Malz; W. Radke. *Macromol. Chem. Phys.* 2015, **216**: 228-234.
14. K. Maiko; H. Pasch. *Macromol. Rapid. Commun.* 2015, **36**: 2137-2142.
15. J. Gerber; W. Radke. *e-Polymers.* 2005, **5:**.1-12.
16. S. Lee; H. Lee; T. Chang; A. Hirao. *Macromolecules.* 2017, **50**: 2768-2776.
17. S. Lee; T. Chang. *Macromol. Chem. Phys.* 2017, **218**: 1700087.
18. L. R. Hutchings; S. Agostini; M. E. Oti; J. Keth. *Eur. Polym. J.* 2015, **73**: 105-115.
19. T. Chang. *J. Polym. Sci. B* 2005, **43**: 1591-1607.
20. H. C. Lee, Chang, T. *Polymer.* 1996, **37**: 5747.
21. H. C. Lee, Chang, T. *Macromolecules.* 1998, **31**: 690-694.
22. H. Pasch In *Polymer Analysis Polymer Physics*; Springer, Berlin: 1997, p 1-45.
23. B. Trathnigg; M. I. Malik; N. Pircher; S. Hayden. *J. Sep. Sci.* 2010, **33**: 2052-2059.
24. Y. Brun. *J. Liq. Chrom. Relat. Tech.* 1999, **22**: 3027-3065.
25. W. Radke. *J. Chromatogr. A.* 2014, **1335**: 62-79

26. H. Pasch In *New Developments in Polymer Analytics I*; Schmidt, M., Ed.; Springer Berlin Heidelberg: Berlin, Heidelberg, 2000, p 1-66.
27. H. Pasch. *Polym. Chem.* 2013, **4**: 2628.
28. P. Kilz; R. Kruger; H. Much; G. Schulz. *Adv. Chem. Ser.* 1995, **247**.
29. J. Gerber; W. Radke. *Polymer*. 2005, **46**: 9224-9229.
30. P. Schoenmakers; P. Aarnoutse. *Anal. Chem.* 2014, **86**: 6172-6179.
31. B. W. J. Pirok; D. R. Stoll; P. J. Schoenmakers. *Anal. Chem.* 2018.**91**: 240-263
32. M. E. Schimpf. *J. Chromatogr. A.*1990, **517**: 405-421.
33. J. R. Runyon; S. K. R. Williams. *J. Chromatogr. A.* 2011, **1218**: 7016-7022.
34. M. I. Malik; H. Pasch. *Prog. Polym. Sci.* 2016, **63**: 42-85.
35. J. C. Giddings; M. N. Myers; J. Janča. *J. Chromatogr. A.*1979, **186**: 37-44.
36. M. E. Schimpf In *Encyclopedia of Separation Science*; Wilson, I. D., Ed.; Academic Press: Oxford, 2000, p 3906-3915.
37. C. Bria; F. Violleau; S. K. R. Williams. *LCGC Eur* 2013: 660-671.
38. M. E. Schimpf; K. Caldwell; J. C. Giddings *Field-flow fractionation handbook*; John Wiley & Sons, 2000
39. B. H. Zimm. *J. Chem. Phys.* 1948, **16**: 1093-1099.
40. P. J. Wyatt. *Anal. Chimica. Acta.* 1993, **272**: 1-40.
41. U. L. Muza; H. Pasch. *Anal. Chem.* 2019, **91**: 6926-6933
42. T. G. Scholte; N. Meijerink; H. Schoffeleers; A. Brands. *J. Appl. Polym. Sci.* 1984, **29**: 3763-3782.
43. D. Murima; H. Pasch. *Anal. Bioanal. Chem.* 2019, **411**: 5063-5078.
44. M. E. Schimpf; J. C. Giddings. *J. Polym. Sci. B.* 1990, **28**: 2673-2680.
45. M. E. Schimpf; J. C. Giddings. *Macromolecules.* 1987, **20**: 1561-1563.
46. G. Greyling; A. Lederer; H. Pasch. *Macromol. Chem. Phys.* 2018, **219**: 1800417.
47. S. Bywater In *Physical Chemistry*; Springer, Berlin: 1979, p 89-116.
48. S. Podzimek; T. Vlcek. *J. Appl. Polym. Sci.* 2001, **82**: 454-460.
49. B. J. Bauer; L. J. Fetters; W. W. Graessley; N. Hadjichristidis; G. F. Quack. *Macromolecules.* 1989, **22**: 2337-2347.
50. G. E. Kassalainen; S. K. R. Williams. *J. Chromatogr. A.* 2003, **988**: 285-295.
51. M. E. Schimpf; J. C. Giddings. *J. Polym. Sci. B* 1989, **27**: 1317-1332.
52. A. von Harpe; H. Petersen; Y. Li; T. Kissel. *J. Control. Release.* 2000, **69**: 309-322.
53. L. Schulz; W. Burchard; R. Dönges; *ACS. Symp*: 1998, **688**: 218-238
54. I. H. Park; E.-J. Choi. *Polymer.* 1996, **37**: 313-319.
55. N. Davidson; L. Fetters; W. Funk; N. Hadjichristidis; W. Graessley. *Macromolecules.* 1987, **20**: 2614-2619.
56. D. Patterson *J. Polym. Sci. Part C: Polym. Symp*. 1967; **16**: 3379-3389.
57. F. Yin; D. Bedrov; G. D. Smith. *Eur. Polym. J.* 2008, **44**: 3670-3675.
58. H. Pasch *Macromol. Symp.* 2001; **174**: 403-412.
59. H. Pasch; M. Adler; F. Rittig; S. Becker. *Macromol. Rapid. Commun.* 2005, **26**: 438-444.
60. S. Cheruthazhekatt; T. F. Pijpers; G. W. Harding; V. B. Mathot; H. Pasch. *Macromolecules.* 2012, **45**: 2025-2034.
61. M. I. Malik; H. Pasch. *Prog. Polym. Sci.* 2014, **39**: 87-123.
62. A. Ndiripo; P. S. Eselem Bungu; H. Pasch. *Polym. Int.* 2019, **68**: 206-217.
63. J. C. Giddings. *Anal. Chem.* 1997, **69**: 552-557.
64. M. Schimpf. *Field-Flow Fractionation Handbook* , Wiley, 2000: pp 618
65. G. E. Kassalainen; S. K. R. Williams. *Anal. Chem.* 2003, **75**: 1887-1894.
66. J. R. Runyon; S. K. R. Williams. *J. Chromatogr. A.* 2011, **1218**: 6774-6779.
67. W. van Aswegen; W. Hiller; M. Hehn; H. Pasch. *Macromol. Rapid. Commun.* 2013, **34**: 1098-1103.
68. G. Greyling; H. Pasch. *J. Chromatogr. A.* 2015, **1414**: 163-172.

69. J. Torres-Lapasió; J. Baeza-Baeza; M. Garcia-Alvarez-Coque. *Anal. Chem.* 1997, **69**: 3822-3831.
70. C. A. Ponyik, MSc Thesis, 2016. Colorado School of Mines. Golden, U.S.A.
71. S. R. Turner; B. I. Voit; T. H. Mourey. *Macromolecules.* 1993, **26**: 4617-4623.
72. S. B. Kharchenko; R. M. Kannan; J. J. Cernohous; S. Venkataramani. *Macromolecules.* 2003, **36**: 399-406.
73. C. Acebo; X. Ramis; A. Serra. *Phys. Sci. Rev.* 2017, 1**27**: 645-654.
74. B. Voit. *Acta. Polym.* 1995, **46**: 87-99.

6.

Summary and Recommendations

6.1 Overall conclusions

Complex branched polymers were successfully analyzed by a combination of HPLC protocols which included multidetector SEC, SGIC, TGIC and 2D-LC. The Mark-Houwink (conformation) plots obtained by triple detector SEC with RI-, MALLS- and viscometer detection showed that the slopes of the intrinsic viscosity vs. molar mass functions decreased with increasing numbers of arms signifying the increased polymer coil densities. Overally, branching ratios and star functionalities were obtained that agreed with the NMR results. The lower than expected average branching numbers calculated by NMR indicate complex mixtures of star-shaped polymers with a different number of arms and linear polymer chains from the RAFT, core first strategy employed to prepare the stars. In this study, the targeted molar masses per star was 120 000 g/mol. However low conversions (56% for 3-arm, 38% for 4-arm and 45% for the 6-arm star) as determined by gravimetric analyses resulted in the low average molar masses obtained. For the 6-arm star PS sample at different molar masses, the Mark-Houwink exponents of 0.78, 0.48 and 0.36 were obtained that indicated the differently branched as well as linear species in this complex sample.

The SGIC and TGIC experiments proved that the 6-arm star PS sample comprised of a significant linear portion in addition to 3-arm, 4-arm and 6-arm star molecules. For SGIC analyses, there was still noticeable peak overlapping between the 3-arm star, 4-arm star and some components of the 6-arm star. The fact that the 2nd peak of the 6-arm star sample co-eluted with the 3/4-arm stars suggests that 3/4-arm stars were formed as by-products in the synthesis of the 6-arm star. Improvements in the selectivity of the SGIC and TGIC experiments will enable the strict quantification of these species. However, the application of SGIC as a sub-technique of LAC may still be associated with drawbacks such as co-elution of linear and branched species with similar molar mass. Comprehensive 2D-TGICxSEC has been demonstrated to be able to separate the star polystyrenes according to molecular topology and molar mass and paves the way for more detailed investigations on the molecular composition of differently branched polymers that are prepared by various Reversible deactivation radical polymerization (RDRP) methodologies.

For the star polybutadienes (PBds), in comparison to the 1D-SGIC and SEC separations, 1D-TGIC had the better resolution to separate each by-product present in the star polymers far beyond what was possible with SEC. For the analysis of polymers before fractionation, TGIC was able to show the presence of incomplete, partially coupled products, in contrast to SEC that was only able to show the fully coupled product as well as any excess precursor still present in the crude samples. SGIC was not able to achieve significant baseline separation between products and a variation of the separation conditions is recommended for a more exhaustive study. For the purified PBd samples, TGIC was also able to detect and quantify the amounts of impurities still present after fractionation, where SEC analysis had indicated complete purity and SGIC was unable to resolve any by-products from the major peak

Miktoarm star polystyrene-polyisoprene and hyperbranched polybutadiene-polystyrene were successfully prepared via Williamson coupling reactions. These complex polymer samples with multivariate distributions in molar mass, architecture and chemical composition of the constituting building blocks were successfully separated using a combination of SGIC and TGIC fractionation techniques. Star polybutadienes varying in number of arms and purity were also successfully characterised by TGIC and SGIC. Although they are superior to SEC in this regard, fractions from either SGIC or TGIC may well be resolved based on one molecular distribution but could still contain polymer species which vary in other molecular distributions. Based on the findings of this comparative study, it was concluded that depending on the type of sample under study, and the separation conditions thereto, a combination of SGIC and TGIC will provide complementary information for a complex polymer mixture. In addition, TGIC is a more flexible IC technique and provides more alternatives of probing into the multiple heterogeneities of complex polymer systems. The fractions from TGIC analysis of the more complex hyperbranched PBd-PS were collected and successfully analysed by offline ^{1}H-NMR and tentative structures were assigned to the collected fractions. As RP-TGIC is known to be a molar mass sensitive technique (in addition to the molecular weight differences between the PBd (23 000 g/mol) and PS (6 200 g/mol) blocks themselves, we concluded that the eluting species were separated according to the total molecular weight and/or degree of branching in the order of increasing amounts of the polybutadiene entities of the hyperbranched PBd-PS sample. For NP-TGIC, NP-TGIC fractionation, it was concluded that the fractionation was mainly based on the interaction of the relative number of free OH groups of the PBd blocks with the stationary phase. From the comparative study on the 1D SGIC and TGIC results and in order to identify exactly the multiple distributions present in the complex polymers analysed in this work, 2D-LC

separation methods were also modelled. The 2D-LC separations were carried out by combining RP-SGIC × SEC and RP-TGIC × SEC and a remarkable contrast of the results was established.

The shape factor (ρ) and Mark-Houwink plots (intrinsic viscosity as a function of molecular weight data) were generated via multi-detector ThFFF for star polystyrenes in both a thermodynamically good solvent (tetrahydrofuran, THF) and a theta solvent (cyclohexane). Additionally, hyperbranched polybutadiene-polystyrene block copolymer was analysed in THF, a good solvent for both polymer blocks. The ThFFF results allowed an alternative way of investigating branching information by investigating several different parameters. From the findings in this contribution, the translational diffusion coefficients for star-branched polystyrenes were determined by online DLS measurements. Unfortunately, there was weak retention and therefore the thermal diffusion coefficients as well as the Soret coefficients could not be calculated based on the Stokes-Einstein relationship. However, since the star-branched polystyrenes were chemically homogeneous, the fractionation was concluded to be solely size-based owing to the differences in the branching density of the star 3-, 4-, and 6-arm polystyrenes. When using the theta solvent (cyclohexane), the Z-average values increased with increasing temperature for the linear PS until 50 °C, while they were relatively stable for the star-branched PSs across the temperature range owing to the thermodynamic quality differences of the solvents and the resulting lower coil expansionAn even more important point is that the multi-detector ThFFF separation of the more complex hyperbranched PBd-PS block copolymer revealed the dependency of the branching density and chemical composition distribution on the fractionation of the crude sample.

For the analysis of star and hyperbranched polymers multidetector ThFFF has been shown to be an interesting alternative to size exclusion chromatography. The unique fractionation mechanism of ThFFF that is based on the interplay between Temperature and translational diffusion allows for the separation of complex branched samples according to the type of branching. The coupling of ThFFF with information-rich detectors such as multiangle light scattering and viscometry may provide quantitative information on the Temperature and translational diffusion coefficients as well as important molecular parameters such as radius of gyration, hydrodynamic size and shape ratio. Finally, the molar mass dependence of the branching ratio can be investigated

6.2 Recommendations

Suggested future work for the miktoarm star-branched polystyrene-polyisoprene and hyperbranched polybutadiene-polystyrene for TGIC as well as SGIC studies, will be the application of a different solvent system (also co-solvent and lower temperature ramp rates for TGIC) to improve resolution between co-eluting species. For a more detailed analysis on correlating TGIC elution and NMR analysis of individual fractions, it would be critical to collect as much material enough to assess molecular weight and calculate compositions based on the molecular weights of the individual blocks then correlate with NMR data as well as assigning structures of fractions/species based on 2D-LC analyses.

Future work for the miktoarm star-branched polystyrene-polyisoprene and hyperbranched polybutadiene-polystyrene includes collecting of fractions from ThFFF analysis for compositional analysis of the eluting species using ^{1}H-NMR. Additionally, the individual fractions will be subjected to ThFFF analyses in order to determine the thermal diffusion coefficients and correlate them with the data obtained from analysis of the bulk hyperbranched PBd-PS sample. Figure 6.1 illustrates the proposed fractionation methodology for a comprehensive characterization of the multiple distributions based on degree of branching, composition and molar mass.

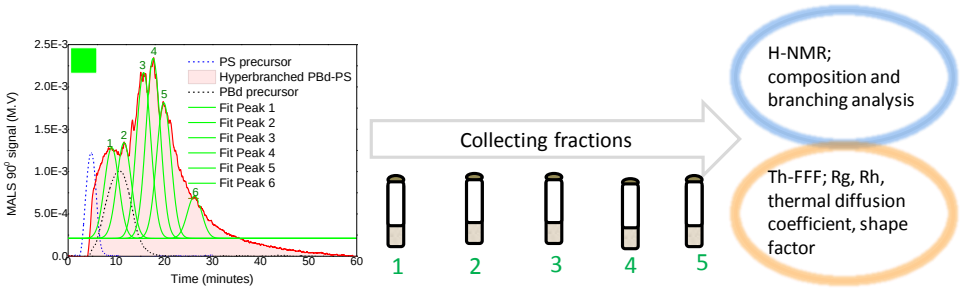

Figure 6.1 Collection of fractions by ThFFF analysis of the bulk hyperbranched PBd-PS

In addition to the positives of Th-FFF analysis of the hyperbranched block copolymer in THF, the multimodal complex fractogram was unattainable by 1D-LC techniques used in this study. Here it is worthy to mention that the use of a gaussian curve fitting was for illustration purposes without the intention of being too optimistic. Owing to that, the alternative method towards a comprehensive analysis would be to perform fractionation and collect individual fractions from the fractogram slices at various times. This, we hope can be achieved by means of using (perhaps) a co-solvent which promotes retention thereby improving resolution of the hyperbranched PBd-PS and the present by-products.